Dissertation

submitted to the

Combined Faculties of the Natural Sciences and for Mathematics
of the Ruperto-Carola University of Heidelberg, Germany

for the degree of

Doctor of Natural Sciences

Put forward by

M.Sc. Sören Lammers

born in Paderborn, Germany

Oral examination: October 19, 2017

Dimensional crossover of nonrelativistic bosons

Referees: Prof. Dr. Christof Wetterich
Prof. Dr. Thomas Gasenzer

Dimensionaler Übergang nichtrelativistischer Bosonen

In dieser Arbeit beschäftigen wir uns mit dem dimensionalen Übergang des nichtrelativistischen Bosegases mit abstoßender Punktwechselwirkung. Unser Fokus liegt auf dem Übergang von zwei zu drei Dimensionen, da dieser Fall besonders relevant für Experimente mit ultrakalten Gasen ist. Sowohl in dem zweidimensionalen als auch in dem dreidimensionalen System gibt es einen Phasenübergang zu einem Superfluid. Wir berechnen die kritische Temperatur dieses Übergangs als Funktion der Ausdehnung der transversalen Dimension, welche durch einen Potentialtopf mit periodischen Randbedingungen beschränkt ist. Für diese Berechnungen nutzen wir Gleichungen der funktionalen Renormierungsgruppe. Weiterhin berechnen wir den Zusammenhang der zwei- und dreidimensionalen Streulänge und erörtern, wie das zweidimensionale System seine Eigenschaften von dem dreidimensionalen System während des Renormierungsgruppenflusses erbt. Als zentrales Objekt des dimensionalen Überganges führen wir die Crossover-Funktion ein. Schließlich betrachten wir noch weitere Kompaktifizierungen. Wir berechnen die Crossover-Funktion für ein Gas, dessen transversale Dimension durch ein Boxpotential begrenzt ist und leiten Flussgleichungen her, welche das Verhalten in einer harmonischen Falle approximieren.

Dimensional crossover of nonrelativistic bosons

In this thesis we study the dimensional crossover of a nonrelativistic Bose gas with pointlike repulsive interactions. Our focus is on the dimensional crossover from two to three dimensions, which is of particular relevance in ultracold experiments. Both the two-dimensional and the three-dimensional Bose gas feature a phase transition to a superfluid state. We investigate how the phase transition temperature changes as a function of the spatial extent of the transverse dimension, which is confined in a potential well with periodic boundary conditions. For these calculations we employ Functional Renormalization Group equations. Further, we relate the 3D and 2D s-wave scattering lengths and show how the lower-dimensional system inherits its properties from the higher-dimensional system during the renormalization group flow. In these calculations we introduce the crossover function, which is of central importance in the dimensional crossover. We also investigate other compactifications. We calculate the crossover function for a box confinement and introduce approximate flow equations for a confinement in a harmonic trap.

Contents

1 Introduction **9**

2 Basics of ultracold quantum gases **13**
2.1 Statistical Physics . . . 13
2.2 Ideal 3D Bose gas . . . 15
2.3 Interacting 3D Bose gas . . . 20
2.4 2D Bose gas . . . 22

3 Functional Renormalization **27**
3.1 The effective action . . . 27
3.2 Derivation of the Wetterich equation . . . 30
3.3 Properties of the Wetterich equation . . . 33

4 Dimensional Crossover of nonrelativistic bosons **37**
4.1 Main concepts of ultracold gases with FRG . . . 38
4.1.1 The special role of the effective potential . . . 38
4.1.2 Microscopic model . . . 41
4.1.3 Ansatz for the effective average action . . . 42
4.1.4 Initial conditions . . . 44
4.2 A game of scales: Introduction of trap size L . . . 47
4.3 Flow equations . . . 50
4.4 Superfluid transition . . . 55
4.5 2D limit . . . 62
4.5.1 Effective 2D coupling constant . . . 62
4.5.2 True 2D gas . . . 69
4.6 Dimensional crossover for fixed a_{2D} . . . 71
4.7 Anisotropic derivative expansion . . . 73
4.8 Non-homogeneous ground states . . . 75
4.8.1 Crossover function in a box . . . 76
4.8.2 Approximate flow equations in a harmonic trap . . . 79

5 Discussion & Outlook **87**

A Flow equations **93**
A.1 Isotropic derivative expansion 93
A.1.1 Flow of the effective potential 93
A.1.2 Flow equations for kinetic coefficients 101
A.2 Anisotropic derivative expansion 108

List of Figures **113**

Bibliography **115**

CHAPTER 1

Introduction

In this thesis we investigate the properties of a gas of ultracold bosons when one spatial dimension is confined by a trap. The history of quantum effects in ultracold gases goes back to the theoretical description of a Bose–Einstein condensate (BEC) in a three-dimensional gas by Bose and Einstein in 1924 (Einstein (1924, 1925); Bose (1924)). This purely quantum mechanical effect was then observed in laboratories in 1995, 70 years after its theoretical description, by Anderson et al. (1995); Bradley et al. (1995); Davis et al. (1995). In order to achieve this, the atoms had to be cooled down to a few μK or below.

The first observation of a BEC was followed by an enormous progress in experimental techniques, see for example Refs. (Pitaevskii and Stringari (2003); Bloch et al. (2008); Pethick and Smith (2002)). Notably, it has become feasible to change the dimensionalities of the system by using strongly anisotropic external potentials (Lewenstein et al. (2006)). At low temperatures the complicated interaction potential between the atoms can be replaced by a simple contact potential and the interactions are sufficiently described by the s-wave scattering length a. This interaction can be tuned with magnetic fields with the help of Feshbach resonances and controlled and measured in experiments with high precision.

Due to the recent progress in trapping ultracold quantum gases it was possible to observe the unusual features of two-dimensional Bose gases. In contrast to a three-dimensional system there is no phase transition that results in the emergence of a condensate, but rather the system develops a superfluid density at low temperatures due to the Berezinskii–Kosterlitz–Thouless mechanism. The corresponding algebraically correlated superfluid has been observed for both bosons (Hadzibabic et al. (2006); Cladé et al. (2009); Tung et al. (2010); Plisson et al. (2011); Desbuquois et al. (2012); Fletcher et al. (2015)) and fermion pairs (Ries et al. (2015); Murthy et al. (2015)).

In general, lower-dimensional systems exhibit unusual features due to the pronounced influence of fluctuations. It is fascinating how these complex macroscopic properties emerge from a quite simple Hamiltonian that describes the underlying microscopic physics of ultracold quantum gases. The system of cold gases is not only attractive because of its own properties, moreover they might help to understand com-

pelling materials like high-temperature superconductors or graphene in the spirit of cold gases as quantum simulators (Feynman (1982)).

In experiments with ultracold atoms in reduced dimensionality the final laboratory setup might still have an influence of the three-dimensional system, because the degree of anisotropy of the trap might be insufficient to be a truly two-dimensional gas. Therefore, the aim of this thesis is to shed light on systems which are in a dimensional crossover without a well-defined dimensionality.

We employ the Functional Renormalization Group approach, which is based on a quantum field theoretical description of the Bose gas (Wetterich (1993)). This method allows us to calculate the properties of a Bose gas in two and three dimensions and in the dimensional crossover in a unified way. We deduce the physics governing the many-body system at macroscopic scales from the rather simple microscopic laws by the successive inclusion of fluctuations. This is done by using an exact flow equation for the effective average action (Wetterich (1993)), which connects effective theories valid at different scales.

The three- and two-dimensional Bose gases have been investigated with the functional renormalization group in Refs. (Wetterich (2008); Floerchinger and Wetterich (2008, 2009b)). We employ this successful ansatz to describe a Bose gas whose transverse spatial dimension is confined via a trapping potential. The results of this thesis will help to answer the question on how to disentangle the influence of dimensionality effects from other aspects.

The thesis is organized as follows. In Ch. 2 we introduce the basic properties of ultracold bosonic gases. In particular, we review the ideal Bose gas in three dimensions, which undergoes a phase transition to a Bose–Einstein condensate. We proceed by explaining why we can define interactions in these systems by a simple s-wave scattering length a. Next we demonstrate that the argument for a Bose–Einstein condensate does not hold in a two-dimensional ideal homogeneous Bose gas. Nonetheless, it undergoes a phase transition to a superfluid state due to the Berezinskii–Kosterlitz–Thouless mechanism, which we will briefly describe.

In Ch. 3 we review the Functional Renormalization Group approach. We introduce important concepts in quantum field theory and define the effective average action, which is the key object in this approach. We show how to derive the Wetterich equation and discuss some properties of the approach such as regulator choice, truncations and error control.

We apply the method of functional renormalization to a Bose gas in Ch. 4. In particular, we introduce the effective potential, which is the key object to distinguish between the normal and the superfluid phase. We discuss the microscopic action for nonrelativistic Bose gases with pointlike interactions and show how this translates to a good ansatz for the effective average action. Next, we introduce the compactification length L in Sec. 4.2 and present our results in the following sections. First, we compute the superfluid transition temperature for all confinement lengths in a box with periodic boundary conditions. Further, when the confinement is very pronounced, we can effectively describe the system as a two-dimensional one and we elaborate how the

two-dimensional gas inherits its properties from the three-dimensional one. We proceed by discussing further properties of the Bose gas in a box with periodic boundary conditions and compare and benchmark results to T-matrix calculations. In Sec. 4.8.1 we calculate the crossover function for a Bose gas confined in a box potential with infinitely high walls and in the last section we introduce an approximate flow equation for the effective potential to describe a Bose gas in a harmonic trap.

We complete the thesis with a discussion in Ch. 5. The appendix gives a detailed derivation of flow equations for the isotropic and anisotropic derivative expansion. A significant part of this work has been published in

- *Dimensional crossover of nonrelativistic bosons*
  with I. Boettcher and C. Wetterich
  Physical Review A **93**, 063631 (2016)

CHAPTER 2

Basics of ultracold quantum gases

This chapter serves as a short introduction into the physics of ultracold bosonic quantum gases. There are uncountably many good reviews and lecture notes, which cover the topics on statistical physics and quantum many-body systems in great detail. If one wants to learn more on this fascinating topic, see for example Ref. (Tong (2012)) for an introduction to statistical physics, Refs. (Pethick and Smith (2002); Pitaevskii and Stringari (2003)) for Bose–Einstein condensation, Refs. (Hadzibabic and Dalibard (2011); Altland and Simons (2010)) for two-dimensional Bose gases and topological phase transitions, Ref. (Bloch et al. (2008)) for a review on many-body physics with ultracold gases and Ref. (Boettcher et al. (2012)) for a review on ultracold gases within the method of functional renormalization group.

Everyday experience tells us that gases are most commonly confined in three-dimensional boxes, like rooms, the refrigerator or the atmosphere. Thus, we start with a basic description of statistical physics in Sec. 2.1 and always keep the intuitive picture of a three-dimensional gas in mind. Then we present the key physical properties of an ideal three-dimensional Bose gas in Sec. 2.2 and evaluate in Sec. 2.3 the key concepts of an interacting Bose gas. In Sec. 2.4 we discuss two-dimensional gases, which is not only of theoretical importance, but further also crucial in order to comprehend technologically interesting materials like graphene. These inherit their fascinating properties at least partially due to reduced dimensionality.

2.1 Statistical Physics

If we want to describe a gas of bosons, or any kind of particles for that matter, we need to employ the tools of statistical physics. This becomes clear by everyday observations such as the following: After four or five hot summer days in Heidelberg even the toughest theoretical physicist stops calculating the Schrödinger equation for 10^{23} particles, which is the typical number of particles in a box, and starts to think about ways to reduce the temperature in the room he is in.

However, it does not make sense to talk about the temperature of one particle, because temperature is an emergent quantity. This means that it is not included in the

underlying equations, which govern the microscopic physics, but is only a feature of a large bundle of particles. In this thesis we also deal with phase transitions, which is another emergent effect and which means that the whole gas changes its characteristics abruptly when temperature is reduced.

The physical quantities that we are interested in, like entropy, temperature or pressure, are encoded in the so called partition function. Consider a system with a fixed energy E. Because of the large number of particles, it is hopeless to solve the Schrödinger equation, but since a realistic system is always to some amount in contact with its surroundings, we can argue, that due to perturbations the system actually keeps on changing the microstate it is in (that is one particular energy eigenstate to the Schrödinger equation). The fundamental assumption that we make is that for an isolated system in equilibrium, all microstates that are accessible to the system are equally likely. With this, we switch to a statistical description of the system, in which each state n comes with a probability $p(n)$ that the system is in this particular state.

In the system under consideration we find

$$p(n) = \frac{1}{\Omega(E)}, \tag{2.1}$$

where $\Omega(E)$ is the number of states with energy E and therefore the number of accessible states. This probability distribution $p(n)$ is called the microcanonical ensemble. From this we find all relevant and interesting properties of the system, like the entropy S

$$S(E) = k_\mathrm{B} \log \Omega(E) \tag{2.2}$$

with Boltzmann constant k_B or the temperature T

$$\frac{1}{T} = \frac{\partial S}{\partial E}. \tag{2.3}$$

In a more realistic scenario, however, we fix the temperature T, and we deduce the average energy from this. We say that the system is in a heat bath, which keeps the temperature constant. One can show that the probability distribution in this case is given by the so called canonical ensemble (for details see Ref. (Tong (2012)))

$$p(n) = \frac{e^{-E_n/k_\mathrm{B}T}}{\sum_m e^{-E_m/k_\mathrm{B}T}}, \tag{2.4}$$

where we have introduced the inverse temperature

$$\beta = \frac{1}{k_\mathrm{B}T}. \tag{2.5}$$

The sum over all microstates in the denominator is called the partition function Z_can, and surprisingly it actually contains all the relevant information about the system. For example, the average energy is found to be

$$\begin{aligned}\langle E\rangle &= \sum_n p(n)E_n = \sum_n \frac{E_n e^{-\beta E_n}}{Z_{\text{can}}} \\ &= -\frac{\partial}{\partial\beta}\log Z_{\text{can}}\end{aligned} \tag{2.6}$$

We can make one more generalization by allowing the system to exchange particles with its surroundings and we fix the average particle number by choosing a certain chemical potential μ. This leads to the grand canonical partition function

$$Z_{\text{grc}} = \sum_n e^{E_n - \mu N_n}. \tag{2.7}$$

The average particle number $\langle N\rangle$ is now given by

$$\langle N\rangle = \frac{1}{\beta}\frac{\partial}{\partial\mu}\log Z_{\text{grc}}. \tag{2.8}$$

In the following we work in the thermodynamic limit $(N, V) \to \infty$, such that the density $n = N/V$ stays fixed. In this limit the fluctuations around the average value (for example the average energy or particle number) scale with $\sqrt{N}$, so that for gases with $N = 10^{23}$ we can safely neglect these fluctuations and just talk about *the* particle number $N = \langle N\rangle$.

2.2 Ideal 3D Bose gas

In this section we apply the tools of statistical physics to an ideal Bose gas, i.e. to a system of noninteracting bosons. Of course, in real systems there is always some level of interaction. However, it is a very simple and instructive example of a system, where a Bose–Einstein condensation emerges. It was first examined in Ref. (Einstein (1925)).

To understand at which temperatures the quantum nature of the particles comes into play, we can look at the scales governing the system. We consider a gas of N bosons, which is trapped in a box with side lengths L and volume $V = L^3$. This sets the average distance between particles to

$$l = n^{-1/3}. \tag{2.9}$$

If we think of the quantum particles as little wavepackets, then we can assign them a spatial extent of the order of

$$\lambda_T = \sqrt{\frac{2\pi\hbar^2}{M k_{\text{B}} T}}, \tag{2.10}$$

with $\hbar$ being the reduced Planck constant and M the mass of the particles. This is known as the thermal de Broglie wavelength, which corresponds to the de Broglie wavelength $\lambda = h/p$ of a particle with kinetic energy $\pi k_{\text{B}} T$, i.e. a typical energy of a particle in a heat bath of temperature T. Quantum effects should come into play when

the wavepackets start to overlap, that is, when the thermal wavelength is comparable to the interparticle distance. This yields

$$\begin{aligned} n^{-1/3} = l \sim \lambda_T &= \sqrt{\frac{2\pi\hbar^2}{Mk_{\mathrm{B}}T}} \\ \Rightarrow T_{\mathrm{c}} &\approx \frac{4\pi\hbar^2}{2Mk_{\mathrm{B}}} n^{2/3} = 4\pi n^{2/3}, \end{aligned} \tag{2.11}$$

where in the last equality we made use of our conventions $\hbar = k_{\mathrm{B}} = 2M = 1$.

The conceptual difference to a classical gas is that the bosons are identical particles with integer spin which are indistinguishable from one another. For bosons, the wavefunction must be symmetric under the exchange of two particles,

$$\phi(\vec{x}_1, \vec{x}_2) = \phi(\vec{x}_2, \vec{x}_1), \tag{2.12}$$

which reduces the number of accessible states (as compared to a classical gas) and therefore leads to major differences at low temperatures.

We calculate the grand canonical partition function Z_{grc} for the Bose gas under consideration. Since we are dealing with noninteracting particles, we can use the single particle energy states to label the possible states of the system and then, in addition, we state how many particles are in each single particle state. This is sufficient since the particles are indistinguishable. Furthermore, since we deal with bosons, there is no restriction on the number of particles in one state. In this manner, we arrive at a simple way to calculate the partition function

$$Z_{\mathrm{grc}} = \sum_{n_i=0}^{\infty} e^{\sum_i -\beta(\epsilon_i - \mu)n_i}, \tag{2.13}$$

which, when written in the form

$$Z_{\mathrm{grc}} = \prod_i \sum_{n_i=0}^{\infty} e^{-\beta(\epsilon_i - \mu)n_i}, \tag{2.14}$$

can be thought of as the product of i independent partition functions for each single particle state. The geometric sum is easily calculated and we arrive at

$$Z_{\mathrm{grc}} = \prod_i \frac{1}{1 - e^{-\beta(\epsilon_i - \mu)}}. \tag{2.15}$$

The average number of particles N turns out to be

$$\begin{aligned} N &= \frac{1}{\beta}\frac{\partial}{\partial\mu} \log Z \\ &= \frac{1}{\beta}\frac{\partial}{\partial\mu} \sum_i \log \frac{1}{1 - e^{-\beta(\epsilon_i - \mu)}} \\ &= \sum_i \frac{1}{e^{\beta(\epsilon_i - \mu)} - 1}. \end{aligned} \tag{2.16}$$

For a given particle number N we need to invert this equation to find the corresponding value of the chemical potential μ. From this equation we can directly deduce the average number of particles in the state i, since

$$N = \sum_i n_i, \tag{2.17}$$

we have

$$n_i = \frac{1}{e^{\beta(\epsilon_i - \mu)} - 1}. \tag{2.18}$$

This is the Bose–Einstein distribution.

For non-relativistic bosons we have

$$\epsilon_i = \frac{\hbar^2 k_i^2}{2M}, \tag{2.19}$$

while for periodic boundary conditions the wavevector k_i is quantized as

$$k_i = \frac{2\pi}{L} n_i = \Delta k \cdot n_i,\ i = \{x, y, z\} \text{ and } n_i \in \mathbb{Z}. \tag{2.20}$$

The lowest energy in the system is $\epsilon_0 = 0$, from which we can deduce that

$$\mu < 0, \tag{2.21}$$

because otherwise we would have negative occupation numbers for states with $\epsilon_i - \mu < 0$, which is clearly unphysical.

Since in the end we consider the thermodynamic limit, which means that the box has a macroscopic volume, it looks like a reasonable approximation if the sum over all states i is replaced by an integral over the momentum states via

$$\sum_i \to \frac{1}{(\Delta k)^3} \int \mathrm{d}^3 k = \frac{4\pi V}{(2\pi)^3} \int_0^\infty \mathrm{d}k\, k^2, \tag{2.22}$$

where in the last equation we have already performed the angular integration, which gives us a factor of 4π. We make a change of integration variable to

$$E = \frac{\hbar^2 k^2}{2M}, \tag{2.23}$$

such that the summation is approximated by

$$\frac{4\pi V}{(2\pi)^3} \int_0^\infty \mathrm{d}k\, k^2 = \frac{V}{2\pi^2} \int_0^\infty \mathrm{d}E \sqrt{\frac{2ME}{\hbar^2}} \frac{M}{\hbar^2}. \tag{2.24}$$

Now we can introduce the density of states

$$g(E) = \frac{V}{4\pi^2} \left(\frac{2M}{\hbar^2}\right)^{3/2} E^{1/2}, \tag{2.25}$$

which tells us how many states there are within an energy interval $[E, E + \delta E]$. We write the (average) number of particles in a Bose gas as

$$N = \int \mathrm{d}E \frac{g(E)}{e^{\beta(E-\mu)} - 1}. \tag{2.26}$$

By introducing

$$\begin{aligned} z &= e^{\beta\mu}, \\ g_{3/2}(z) &= \frac{2}{\sqrt{\pi}} \int_0^\infty \mathrm{d}x \frac{x^{1/2}}{z^{-1}e^x - 1}, \end{aligned} \tag{2.27}$$

we can rewrite the particle density $n = N/V$ as

$$n(\mu, T) = \frac{1}{\lambda_T^3} g_{3/2}(z). \tag{2.28}$$

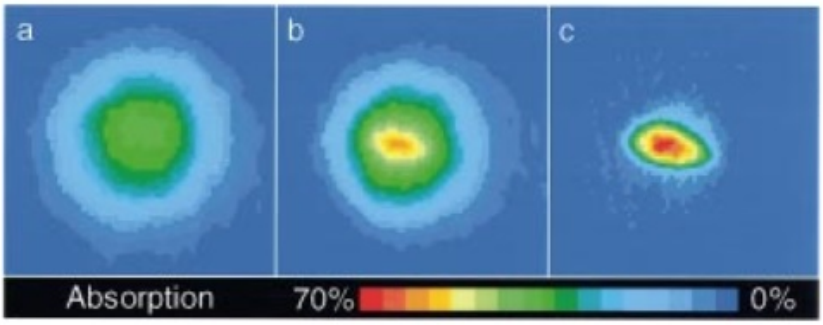

Figure 2.1: One of the very first Bose–Einstein condensations achieved with sodium atoms by Davis et al. (1995). (a) shows the velocity distribution of the normal thermal gas above the critical temperature. In (b) one can see the emergence of a condensate just below an estimated critical temperature of $T_\mathrm{c} \sim 2\mu$K, which is even more pronounced after further evaporative cooling, depicted in (c).

When we decrease the temperature T while keeping the density n fixed, we need to increase the chemical potential and therefore z. But eventually, the chemical potential becomes zero, or equivalently $z = 1$. At this point it seems as if we cannot increase the particle number for a fixed temperature. We can calculate the temperature when this scenario happens. We just have to insert $z = 1$ into Eq. (2.28). With

$$g_{3/2}(1) = \zeta\left(\frac{3}{2}\right), \tag{2.29}$$

where ζ denotes the Riemann zeta function, we obtain

$$\lambda_{T_\mathrm{c}}^3 n = \zeta\left(\frac{3}{2}\right) \approx 2.612 \tag{2.30}$$

or

$$\begin{aligned} T_\mathrm{c} &= \frac{2\pi\hbar^2}{M k_\mathrm{B}} \zeta\left(\frac{3}{2}\right)^{-2/3} n^{2/3} \\ &= \frac{4\pi}{\zeta\left(\frac{3}{2}\right)^{-2/3}} n^{2/3} \approx 6.625 n^{2/3}. \end{aligned} \tag{2.31}$$

Of course, the implication that we can add no more particles at the critical temperature is unphysical. The mistake that we made during this derivation was the substitution of the sum by an integral. Because of the weight $\sqrt{E}$ in the integral, see Eq. (2.25), the zero energy state did not contribute at all. However, as we get closer to T_c and below, z gets very close to one, which results in a macroscopic occupation of the lowest state. Thus, the problem was solved by Einstein and Bose by treating the zero momentum state separately. We denote the number of so-called condensed particles by N_0. By imposing that the total number of particles N is given by the condensed particles N_0 and the excited particles N_ex, where the number of excited particles is given by our integral approximation, we find, together with Eq. (2.31),

$$\frac{N_\mathrm{ex}(T)}{N} = \left(\frac{\lambda_{T_\mathrm{c}}}{\lambda_T}\right)^3 = \left(\frac{T}{T_\mathrm{c}}\right)^{3/2}. \tag{2.32}$$

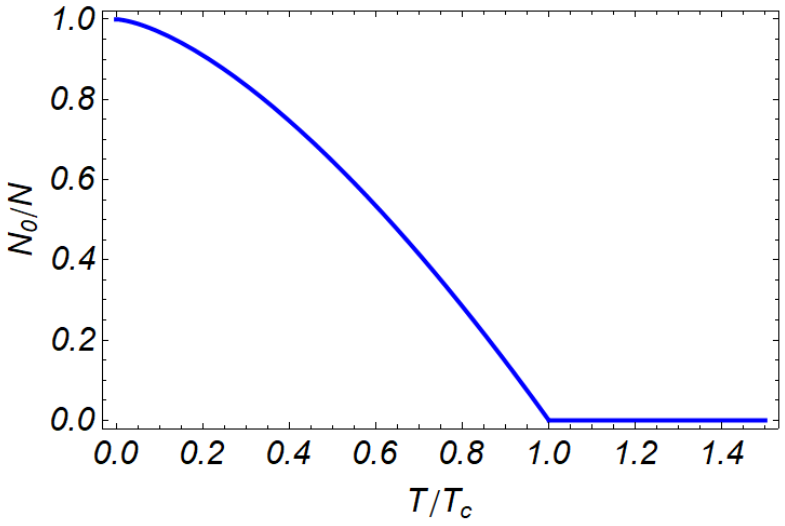

Figure 2.2: Condensate fraction N_0/N as a function of temperature T. Below the critical temperature T_c a Bose–Einstein condensate emerges, where the lowest energy state N_0 is macroscopically occupied, i.e. $N_0 = \mathcal{O}(N)$. For vanishing temperature all particles are in the lowest state, so that the condensate fraction N_0/N is unity. For $T \to T_\mathrm{c}^-$ the condensate vanishes continuously, which is typical for a second order phase transition.

This translates to a condensate fraction given by

$$\frac{N_0(T)}{N} = 1 - \left(\frac{T}{T_c}\right)^{3/2} \quad \text{for } T \leq T_c. \tag{2.33}$$

This macroscopic occupation is known as a Bose–Einstein condensate. We show the condensate fraction as a function of temperature in Fig. 2.2. 70 years after the first theoretical description of a Bose–Einstein condensation, experiments in 1995 with vapors of Rubidium (Anderson et al. (1995)), Sodium (Davis et al. (1995)) and Lithium (Bradley et al. (1995)) showed the first realization of such a condensate. One of the first pictures obtained from a BEC is depicted in Fig. 2.1.

As mentioned in the beginning of this section, an ideal Bose gas is an incomplete model, because it completely neglects interactions. Thus, the following section addresses the changes that occur when the interactions are included.

2.3 Interacting 3D Bose gas

In this section we show how particles interact with each other and how we can approximate the interactions in a simple manner. For this, let us first consider how the interaction potential between neutral atoms looks like. At very short distances, comparable to the size of the atoms, the interaction is strongly repulsive due to the Pauli exclusion principle, which prevents two atoms from occupying the same space. We will show, however, that the precise form of this interaction potential is not relevant for our purposes. For larger separations of the atoms the interaction is governed by an attractive $1/r^6$ force, where r is the distance between the atoms. Its origin are fluctuating dipoles from the atoms, thus again a quantum mechanical reason. To understand how this results in a $1/r^6$ force, suppose that one atom acquires a temporary dipole p_1. This in turn induces an electric field E, which then induces a dipole $p_2 \sim E$ in a nearby atom. Therefore, the resulting so-called van der Waals potential has the form $p_1 p_2/r^3 \sim 1/r^6$, which causes a weak attraction between the atoms.

Often, the repulsive part is modeled by a $1/r^{12}$ term. The corresponding potential $U(r) \sim \left(\frac{r_0}{r}\right)^{12} - \left(\frac{r_0}{r}\right)^6$ is called the Lennard–Jones potential. But it is also possible to include a hard core repulsion instead, which looks like

$$U(r) = \begin{cases} \infty & r \leq r_0 \\ -A\left(\frac{r_0}{r}\right)^6 & r > r_0. \end{cases} \tag{2.34}$$

So which interaction potential should we use? The answer is that it does not matter, because the details of the interaction potential are not important in the system under consideration. When we compare the associated length scale $l_{\mathrm{vdW}} = \left(\frac{M r_0}{\hbar^2}\right)^{1/4}$ to the de Broglie wavelength λ_T, then we find

$$\lambda_T \gg l_{\mathrm{vdW}}. \tag{2.35}$$

Thus, if we think of the atoms as little wavepackets with a spatial extent of λ_T, then they can never resolve the short-range details of the potential. Therefore, we can replace the complicated van der Waals potential with a simple short-range potential, which nevertheless features the same low-energy physics. The interaction between two atoms can be described by the behavior of the relative wave function before and after the scattering event. We may write it as an incoming plane wave and a scattered wave

$$\psi_k(r) = e^{ikz} + \psi_{\text{sc}}. \tag{2.36}$$

For large separations the scattered wave is a spherical wave

$$\psi_{\text{sc}}(r) = f_k(\theta, \varphi)\frac{e^{ikr}}{r}, \tag{2.37}$$

where we introduced the scattering amplitude $f_k(\theta, \varphi)$. Since our interaction potential only depends on the distance, the scattering amplitude is independent of φ. Furthermore, we can expand the scattering amplitude in Legendre polynomials P_l, such that it is described as a sum over partial wave scattering amplitudes, each associated with a different relative angular momentum. Since we deal with low collision energies $E \ll \frac{\hbar^2}{M l_{\text{vdW}}^2}$, scattering with nonvanishing relative angular momenta is not allowed and only s-wave scattering occurs. Actually, the scattering process is then completely determined by the scattering length a, which in turn defines the now constant scattering amplitude

$$f = -a. \tag{2.38}$$

So as long as the interaction potential reproduces the same s-wave scattering length a, we are free to choose a simpler potential than the van der Waals potential. In particular, we choose a pointlike contact potential

$$V(r) = \lambda\delta(r) \tag{2.39}$$

with coupling constant λ. We can use the Born approximation to determine the scattering amplitude from the potential via

$$f(\theta) = -\frac{m_r}{2\pi\hbar^2}\int \mathrm{d}^3x e^{-i\vec{q}\vec{x}}V(\vec{x}), \tag{2.40}$$

where $m_r = M/2$ is the reduced mass. For the contact potential this yields

$$a = \frac{M}{4\pi\hbar^2}\lambda. \tag{2.41}$$

Later in Ch. 4.1.4 we use this relation to find the correct initial condition for the ultraviolet coupling constant.

The scattering length a can be changed in experiments with the help of so called Feshbach resonances in a very controlled manner.

2.4 2D Bose gas

In this section we focus on a two-dimensional system and as before we calculate the average particle number to see if the argument for Bose–Einstein condensation still holds. The average number of particles can be written as

$$\begin{aligned} N &= \frac{1}{(\Delta k)^2} \int \mathrm{d}^2 k \frac{1}{e^{\beta(\epsilon_i - \mu)} - 1} \\ &= \frac{V_{2\mathrm{D}}}{2\pi} \int \mathrm{d}k \frac{k}{e^{\beta(\frac{\hbar^2 k^2}{2M} - \mu)} - 1}, \end{aligned} \tag{2.42}$$

where $V_{2\mathrm{D}} = L^2$ is the two-dimensional volume. With $x = \beta\hbar^2 k^2/(2M)$ we find

$$N = \left(\frac{V_{2\mathrm{D}}}{\lambda_T}\right)^2 \int \mathrm{d}x \frac{1}{z^{-1}e^x - 1}. \tag{2.43}$$

We can solve the integral and introduce the two-dimensional particle density $n = N/V_{2\mathrm{D}}$ to obtain

$$n\lambda_T^2 = -\log\left(1 - e^{\beta\mu}\right). \tag{2.44}$$

Thus, in two dimensions, we can always find a suitable chemical potential μ for any value of $n\lambda_T^2$ and therefore we do not find a condensate in a homogeneous ideal two-dimensional Bose gas.

In the language of correlation functions, for a condensate to appear we need the first-order correlation function

$$g_1(r) = \langle \varphi^*(\vec{r})\, \varphi(0) \rangle \tag{2.45}$$

to approach a constant in the limit $r \to \infty$, which is then called long-range order. The correlation function $g_1(r)$ characterizes the correlations of the complex Bose field $\varphi(\vec{x})$ for two points of distance r (we only consider homogeneous gases, so that the correlations only depend on the relative distance). In contrast to a condensate, where even for infinitely large separations between two points spatial coherence is still present, the correlations of a thermal classical gas decay exponentially, i.e. $g_1(r) \sim e^{-r/\lambda_T}$ for $r \to \infty$ and λ_T denoting the thermal de Broglie wavelength.

The Mermin–Wagner theorem (Mermin and Wagner (1966); Hohenberg (1967)) states that a continuous symmetry cannot be spontaneously broken in two or less dimensions at any finite temperature (see Ch. 4.1.1 where we describe the phase transition to a Bose–Einstein condensate in terms of the spontaneous breaking of the $U(1)$ symmetry of the effective potential). What we have shown above, that there is no condensate present in two dimensions, is therefore a special case of the more general Mermin–Wagner theorem. We can write this as $g_1(r) \to 0$ for $r \to \infty$.

However, a two-dimensional system can still undergo a phase transition to a superfluid state for low enough temperatures. This phase features so-called quasi-long-range order, which means that the first-order correlation function $g_1(r)$ decays algebraically,

i.e. $g_1(r) = r^{-\eta}$ for $r \to \infty$. The exponent η is at most $1/4$, which is quite small and thus leads only to a slow decay of correlations. This superfluid state is often called a "quasi-condensate", which refers to a condensate with a fluctuating phase (Kagan et al. (1987); Popov (1988)). In the language of the complex bosonic field, we approximate $\varphi(\vec{r}) = \sqrt{\rho}e^{\theta(\vec{r})}$, i.e. we have a superfluid density ρ with no fluctuations, and a fluctuating phase $\theta(\vec{r})$, which still possesses correlations.

The mechanism behind the so-called Berezinskii-Kosterlitz-Thouless (BKT) phase transition (Berezinskii (1971, 1972); Kosterlitz and Thouless (1973); Kosterlitz (1974)) is of a topological nature: In the low temperature phase the superfluid contains pairs of quantized vortices of opposite rotation. When the temperature is increased, at some point the vortices can proliferate and destroy the quasi-long-range order. We can understand how vortices drive the phase transition with a simple thermodynamic argument. For a more detailed discussion, see Refs. (Hadzibabic and Dalibard (2011); Pethick and Smith (2002); Altland and Simons (2010)).

Consider again a bosonic field $\varphi = \sqrt{\rho}e^{\mathrm{i}\theta}$, where we only allow for phase fluctuations. Suppose now, that we move through this field while keeping track of the phase $\theta(\vec{x})$. Of course, when we come back to the starting point, the bosonic field needs to have the same value as in the beginning. Vortices are field configurations where θ changes by a multiple of 2π, i.e.

$$\oint \mathrm{d}\theta = \oint \vec{\nabla}\theta(\vec{x})\mathrm{d}\vec{l} = 2\pi n, \tag{2.46}$$

where n is an integer. These vortex configurations can not be continuously deformed to a zero-vortex configuration and we need to take these possible excitations additionally into account. One possible phase configuration of such an $n = 1$ vortex is depicted in Fig. 2.3.

The energy associated with the creation of a single vortex is given by

$$E = \int \mathrm{d}^2x\varphi^* \left(-\frac{\hbar^2\nabla^2}{2M}\right)\varphi. \tag{2.47}$$

With $\varphi(\vec{x}) = \sqrt{\rho}e^{\mathrm{i}\theta(\vec{x})}$ we find

$$E = \int \mathrm{d}^2x\rho\frac{\hbar^2}{2M}\left(\vec{\nabla}\theta\right)^2. \tag{2.48}$$

For a vortex sitting at the origin we can approximate the energy by evaluating Eq. (2.46) for a circle of radius r to

$$2\pi n \stackrel{!}{=} 2\pi r|\vec{\nabla}\theta| \tag{2.49}$$

and thus for $n = 1$ we have

$$|\vec{\nabla}\theta| = \frac{1}{r}. \tag{2.50}$$

We can estimate the energy to

$$E = \frac{\rho\hbar^2}{2M}\int \mathrm{d}^2x\frac{1}{r^2} = \frac{\rho\hbar^2}{2M}2\pi\int \mathrm{d}r\frac{1}{r} = \frac{\rho\hbar^2\pi}{M}\log\left(\frac{L}{\xi}\right), \tag{2.51}$$

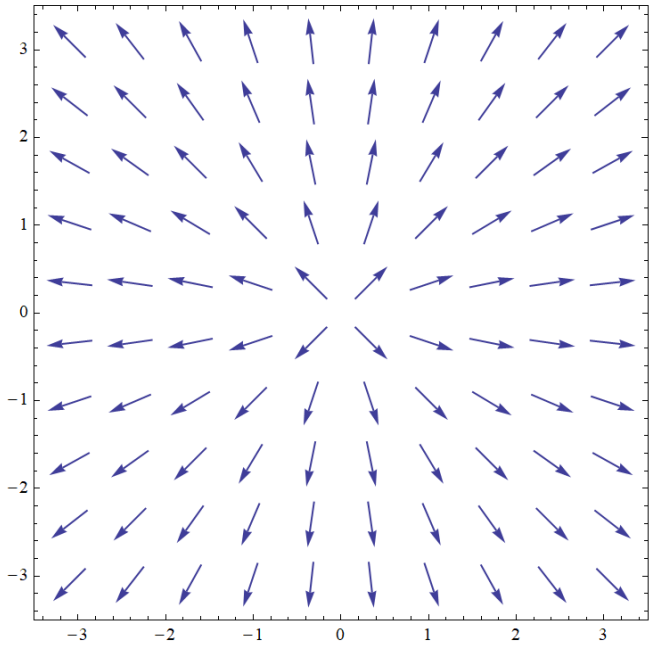

Figure 2.3: The phase of the Bose field in presence of a possible vortex configuration for $n = 1$. If we consider a path that circulates once around the origin, the phase picks up an additional value of 2π. These configurations cannot be continuously deformed to a uniform $n = 0$ solution. Below the critical temperature T_{BKT} vortices only appear as tightly bound vortex-antivortex pairs, who proliferate at the critical temperature and destroy the superfluid.

where ξ is the size of the vortex and L the size of the system. Thus, in the thermodynamic limit $L \to \infty$, the energy diverges logarithmically.

Further, there are L^2/ξ^2 places to put a vortex of size ξ^2 into the plane of size L^2. Thus, the entropy S evaluates to

$$S = k_{\mathrm{B}} \log\left(\frac{L^2}{\xi^2}\right) = 2k_{\mathrm{B}} \log\left(\frac{L}{\xi}\right). \tag{2.52}$$

The free energy F associated with a single vortex is therefore given by

$$\begin{aligned} F &= E - TS \\ &= \left(\frac{\rho\hbar^2\pi}{M} - 2k_{\mathrm{B}}T\right) \log\left(\frac{L}{\xi}\right). \end{aligned} \tag{2.53}$$

Thus, right at the temperature given by

$$k_{\mathrm{B}}T_{\mathrm{c}} = \rho\frac{\pi\hbar^2}{2M} \tag{2.54}$$

the free energy changes sign: For temperatures lower than T_c the free energy is positive and the energy effects will suppress the creation of (free) vortices. For temperatures higher than T_c the free energy is negative and vortices are favorable. If one repeats the calculation for a vortex-antivortex pair, then what one sees is that these are actually not that energetically suppressed - as long as they are very close together. Therefore, one can think of the phase transition as a proliferation of bound vortex-antivortex pairs as one raises the temperature and the free vortices, then, destroy the quasi-long-range order and the superfluid.

We can rewrite the condition for the critical temperature as

$$\rho\lambda_{T_{\mathrm{BKT}}}^2 = 4. \tag{2.55}$$

In a homogeneous two-dimensional Bose gas the BKT theory predicts that the exponent η is connected to the superfluid density via

$$\eta = \frac{1}{\rho\lambda_T^2}. \tag{2.56}$$

At the critical temperature T_{BKT} the superfluid density undergoes a universal jump from $\rho = 0$ for $T > T_{\mathrm{BKT}}$ to $\rho = \frac{4}{\lambda_T^2}$ for $T = T_{\mathrm{BKT}}^-$, while the critical exponent η behaves like

$$\eta(T) = \begin{cases} \frac{1}{\rho\lambda_T^2} & T \leq T_{\mathrm{BKT}} \\ 1/4 & T = T_{\mathrm{BKT}} \\ 0 & T > T_{\mathrm{BKT}}. \end{cases} \tag{2.57}$$

The relation between the critical temperature and the superfluid density is universal and in particular does not depend on the interaction strength. This does not hold for the total density n, because at the transition one has the critical phase space density (Popov (1983); Fisher and Hohenberg (1988); Holzmann et al. (2007))

$$n\lambda_T^2 = \log(\xi/\tilde{g}), \tag{2.58}$$

where $\tilde{g}$ is the interaction strength and ξ is a constant. Monte Carlo calculations have shown that $\xi = 380$ (Prokof'ev et al. (2001); Prokof'ev and Svistunov (2002)). In Sec. 4.5.2 we calculate a similar quantity ξ_μ with the functional renormalization group.

Thus, in two as well as in three dimensions we find a transition to a superfluid state. Within the framework of functional renormalization group we want to examine the dimensional crossover from two to three dimensions. In the next chapter we discuss the basics of this method.

CHAPTER 3

Functional Renormalization

This chapter serves as a short introduction to the method of functional renormalization group (FRG). We use this method to deduce the large scale macroscopic physics of the ultracold quantum gas from its rather simple microscopic laws. For this, we briefly recall some concepts of quantum field theory and, in particular, introduce the effective action. Then we derive the Wetterich equation and discuss its properties. The derivation follows the scheme presented in Refs. (Gies (2012)) and (Boettcher et al. (2012)).

3.1 The effective action

For a single scalar quantum field $\varphi(X)$ the n-point correlation function is defined as

$$\langle \varphi(X_1) \cdots \varphi(X_n) \rangle = N \int \mathcal{D}\varphi \varphi(X_1) \cdots \varphi(X_n) e^{-S[\varphi]}, \tag{3.1}$$

where $N = (\int \mathcal{D}\varphi e^{-S[\varphi]})^{-1}$ denotes the normalization factor and S is the microscopic action of the theory. In the following we will think of φ as a complex scalar field, since this is the proper description for a gas of bosons, but generalizations to fermions and additional fields are straightforward.

From this set of n-point correlation functions we can extract all the desired information about the system: The 2-point correlation function, for example, determines the propagation of a particle, whereas n-point correlation functions can be used for scattering experiments with two incoming and $(n-2)$ outgoing particles.

Since a quantum field theory is fully described by this set of correlation functions, one could say that quantum field theory "consists of doing one big integral" (Zee (2010)), which is

$$Z[J] = \int \mathcal{D}\varphi e^{-S[\varphi] + \int J \cdot \varphi}. \tag{3.2}$$

Suppose we know an exact solution to the generating functional $Z[J]$. Then we can recover the correlation functions by a suitable number of functional derivatives with respect to the source J, followed by setting the source to zero,

$$\langle\varphi(X_1)\cdots\varphi(X_n)\rangle = \frac{1}{Z\,[0]}\frac{\delta^n Z\,[J]}{\delta J(X_1)\cdots\delta J(X_n)}\bigg|_{J=0}. \tag{3.3}$$

However, for most physical systems it is impossible to solve the integral exactly. Therefore we have to rely on truncations, one example being an expansion in a small parameter, e.g. a coupling constant. However, we want to use a genuinely nonperturbative approach.

From the generating functional $Z[J]$ we can define the Schwinger functional

$$W[J] = \log Z[J], \tag{3.4}$$

which is the generating functional of the connected n-point correlation functions, or Green's functions. The expectation value of $\varphi(X)$ is given by

$$\langle\varphi(X)\rangle_J = \frac{1}{Z\,[J]}\frac{\delta Z\,[J]}{\delta J(X)} = \frac{\delta W\,[J]}{\delta J(X)} \tag{3.5}$$

and can be understood as a classical field, where the quantum fluctuations are already included. In our Bose gas system $\phi(X) \equiv \langle\varphi(X)\rangle$ is the field that describes the condensate, see Ch. 4.1, where we discuss this in detail.

By taking a second functional derivative

$$\begin{aligned}\frac{\delta^2 W\,[J]}{\delta J(X)\delta J(Y)} &= \frac{\delta}{\delta J(X)}\left(\frac{1}{Z\,[J]}\frac{\delta Z\,[J]}{\delta J(Y)}\right)\\ &= \frac{1}{Z\,[J]}\frac{\delta^2 Z\,[J]}{\delta J(X)\delta J(Y)} - \left(\frac{1}{Z\,[J]}\frac{\delta Z\,[J]}{\delta J(X)}\right)\left(\frac{1}{Z\,[J]}\frac{\delta Z\,[J]}{\delta J(Y)}\right)\\ &= \langle\varphi(X)\varphi(Y)\rangle_J - \langle\varphi(X)\rangle_J\langle\varphi(Y)\rangle_J\\ &= G(X,Y)\end{aligned} \tag{3.6}$$

we obtain the propagator.

Instead of the Schwinger functional, which is a function of the source J, we can also use the effective action $\Gamma[\phi]$, from which we can extract all physical information, too, but which is a functional of the field ϕ and therefore far more intuitive. Looking at Eq. (3.5) we see that $Z[J]$ and $\Gamma[\phi]$ are connected via a Legendre transformation

$$\Gamma\,[\phi] = \sup_J\left(\int_X J(X)\phi(X) - W\,[J]\right). \tag{3.7}$$

The effective action is the quantum analogue to the classical action S, but now with all quantum fluctuations included. Variation with respect to the field

$$\begin{aligned}\frac{\delta\Gamma\left[\phi\right]}{\delta\phi(Y)} &= \frac{\delta}{\delta\phi(Y)}\left(\int_X J(X)\phi(X)\right) - \frac{\delta W\left[J\right]}{\delta\phi(Y)} \\ &= \int_X J(X)\frac{\delta\phi(X)}{\delta\phi(Y)} + \int_X \frac{\delta J(X)}{\delta\phi(Y)}\phi(X) - \frac{\delta W\left[J\right]}{\delta\phi(Y)} \\ &= J(Y) + \int_X \frac{\delta J(X)}{\delta\phi(Y)}\left(\phi(X) - \frac{\delta W\left[J\right]}{\delta J(X)}\right) \\ &= J(Y)\end{aligned} \tag{3.8}$$

gives us the quantum equation of motion. In the derivation we implicitly assumed that the supremum is taken and we will omit the notation in the following. In the last equation we have used Eq. (3.5). The effective action $\Gamma[\phi]$ is the generating functional of one-particle irreducible correlation functions. In particular, $\Gamma^{(2)} = \delta^2\Gamma/(\delta\phi(X)\delta\phi(Y))$ yields the inverse propagator.

For a vanishing source $J = 0$ we see that the ground state minimizes the effective action. Often we are only interested in homogeneous ground states, because if the system, in which the Bose gas is confined in, is homogeneous itself, then this is a reasonable assumption. If we exclude inhomogeneous ground states and evaluate the effective action for a homogeneous solution, then the effective action reduces to an integral over the effective potential. The effective potential $U(\phi)$ is that part of the effective action which does not vanish for a constant solution, i.e.

$$\begin{aligned}\Gamma\left[\phi_0\right] &= \int_X U(\phi)\Big|_{\phi(X)=\phi_0} \\ &= U(\phi_0)\int_X = U(\phi_0)\beta V_{3\mathrm{D}},\end{aligned} \tag{3.9}$$

where $V_{3\mathrm{D}}$ is the three-dimensional spatial volume. In this case the task of finding the ground state reduces to minimizing the effective potential

$$\left.\frac{\partial U}{\partial\phi}\right|_{\phi=\phi_0} = 0. \tag{3.10}$$

For a vanishing source the effective action can also be written as

$$e^{-\Gamma[\phi_0]} = \int \mathcal{D}\varphi e^{-S[\varphi]}, \tag{3.11}$$

which shows us that $\Gamma[\phi_0]$ can be identified with the grand-canonical potential Φ_G via

$$\Gamma[\phi_0] = -\log Z = \beta\Phi_G. \tag{3.12}$$

This implies that the effective potential $U = \Phi_G/V_{3\mathrm{D}}$ can be identified with the pressure of the system via

$$P(\mu, T) = -U(\phi_0, \mu, T). \tag{3.13}$$

This is the equation of state, from which we can calculate thermodynamic properties of the system. For example, the particle density n then evaluates to

$$n\left(\mu,T\right)=-\frac{\partial U}{\partial\mu}(\phi_0,\mu,T). \tag{3.14}$$

These considerations are important for us, because the effective potential is the key object to distinguish the superfluid from the normal phase of the system. In Ch. 4.1.1 we explain the properties of the effective potential in the language of symmetry breaking in more detail. In addition, we use Eq. (3.14) to arrive at a flow equation for the density, see Eq. (4.60).

3.2 Derivation of the Wetterich equation

Our goal is to calculate the effective action Γ. We have seen that it is the quantum analogue to the classical action S, but with all quantum fluctuations already included. From this object we can calculate everything: we get the quantum equation of motion by varying Γ with respect to the fields, we get scattering amplitudes, or we can calculate thermodynamic quantities and relations from the equation of state, see Eq. (3.13).

The effective action Γ, however, is difficult to obtain. The method of functional renormalization group provides an effective tool to calculate Γ, where we do not include the quantum fluctuations all at once, but stepwise. This idea was employed in Kadanoff's renormalization group transformations of block spins (Kadanoff (1966)) and further developed to a continuum version by Wilson (Wilson (1971)).

The method of functional renormalization allows us to interpolate smoothly between the full effective action Γ, which describes the physics at macroscopic scales, and the microscopic action S, which describes the physics of the known microscopic laws. In the following derivation we introduce the effective average action Γ_k, which is the central object in the FRG approach. By introducing a regulator $R_k(Q)$, which decouples the low momentum modes from the high momentum modes, we make the effective average action Γ_k dependent on the scale k. This average action describes the physics at some momentum scale k, where fluctuations with momenta larger than k are already included.

Starting point of our calculations is the classical microscopic action S, which we define to describe the physics at the microscopic ultraviolet scale Λ. The effective average action Γ_k obeys an exact flow equation

$$\partial_t\Gamma_k\left[\phi\right]=\frac{1}{2}\mathrm{STr}\left[\frac{1}{\Gamma_k^{(2)}\left[\phi\right]+R_k}\partial_t R_k\right], \tag{3.15}$$

which was first derived by Wetterich (1993). This equation tells us how the effective average action changes with the scale k. Thus, in the FRG approach, we integrate out one momentum shell after another, until we finally arrive at the full effective action

Γ for $k \to 0$. Therefore the effective average action Γ_k needs to obey the boundary conditions

$$\Gamma_{k\to\Lambda} = S,\ \Gamma_{k\to 0} = \Gamma. \tag{3.16}$$

To derive the flow equation for Γ_k we now modify the generating functional by adding a regulator term ΔS_k

$$Z_k[J] = \int \mathcal{D}\varphi e^{-S[\varphi]-\Delta S_k[\varphi]+\int_X J(X)\varphi(X)}, \tag{3.17}$$

where the regulator term is chosen to be quadratic in the field

$$\Delta S_k[\varphi] = \int_Q \varphi^*(Q) R_k(Q) \varphi(Q). \tag{3.18}$$

Throughout this derivation we think of φ as a complex scalar field, because this is the correct description for the ultracold Bose gases that we consider. R_k is now the regulator or cutoff function, which ensures that we only integrate out momentum modes that are higher than k. The regulator needs to fulfill some constraints on its shape to possess the desired properties. But besides these general constraints the regulator can be chosen quite arbitrarily. We will talk about regulators after the derivation of the flow equation in Sec. 3.3.

We can calculate the derivative of the now scale-dependent Schwinger functional. In the following, we sometimes make use of the dimensionless scale t instead of k, which is defined as $t = \log(k/\Lambda)$. A derivative with respect to t is often described with a dot, i.e.

$$\dot{\Gamma} = \partial_t \Gamma_k = k\partial_k \Gamma_k. \tag{3.19}$$

We find, keeping the source J fixed,

$$\begin{aligned}
\partial_t W_k[J]\Big|_J &= \partial_t \log Z_k[J] \\
&= \frac{1}{Z_k[J]} \int \mathcal{D}\varphi \left(-\partial_t \Delta S_k[\varphi]\right) e^{-S[\varphi]-\Delta S_k[\varphi]+\int_X J\varphi} \\
&= -\frac{1}{2}\int_Q \partial_t R_k(Q) \frac{1}{Z_k[J]} \int \mathcal{D}\varphi \left(\varphi^*(Q)\varphi(Q)\right) e^{-S[\varphi]-\Delta S_k[\varphi]+\int_X J\varphi}.
\end{aligned} \tag{3.20}$$

In the last line the now scale-dependent two-point correlation function appears. With the definition of the full propagator

$$\begin{aligned}
G(X,Y) &= \langle\varphi(X)\varphi(Y)\rangle - \langle\varphi(X)\rangle\langle\varphi(X)\rangle \\
&= \frac{\delta^2 W_k[J]}{\delta J(X)\delta J[Y]},
\end{aligned} \tag{3.21}$$

which is the connected two-point function, we can rewrite the derivative of the Schwinger functional as

$$\begin{aligned}\partial_t W_k[J]\Big|_J &= -\frac{1}{2}\int_Q \partial_t R_k(Q) G_k(Q,Q) - \frac{1}{2}\int_Q \phi^*(Q)\partial_t R_k(Q)\phi(Q) \\ &= -\frac{1}{2}\int_Q \partial_t R_k(Q) G_k(Q,Q) - \partial_t \Delta S_k[\phi]\,.\end{aligned} \tag{3.22}$$

To obtain the effective average action we define a modified Legendre transformation according to

$$\Gamma_k[\phi] = \int_X J(X)\phi(X) - W_k[J] - \Delta S_k[\phi]\,. \tag{3.23}$$

The scale derivative of Γ_k now evaluates to

$$\begin{aligned}\partial_t \Gamma_k[\phi] &= \int_X (\partial_t J)\phi - \partial_t W_k[J]\Big|_J - \int_X \frac{\delta W_k[J]}{\delta J(X)}\partial_t J - \partial_t \Delta S_k[\phi] \\ &= -\partial_t W_k[J]\Big|_J - \partial_t \Delta S_k[\phi]\,,\end{aligned} \tag{3.24}$$

where we have used that J is determined by

$$\phi(X) = \frac{\delta W_k[J]}{\delta J(X)}. \tag{3.25}$$

Inserting (3.22) yields

$$\partial_t \Gamma_k[\phi] = \frac{1}{2}\int_Q \partial_t R_k(Q) G_k(Q,Q). \tag{3.26}$$

We can rewrite this equation to express G in terms of Γ_k. For this we need the equation of motion

$$\frac{\delta \Gamma_k[\phi]}{\delta \phi^*} = J - \frac{\delta}{\delta \phi^*}\Delta S_k = J - R_k \phi. \tag{3.27}$$

A second variation with respect to ϕ and using that G can be expressed as $G_k(Q,Q) = \delta\phi(Q)/\delta J(Q)$ we find

$$\frac{\delta J}{\delta \phi} = \Gamma_k^{(2)}[\phi] + R_k, \tag{3.28}$$

where $\Gamma_k^{(2)} = \delta^2\Gamma_k/(\delta\phi^*\delta\phi)$ is the second functional derivative. This yields

$$\mathbb{1} = \left(\Gamma_k^{(2)}[\phi] + R_k\right)(Q,Q)\cdot G_k(Q,Q). \tag{3.29}$$

With this we obtain the flow equation of the effective average action, the Wetterich equation

$$\partial_t \Gamma_k[\phi] = \frac{1}{2}\int_Q \partial_t R_k(Q)\frac{1}{\Gamma_k^{(2)}[\phi] + R_k}(Q,Q). \tag{3.30}$$

More generally, this can be rewritten as

$$\partial_t \Gamma_k [\phi] = \frac{1}{2} \mathrm{STr} \left[\frac{1}{\Gamma_k^{(2)} [\phi] + R_k} \partial_t R_k \right], \tag{3.31}$$

where the supertrace includes the momentum integration and a summation over field indices. For example, the Bose gas is described by a complex field ϕ, which could be decomposed into two components $\phi = \frac{1}{\sqrt{2}}(\phi_1 + \mathrm{i}\phi_2)$. The supertrace then includes the summation over the internal index $i = (1, 2)$. Next we discuss the properties of the Wetterich equation.

3.3 Properties of the Wetterich equation

First of all, no approximations have been used in the derivation of the flow equation, therefore the Wetterich equation is an exact equation and solving it is equivalent to solving, for example, the path integral. Its simple one-loop structure is an advantage to perturbation theory, where higher order loops have to be taken into account. Further, it is a nonperturbative approach, which does not rely on the existence of a small perturbation parameter.

We still have to specify how the regulator $R_k(Q)$ actually looks like. For the function $R_k(Q)$ to behave like a regulator it needs to fulfill some conditions, specified below, such that the effective average action is actually interpolating between the microscopic action and the full quantum action. First of all, the regulator needs to regulate the infrared modes, i.e. it needs to suppress momenta q that are lower than the sliding scale k. This ensures that infrared singularities do not pop up, because essentially the regulator adds a mass-like term $\sim k^2$ in the propagator. This means the regulator needs to fulfill

$$\lim_{q^2/k^2 \to 0} R_k(Q) > 0. \tag{3.32}$$

The next constraint ensures that for $k \to 0$ we obtain the full effective action $\Gamma = \Gamma_{k \to 0}$, such that all fluctuations are included for $k \to 0$. We ensure this by choosing a regulator which vanishes in the infrared, so that for $k \to 0$ no fluctuations are suppressed anymore,

$$\lim_{k^2/q^2 \to 0} R_k(Q) = 0. \tag{3.33}$$

On the other end of the scale, as we approach the ultraviolet limit $k \to \Lambda$, we want to reproduce the microscopic action S. Thus, the regulator needs to suppress all fluctuations. This translates to

$$\lim_{k = \Lambda \to \infty} R_k(Q) \to \infty. \tag{3.34}$$

Note, however, that we can treat the microscopic action itself as an effective theory, with fluctuations above Λ already integrated out.

Besides these general constraints the regulator can be chosen arbitrarily. The behavior of the effective average action during the flow is depicted in Fig. 3.1. The effective

average action traces out a line in theory space, which is a space spanned by all possible couplings. Even if particular couplings are not present in the microscopic action, quantum fluctuations might generate them during the flow. We see how Γ_k connects the microscopic action S in the UV with the full effective action Γ in the IR. But the particular way how Γ_k reaches Γ depends on the choice of regulator. As long as we ensure the properties of a regulator above we can be sure that for $k \to 0$ the full effective action Γ is reached. This freedom in the choice of a regulator also gives us the option to choose one which best suits our particular physical problem.

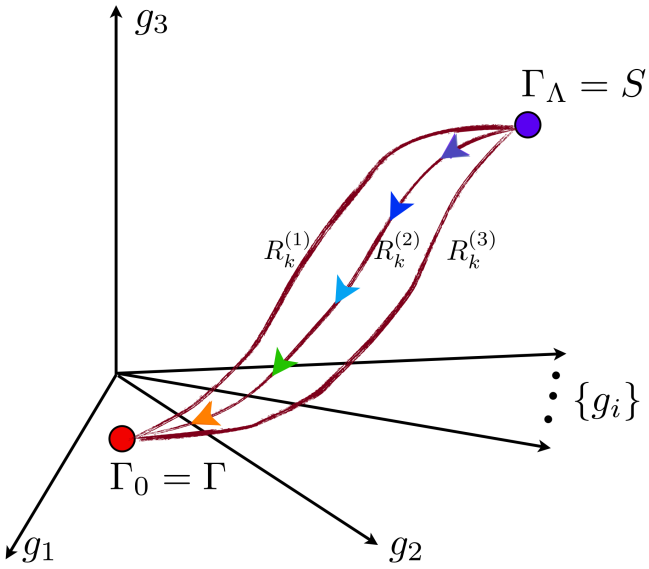

Figure 3.1: The theory space is spanned by all possible flowing couplings $\{g_i\}$ of the theory. The effective average action Γ_k coincides with the microscopic action S in the ultraviolet and its flow towards the full effective action Γ in the infrared can be represented as a line. We see that in general different regulators lead to different paths in theory space. As long as we do not approximate the flow equations, then eventually the different paths lead to the same effective action. Figure taken from Boettcher et al. (2012).

Note, however, that these considerations only hold in the case where we can solve the Wetterich equation exactly. In general, however, we have to rely on truncations. To understand this, notice that we get the flow equations for n-point functions by taking a suitable number of functional derivatives of the Wetterich equation. For example, the flow for the 2-point function is schematically given by

$$\partial_t \Gamma_k^{(2)}[\phi] = \frac{\delta^2}{\delta\phi^2} \partial_t \Gamma_k[\phi] \,. \tag{3.35}$$

Since the flow of the effective average action depends on the 2-point function, the flow for the 2-point function will depend on the 3- and 4-point functions. This is true for any

nth order flow equation: The flow equation for $\Gamma_k^{(n)}$ contains $(n+1)$- and $(n+2)$-point functions $\Gamma_k^{(n+1)}$ and $\Gamma_k^{(n+2)}$, which means that in this way we get an infinite hierarchy of differential equations. This expansion needs to be truncated at some point to gain a finite number of running couplings. This means that the theory space in Fig. 3.1 is approximated by a subspace with a finite number of dimensions. But if we restrict Γ_k to contain at most correlators of n fields (setting higher correlators to zero), then we do not have a closed set of equations anymore. We have to specify how to project onto the flow equations for the running couplings, and we need to use physical insight to find a good approximation. One can compute observables in different projection prescriptions to test the quality of a certain truncation, see Ref. (Schnoerr et al. (2013)).

In this thesis we use the derivative expansion (Morris (1994a,b)), see Sec. 4.1.3, which is an expansion in powers of derivatives of the field. Moreover, we employ a Taylor expansion in powers of the field in the effective potential. Because the functional renormalization group approach is so intuitive (e.g. the effective average action is a function of the condensate field, and therefore directly connected to physical observables), a small number of cleverly chosen couplings is often enough to capture the relevant physics. In our truncation, we stop the Taylor expansion for the effective potential at the order $\rho^2 = \phi^4$. We will see, that this already leads to good results, qualitatively and quantitatively. Incorporating higher order couplings in the effective potential is another way to improve and also check the current truncation, since more terms should not alter the results in a significant way.

Since we have to rely on truncations, different choices of regulators might yield different effective actions. Thus, the choice of the regulator is not completely arbitrary anymore (this statement only holds for the exact flow equation), but one should use one that fits the physical problem. In particular, one should use a regulator that obeys the symmetries of the system, see Sec. 4.3, because then couplings which would spoil the underlying symmetry are not generated during the flow. One question is, if there is a best choice of regulator for a given truncation, that is, a regulator which brings us closest to the "true" effective action. The answer to this question leads to optimized regulators, see Refs. (Litim (2000, 2001b); Pawlowski (2007)). Since the results depend on the choice of regulator, we obtain another opportunity to check the quality of the truncation by repeating the calculations with a different regulator.

A great advantage of the functional renormalization group approach is that it includes fluctuations only stepwise. This not only ensures that we do not have to deal with infrared singularities, but it also helps to cope with physical problems where a lot of different scales are present. We look at particular momentum scales only one at a time and especially in this thesis the intuitive picture of a flow from one scale to another helps to understand the emergence of two-dimensional physics from three-dimensional physics in strong confining potentials, see Sec. 4.5.1.

To summarize, we find that we need to rely on truncations, because we cannot solve the flow equation exactly. Since the functional renormalization group approach is nonperturbative, it is nontrivial to estimate the magnitude of the errors. However, we have different ways to check and improve our truncation. This method provides an intuitive

approach to physical problems, so that physical insight leads in most cases to relatively simple truncations with a manageable number of running couplings.

Now we have all the tools that we need to apply the method of functional renormalization group to a gas of ultracold bosons. In the next chapter we describe the implementation in detail, derive the flow equations and present the results.

CHAPTER 4

Dimensional Crossover of nonrelativistic bosons

In Ch. 2 we introduced and discussed properties of two- and three-dimensional Bose gases. In particular, we saw that both systems undergo a phase transition to a superfluid state: The three-dimensional system develops a Bose–Einstein condensate for low enough temperatures, whereas the two-dimensional system can be in a superfluid state due to the BKT mechanism. Because of the more pronounced influence of fluctuations, lower dimensional systems exhibit several unusual features, which make them interesting also for cold atom experiments. The final setup of the experiment, however, might still feature aspects of the three-dimensional system, since the preparation of a truly two-dimensional system in a laboratory is very challenging. This motivates us to discuss Bose gases in a system with a finite anisotropy ratio, so that the system is in a dimensional crossover without a well-defined dimensionality.

One of the questions that we want to answer is: What is the residual influence of the finite extension in the third dimension? In the following we want to deduce properties of the cold atom system by employing the functional renormalization group approach. We have described basic features of this method in Ch. 3. The Wetterich equation allows us to deduce the full effective action from the microscopic or classical action by successively integrating out thermal and quantum fluctuations. To accomplish this we introduced the central object in this approach, which is the effective average action. In the next section we will discuss the key ingredients to make the functional renormalization work for ultracold gases. More specifically, we introduce and explain the role of the effective potential, its relation to the underlying $U(1)$ symmetry and the connection to the superfluid phase. We then proceed and set up the microscopic model of a three-dimensional Bose gas and discuss how this translates to a good ansatz of the effective average action. To fully match the ansatz to the microscopic model we specify the initial conditions of the running couplings. We then explain how we confine the transverse spatial dimension, derive the necessary flow equations and present our results for this system. In Sec. 4.8 we discuss some specific properties of systems with a different kind of confinement.

4.1 Main concepts of ultracold gases with FRG

4.1.1 The special role of the effective potential

Our main goal is to compute the few- and many-body properties of a Bose gas in a three-dimensional setting, where the third dimension is confined due to a potential well. We found in Ch. 2 that a Bose gas undergoes a phase transition to a superfluid state in two and in three dimensions, whenever the temperature is low enough for a given fixed density. The quantity which we are interested in is therefore the phase diagram, which gives us the critical temperature $T_\mathrm{c}\,(n)$ as a function of the density of the system as well as other external parameters, which we will introduce later on. The underlying mechanism behind the phase transition is the spontaneous breaking of a symmetry. To understand this recall from Ch. 3 how the effective action Γ is connected to the microscopic action S. In most cases the effective action might be quite different from the microscopic action, because collective phenomena might appear while information about microscopic physics is lost when incorporating thermal and quantum fluctuations. However, the effective action shares the same symmetries as the microscopic action. The symmetry that we are dealing with when we consider a Bose gas is a global $U(1)$ symmetry, which means that the microscopic action is invariant under global phase rotations of the field

$$\begin{aligned} \varphi &\to e^{\mathrm{i}\alpha}\varphi \\ \varphi^* &\to e^{-\mathrm{i}\alpha}\varphi^* \end{aligned} \tag{4.1}$$

with real parameter α. The physical implication of this symmetry is the conservation of the corresponding Noether charge, which for this $U(1)$ symmetry is the particle number

$$N = \int_{\vec{x}} \langle \varphi^* \varphi \rangle \,. \tag{4.2}$$

The effective action also shares this symmetry, because there are no anomalies present in the functional integral measure. If no external sources are present which would break the symmetry explicitly (and therefore rather trivially), the symmetry can break spontaneously if the ground state of the system develops a nonzero expectation value. So even though the action is invariant under a certain symmetry, the physical state of the system might break it, because the ground state now transforms nontrivially under phase rotations.

In the functional renormalization group approach we connect the full effective action Γ with the microscopic action S via the introduction of the effective average action Γ_k. Since the effective action shares the same symmetries as the microscopic action, we should choose an ansatz for Γ_k which shares these symmetries as well because couplings that do not obey these symmetries are then not generated during the flow. We will discuss the choice of a suitable ansatz in Sec. 4.3. First, we investigate how the breaking of this symmetry, which distinguishes the superfluid from the normal phase, is connected to the effective potential. The effective potential U is the part of the ef-

fective action which does not contain derivatives of the field. The symmetry considerations have profound consequences on the effective potential, because it can only depend on combinations of fields that respect the underlying symmetry. Therefore, the effective potential is not a function of the individual fields ϕ and ϕ^*, but rather it is a function of the $U(1)$-invariant combination $\rho = \phi^*\phi$

$$U = U(\rho). \tag{4.3}$$

Further, we know that the physical expectation value minimizes the effective action. If we assume that a constant field is the configuration which minimizes the part of the effective action which contains derivatives, then the effective action reduces to the effective potential and the physical solution is the field configuration which also minimizes the effective potential. We showed this in Eq. (3.10) where we evaluated the equation of motion with vanishing source for a homogeneous ground state. Since for the most part of this thesis we work with a homogeneous setting, the assumption of a homogeneous ground state is justified. The equation to determine the ground state reduces to

$$U(\rho_0) = \min_{\rho} [U(\rho)] \tag{4.4}$$

and we can distinguish two distinct phases: If the system does not develop a nonzero expectation value, i.e. $\rho_0 = 0$, then the state does not spoil the symmetry of the underlying physical action and we are in the so called "normal phase". If $\rho_0 \neq 0$, however, then even though we started with a theory that respects the $U(1)$ symmetry, quantum and thermal fluctuations drive the system to a state where it develops a nonvanishing expectation value ρ_0. We plot the general shape of the effective potential in Fig. 4.1, which is often called a mexican hat potential.

At the classical level it is given by

$$U(\rho) = -\mu |\phi|^2 + \frac{\lambda}{2} |\phi|^4 , \tag{4.5}$$

where it becomes evident that the symmetry is broken for positive chemical potential. Notice that in this case, the requirement to minimize the effective potential only fixes the amplitude of the complex field $\phi = |\phi| e^{i\theta}$. Thus, there is still the freedom to choose a phase. However, none of these values is singled out, but the system chooses one particular value determined by uncontrollable fluctuations. Without loss of generality we might choose a particular value of the phase which makes our calculations most convenient. We therefore work with a decomposition of the complex field ϕ into a real and an imaginary part

$$\begin{aligned} \phi &= \frac{1}{\sqrt{2}} (\phi_1 + i\phi_2) \\ \phi^* &= \frac{1}{\sqrt{2}} (\phi_1 - i\phi_2) \end{aligned} \tag{4.6}$$

and use our freedom to choose a phase to force the ground state to be real, i.e. we set $\phi_2 = 0$, so that $\rho_0 = \phi^2$ with ϕ being real valued. If we now consider a field

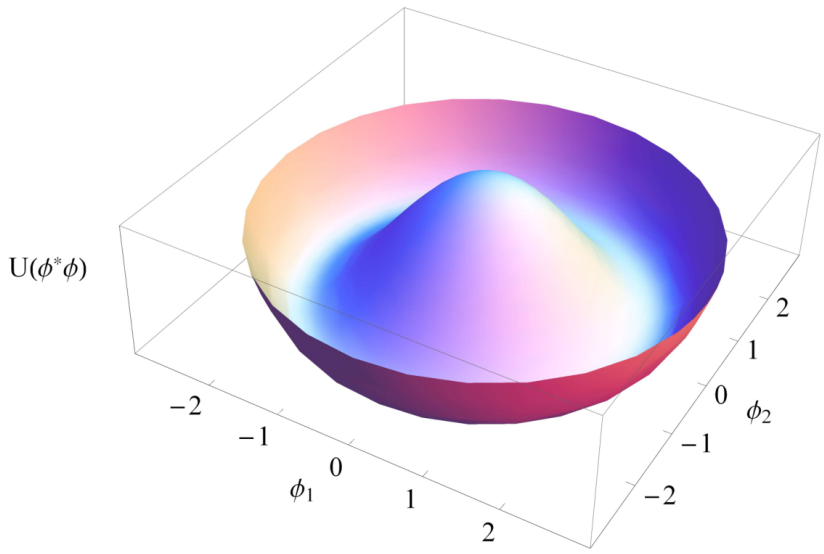

Figure 4.1: The effective potential U as a function of the complex field ϕ resembles the form of a mexican hat. $U(\phi^*, \phi)$ does not depend on the phase, which is chosen spontaneously in the superfluid phase, but only on the amplitude $\rho = \phi^*\phi$. Without loss of generality we demand ϕ to be real-valued.

φ which fluctuates around the ground state, we can decompose the fluctuations into two groups: Fluctuations along the amplitude direction are energetically suppressed, because it costs energy to move up inside the effective potential. However, phase fluctuations do not cost energy and give therefore rise to gapless modes, the so called Goldstone modes, which eventually are responsible for the superfluidity of the system. The appearance of Goldstone modes in a system with a spontaneously broken symmetry is a general result of Goldstone's theorem, see Ref. (Goldstone (1961)).

We have seen that the effective potential is the key object to distinguish between the normal and the superfluid phase, depending on whether its minimum is zero or nonzero. In general, the minimum of the effective potential depends on external parameters like temperature, chemical potential or scattering length

$$\rho_0 = \rho_0 \left(\mu, T, a\right). \tag{4.7}$$

We can therefore drive the system from one phase to the other by changing an external parameter, like the temperature. In our case we deal with a second order phase transition, which means that the order parameter vanishes continuously as temperature is increased. The two phases are separated at the critical temperature, which is characterized by

$$\rho_0 = 0, \quad U'\left(\rho_0\right) = 0. \tag{4.8}$$

We plot the effective potential as a function of the symmetry invariant in presence of a second order phase transition in Fig. 4.2.

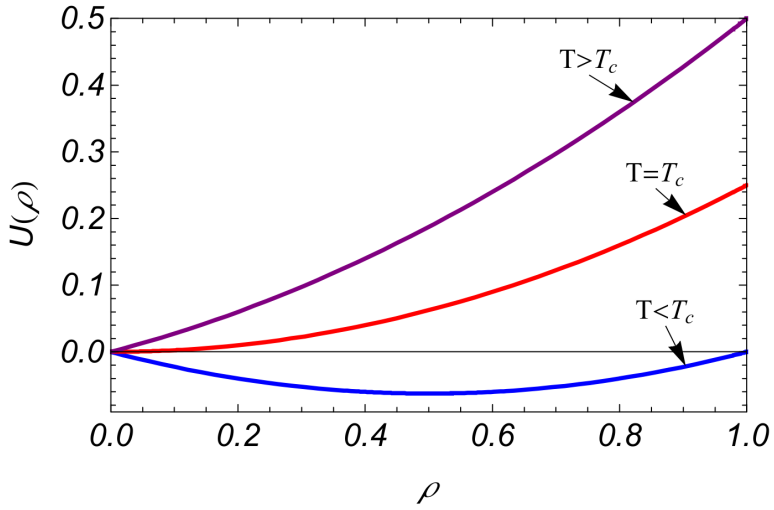

Figure 4.2: This figure shows the effective potential U as a function of the symmetry invariant ρ for different temperature regimes. For large temperatures the gas is in the normal or symmetric phase, which translates to a vanishing order parameter, i.e. the minimum of the effective potential ρ_0 is zero (purple line). For low temperatures the system is in the superfluid phase, where the minimum of the effective potential takes on a nonvanishing value $\rho_0 \neq 0$ (blue line). In between those two phases is the phase transition (red line).

To summarize, we explained that the task to find the ground state of a system reduces for homogeneous states to find the minimum of the effective potential. The effective potential is a function of the symmetry invariant only and is the key observable to distinguish between the two phases the system can be in.

4.1.2 Microscopic model

We want to study nonrelativistic bosons with repulsive interactions. As a reminder, we saw in Ch. 3 that the grand canonical partition function, which encodes all thermodynamic properties of the system, has a functional integral representation

$$Z(\mu, T) = \int \mathcal{D}\varphi e^{-S[\varphi]}, \tag{4.9}$$

where the integral is a summation over all possible field configurations $\varphi(\tau, \vec{x})$. The Euclidean microscopic action of the system is given by

$$S[\varphi] = \int_X \left(\varphi^* \left(\partial_\tau - \frac{\nabla^2}{2M} - \mu\right)\varphi + \frac{\lambda}{2}|\varphi|^4\right). \tag{4.10}$$

Herein, the bosonic degrees of freedom are described by the complex scalar field φ. Further, we use the abbreviation $\int_X = \int_0^\beta \mathrm{d}\tau \int \mathrm{d}^d x$, the number of spatial dimensions is d, and τ denotes imaginary time. For a finite temperature T the imaginary time is compactified to a torus of circumference $\beta = (k_\mathrm{B} T)^{-1}$ with Boltzmann constant k_B. The chemical potential and atomic mass are denoted by μ and M, respectively. Further we use natural units $\hbar = k_B = 1$ and later on we will also use energy units such that $2M = 1$. Notice that we introduced a pointlike s-wave interaction with strength λ, therefore assuming a simple contact potential between the particles. In Ch. 2.3 we justified this simplification with the reasoning that the short distance details of the true interaction potential cannot be resolved by many-body effects, since the thermal de Broglie wavelength λ_T is much larger than the van-der-Waals interaction length l_vdW. So as long as the contact potential gives rise to the same physically measurable scattering length a, we can savely neglect the complicated details of the true interaction potential. Therefore, this action provides an excellent description for ultracold quantum gases of Alkali atoms, but it may, however, also be used as an effective description for nonrelativistic bosonic degrees of freedom in other condensed matter setups.

In our functional renormalization group approach we extract the physical content of the theory by successively including quantum and thermal fluctuations. In this way, the microscopic action S serves as an effective description of the physics at some ultraviolet momentum scale Λ, which is on the order of the inverse van der Waals length. This scale will always be larger than the many-body scales of the system, given by density, temperature and scattering length (otherwise our approximation of a contact potential does not hold anymore). The effective average action Γ_k can be understood in a similar way as an effective description of the physics at the scale k, with fluctuations between k and Λ included. By the inclusion of fluctuations the couplings that define the system might change, so that we denote them with an index k in the following. The effective average action should then coincide with the microscopic action at the scale Λ, because we want the microscopic action to be the effective description of the physics at scale Λ

$$\Gamma_\Lambda[\varphi] = S[\varphi] = \int_X \Big(\varphi^* \left(\partial_\tau - \nabla^2 - \mu \right) \varphi + \frac{\lambda_\Lambda}{2} |\varphi|^4 \Big), \tag{4.11}$$

where we now labeled the interaction strength λ with an index Λ to directly show its scale dependence.

4.1.3 Ansatz for the effective average action

The effective action is in most cases quite different from the microscopic action. To find a suitable ansatz for the effective average action, we should take into account the physical insight that we have of the system. A major guiding principle for this has been introduced in Sec. 4.1.1, namely symmetries. If we employ an ansatz that respects the symmetries of the microscopic action, then couplings that do not obey these symmetries are not generated during the flow. We may now try to mimic the form of the

microscopic action by applying a derivative expansion with the ansatz

$$\bar{\Gamma}_k\left[\bar{\phi}^*,\bar{\phi}\right]=\int_X\Big(\bar{\phi}^*(\bar{Z}_k\partial_\tau-A_k\nabla^2)\bar{\phi}+\bar{U}_k(\bar{\phi}^*\bar{\phi})\Big). \tag{4.12}$$

This implementation has been used in Refs. (Wetterich (2008); Floerchinger and Wetterich (2008, 2009b)). Notice that the now scale dependent effective average potential is only a function of the symmetry invariant $\bar{\rho}$, so that we do not spoil the symmetries of the microscopic action. We have also introduced the kinetic coefficients $\bar{Z}_k$ and A_k. For $\bar{Z}_k=A_k=1$ we recover the kinetic part of the microscopic action, but due to the inclusion of fluctuations these might deviate from 1, so that we go beyond this lowest order. This ansatz for the effective average action forces the resulting effective action into a specific form. We only use a finite number of running couplings, which are needed to be cleverly chosen, so that they can describe the relevant physics, which in this case is above all the second order phase transition to a superfluid state. We denote the bare or "unrenormalized" couplings with an overbar. The wave function renormalization A_k can be used to define renormalized fields via

$$\phi=A_k^{1/2}\bar{\phi}. \tag{4.13}$$

Accordingly we will introduce renormalized couplings, which differ from the bare couplings by a suitable rescaling with powers of A_k such that the effective action fulfills

$$\bar{\Gamma}\left[\bar{\phi}\right]=\Gamma\left[\phi\right]. \tag{4.14}$$

We can rewrite our ansatz for the effective average action as

$$\Gamma_k\left[\phi\right]=\int_X\Big(\phi^*\left(Z_k\partial_\tau-\nabla^2\right)\phi+U_k\left(\rho\right)\Big) \tag{4.15}$$

with $Z_k=\bar{Z}_k/A_k$. With this renormalized field ϕ the prefactor of $\phi^*\nabla^2\phi$ is fixed to unity. This choice ensures that the expectation value of ϕ, which is related to the superfluid density via $\rho=\phi^*\phi$, can be nonzero even in the two-dimensional limit, where the Mermin–Wagner theorem (Mermin and Wagner (1966); Hohenberg (1967)) forbids long-range order, see Ch. 2.4.

We further expand the effective average potential in a Taylor series in ρ. More specifically, we do not use an expansion around a fixed value, but we rather expand the potential around its minimum value $\rho_{0,k}$, which is obviously scale-dependent, too. To be able to describe a second order phase transition we need to include at least the fourth order in the field ϕ, which translates to the following expansion in ρ

$$\begin{aligned}U_k\left(\rho\right)=&\,m_k^2\left(\rho-\rho_{0,k}\right)+\frac{\lambda_k}{2}\left(\rho-\rho_{0,k}\right)^2\\&-n_k\left(\mu'-\mu\right)+\alpha_k\left(\mu'-\mu\right)\left(\rho-\rho_{0,k}\right).\end{aligned} \tag{4.16}$$

We added further terms to the Taylor expansion in ρ, so that we can later project flow equations for the density n_k and α_k.

The flowing minimum is determined by the requirement

$$\left(\partial_\rho U\right)\left(\rho_{0,k}\right) \stackrel{!}{=} 0 \text{ for all } k. \tag{4.17}$$

During the flow the minimum $\rho_{0,k}$ is the quantity that decides in which phase the system is in. In the symmetric regime the minimum vanishes, while in the broken phase we have $m_k^2 = 0$ and $\rho_{0,k} \neq 0$. This will be important when we define the flow equations in Sec. 4.3, because we will switch flow equations for m_k^2 and $\rho_{0,k}$ whenever the minimum changes from zero to a nonzero value.

The ansatz in Eq. 4.16 has a successful history. For example, it has been applied to calculate the thermodynamic equation of state (Floerchinger and Wetterich (2009a); Rançon and Dupuis (2012)), critical exponents (Tetradis and Wetterich (1994a); Berges et al. (2002)), and critical temperature T_c (Floerchinger and Wetterich (2009b); Rançon and Dupuis (2012)). The results do not only agree with other theoretical approaches (Prokof'ev et al. (2001); Prokof'ev and Svistunov (2002); Holzmann et al. (2007); Holzmann and Krauth (2008)) but also with experimental results (Hung et al. (2011); Yefsah et al. (2011); Zhang et al. (2012)). Of course, one can extend the ansatz in Eq. (4.16), e.g. one can incorporate higher order scattering by using a ϕ^{2N}-expansion with a suitable N. In Refs. (Gersdorff and Wetterich (2001); Dupuis (2009); Jakubczyk et al. (2014)), for example, the ansatz for the effective average action of the two-dimensional gas has been extended to capture the emergence of Popov's hydrodynamic description at low energies and the essential scaling at the BKT transition.

To summarize, we introduced an ansatz for the effective average action Γ_k, with which we try to incorporate all the relevant physics by a finite number of running couplings, that are: $\bar{Z}_k, A_k, m_k^2, \rho_{0,k}, \lambda_k, n_k$ and α_k. The way these couplings might change during the flow with the scale k will depend crucially on the external parameters like temperature T or the size L of the confinement of the transverse direction, which we will introduce in detail in Sec. 4.2. Because we have chosen a particular set of a finite number of couplings, the corresponding set of flow equations is not closed at this point. How we project flow equations for the wave function renormalization coefficients will be discussed in Sec. 4.3.

4.1.4 Initial conditions

Before we look at how the running couplings change during the flow we need to specify with which values they start with. These "inital" conditions are fixed by the requirement that our ansatz for the effective average action Γ_k coincides with the microscopic action S at the UV momentum scale Λ

$$\Gamma_\Lambda\left[\phi\right] = S\left[\phi\right]. \tag{4.18}$$

The kinetic part can be easily compared to yield

$$\bar{Z}_\Lambda = A_\Lambda = 1. \tag{4.19}$$

To find a suitable ansatz for m_k and $\rho_{0,k}$ we have a closer look at the microscopic action S, which as we have argued reduces to the classical effective potential for homogeneous solutions. It reads

$$U(\rho) = -\mu\rho + \frac{\lambda}{2}\rho^2. \tag{4.20}$$

In Sec. 4.1.1 we discussed the properties of the effective potential. Already at the classical level we can distinguish the two distinct regimes. For $\mu < 0$ we can write $U(\rho) = |\mu|\,\rho + \frac{\lambda}{2}\rho^2$. Since ρ, the vacuum expectation value, is nonnegative, the minimum of U is clearly given by $\rho_0 = 0$. For $\mu > 0$, however, we find

$$\begin{aligned} U'(\rho_0) &= -\mu + \lambda\rho_0 \stackrel{!}{=} 0 \\ \Leftrightarrow \rho_0 &= \frac{\mu}{\lambda}. \end{aligned} \tag{4.21}$$

This macroscopic field breaks the $U(1)$ symmetry spontaneously. Since this only fixes the amplitude of the complex field ϕ, we are free to choose any value for the phase, which we do in a way that the field is real, i.e. $\phi_0 = \phi_0^* = \sqrt{\frac{\mu}{\lambda}}$. Evaluating the equation of state for the physical solution yields

$$n = -\left.\frac{\partial U}{\partial \mu}\right|_{\phi_0} = |\phi_0|^2 = \rho_0, \tag{4.22}$$

which tells us that all particles are condensed. However, this only holds in the classical approximation for zero temperature. We further notice that

$$\frac{\partial^2 U}{\partial\mu\partial\rho} = -1. \tag{4.23}$$

The inital conditions are therefore given by

$$\begin{aligned} \rho_{0,\Lambda} = n_\Lambda &= \frac{\mu}{\lambda_\Lambda}\theta(\mu), \\ m_\Lambda^2 &= -\mu\theta(-\mu), \\ \alpha_\Lambda &= -1. \end{aligned} \tag{4.24}$$

What is left is the initial condition for λ. We argued before that we can savely work with a pointlike s-wave coupling constant as long as we reproduce the same scattering length a, which can actually be measured in experiments. In contrast, the microscopic coupling λ_Λ is only valid at high energy scales and cannot be measured in experiments - only the renormalized couplings obtained in the $k \to 0$ limit are physical quantities. The scattering length a is connected to λ by the relation (see Ch. 2.3)

$$a = \frac{1}{8\pi}\lambda(k = 0, T = 0, n = 0), \tag{4.25}$$

that is, the scattering length is defined in vacuum for zero temperature. But notice that it is only directly connected to the renormalized coupling constant $\lambda_{k=0}$. Even though we

work in the zero temperature limit, there are still quantum fluctuations that renormalize the microscopic coupling λ_Λ. In order to compare to real experiments, we have to solve the flow equation twice: First we need to connect the unphysical microscopic coupling λ_Λ to the scattering length by solving the vacuum flow. Second, we can "switch on" temperature and chemical potential to calculate the desired many-body properties of the system. The general procedure is shown in Fig. 4.3. It is actually a strong feature of the method of functional renormalization that it can cope with the vacuum or scattering physics and the many-body physics in a unified way. This feature is discussed in more detail in Sec. 4.2.

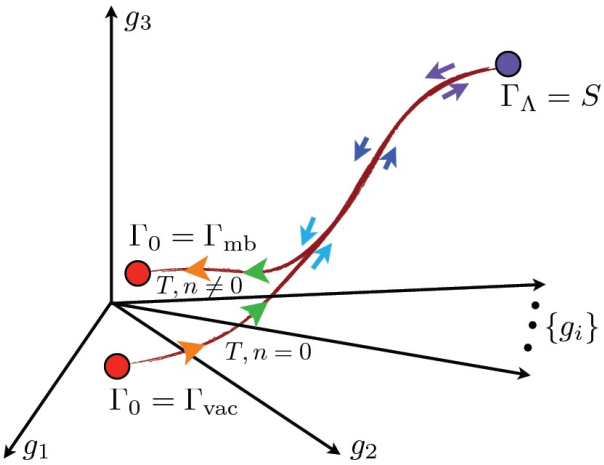

Figure 4.3: To connect the unphysical microscopic coupling λ_Λ to a physical observable, we first solve the flow in vacuum, given by $T = n = 0$, to arrive at $\Gamma_{\rm vac}$. Then we can "switch on" the density and temperature to arrive at the effective action $\Gamma_{\rm mb}$. We always choose the cutoff scale Λ to be much larger than the many-body scales. Then the two different flows coincide in the ultraviolet, because the system does not yet notices many-body effects. Figure taken from Boettcher et al. (2012).

We discuss how we project a suitable flow equation for λ_k and the other couplings in Sec. 4.3, but note that the zero temperature vacuum flow equation for λ_k can be solved analytically, as was shown in Ref. (Floerchinger and Wetterich (2008)). The corresponding differential equation reads

$$\partial_k \lambda = \frac{\lambda^2}{6\pi^2}. \tag{4.26}$$

This is solved by

$$\lambda(k) = \frac{1}{\frac{1}{\lambda_\Lambda} + \frac{\Lambda - k}{6\pi^2}}. \tag{4.27}$$

Using $a = \lambda_{k=0}/(8\pi)$ we find

$$\lambda_\Lambda = \frac{1}{\frac{1}{8\pi a} - \frac{\Lambda}{6\pi^2}}. \tag{4.28}$$

4.2 A game of scales: Introduction of trap size L

The ansatz that we introduced in the previous sections has been very successful to provide a qualitative and mostly quantitative description of the three- and two-dimensional nonrelativistic Bose gas. Thus, we expect this ansatz to be successful in a similar manner when applied to the dimensional crossover from two to three dimensions. In this crossover, the system features long-range order below a critical temperature T_c for all $2 < d \leq 3$. Even for $d = 2$ we find a superfluid phase with an algebraic decay of correlations due to the BKT mechanism, see Ch. 2.4. We can therefore describe a superfluid transition for all $2 \leq d \leq 3$ by monitoring the minimum of the effective average potential U_k in the limit $k \to 0$.

We want to describe the crossover from two to three dimensions by means of compactifying the "transverse" z-direction in the sense that we introduce a potential well of length L. The boundary conditions at the end points may either be chosen periodic or we may restrict the gas to a box potential with infinitely high walls given by

$$V_\mathrm{box}(z) = \begin{cases} 0 & 0 \leq z \leq L \\ \infty & \text{else} \end{cases}. \tag{4.29}$$

In the case of periodic boundary conditions we say that the system is confined to a torus in z-direction. Since the trapping potential vanishes inside the box potential, the confinement reduces in both cases to boundary conditions on the field ϕ. Explicitly they are given by

$$\phi\left(\tau, x, y, z = 0\right) = \phi\left(\tau, x, y, z = L\right) \tag{4.30}$$

for periodic boundary conditions (pbc) and

$$\phi\left(\tau, x, y, z = 0\right) = \phi\left(\tau, x, y, z = L\right) = 0 \tag{4.31}$$

for the box. An important physical implication is the quantization of energies and therefore a discrete excitation spectrum in z-direction.

We want to build this into our method of functional renormalization. Within such a formulation the boundary conditions appear as restrictions on the appropriate function space. That is, if we want to sum over all possible field configurations then we have to take into account that only the ones satisfying the corresponding boundary conditions are included in the summation. Eigenfunctions in z-directions are described as superpositions of plane waves with momentum component q_z. In z-direction the boundary conditions lead to a quantization of energies $E_z = \hbar^2 q_z^2/2M$. For a torus the momenta are restricted to $q_z \to k_n$ with

$$k_n = \frac{2\pi n}{L},\ n \in \mathbb{Z}. \tag{4.32}$$

The key difference to the box is not that the energies are now quantized according to $E_z = \hbar^2\kappa_n^2/2M$ with $\kappa_n = \pi n/L$, $n = 1, 2, \ldots$, but rather that the smallest possible energy, setting $n = 1$, is nonvanishing. In Sec. 4.8.1 we think about how to incorporate this correctly into the functional renormalization group approach.

In experiments the trapping potentials are often harmonic, therefore varying smoothly. However, the qualitative behavior is similar to a trap using potential wells, as can be seen in Fig. 4.4.

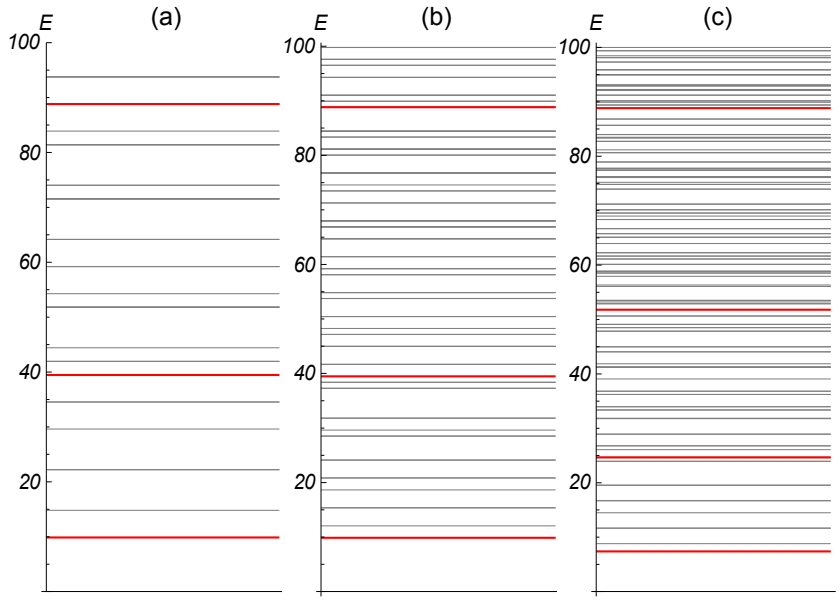

Figure 4.4: Schematics of the energy spectrum in the dimensional crossover from three to two dimensions. The lines represent the eigenenergies of different systems. In panel (a) we consider a noninteracting system in a three-dimensional box potential which confines the system to the cuboid $(x, y, z) \in [0, L_x]^2 \times [0, L]$ with $L_x/L = 2$, whereas panel (b) displays the case of $L_x/L = 3$. We clearly see how the increase in the ratio L_x/L leads to an effective two-dimensional continuum of states (thin gray lines) between the discrete spectrum of excitations in the transverse z-direction (thick red lines). The lowest excitations appear above the zero-point energy, which is generally not zero. In (c) we sketch the more realistic scenario of a system which is interacting and confined by a smooth trapping potential. Although the concrete mode spectrum and level spacing in (c) differ from (a) and (b), we find the same qualitative behavior. Figure taken from Lammers et al. (2016).

Given a particular value of L, how can we decide whether the system under consideration resembles more a two- or a three-dimensional system? For this we need to compare L with the other length scales that are present in the system, i.e. the many-

body length scales which are set by the temperature and density. Suppose L is much smaller than all those other length scales, then we call this the two-dimensional (2D) limit, because the system is frozen in its ground state in z-direction and the low-energy excitations are limited to the two-dimensional continuum (q_x, q_y) in momentum space, just above the zero-point energy. Macroscopically we cannot distinguish it from a 2D system then. In Sec. 4.5.1 we show how the parameters of the effective 2D system are inherited from the 3D system.

It is instructive to compare our formulation of confinement to other systems where dimensional reduction occurs. For example, if the temperature T drops below the relevant energy scales of a system, the statistics change from a quantum to a classical nature. Further, when we derive the flow equations of our running couplings, we make use of the Matsubara formalism, where $1/T$ plays the same role as L in our case. Another example is the dimensional reduction of higher-dimensional Kaluza-Klein theories compactified on a torus (Kaluza (1921); Klein (1926)).

A nice feature of the renormalization group approach is a pronounced separation of scales due to the successive inclusion of fluctuations on different momentum shells. Since we start at some ultraviolet cutoff of the theory and include information about the physics at larger scales only later during the flow, the many-body scales set by temperature T or chemical potential μ do not influence the effective average action Γ_k at the beginning of the flow. As long as the scale k is much larger than the scales set by the many-body effects, i.e. $k \gg T^{1/2}$ and $k \gg \mu^{1/2}$, the flow does not yet "know" that it has a density or temperature, therefore the flow is not different from the vacuum zero temperature flow. First at a scale $k \sim T^{1/2}$ the system starts to feel a temperature. This means that the method of functional renormalization can easily cope with a number of different scales present in the system, because we look at them only one at a time. Thus, we obtain a good intuition about whether we are in a more two- or three-dimensional system by comparing the momentum scale set by the confinement of the transverse direction, L^{-1}, with the many-body scales $\sqrt{\mu}$ and $\sqrt{T}$. For L^{-1} being much larger than $\sqrt{\mu}$ and $\sqrt{T}$ the Bose gas first experiences the confinement, long before many-body effects set in. In this case we are in a quasi 2D system, and it should be possible to describe the system by an effective 2D model. Indeed, we show in Sec. 4.5.1 how the properties of the 2D system are inherited from the 3D system. It is particularly important to realize that we always start with a 3D system at the UV scale Λ, that is, even for very small L, we choose a UV scale such that $\Lambda \gg L^{-1}$ always holds. Therefore, our ansatz of the effective average action and also the microscopic action contain three-dimensional quantities, for example the field $\rho = |\phi|^2$ has the physical dimension of a three-dimensional number density.

It is instructive to see how a 2D effective action emerges from our 3D effective action ansatz

$$\Gamma[\phi] = \int_X \int_0^L \mathrm{d}z \left(\phi^* \left(Z_k \partial_\tau - \nabla^2 - \partial_z^2 + m^2 \right) \phi + \frac{\lambda_{3\mathrm{D}}}{2} |\phi|^4 \right), \tag{4.33}$$

where we now have $X = (\tau, \vec{x})$ with $\vec{x} = (x, y)$. In a 3D system with $L = \infty$ the ground state $\phi_0(\tau, \vec{x}, z)$ is given by a constant value ϕ_0 with arbitrary complex phase. If we now

consider a finite confinement length L with periodic boundary conditions, the ground state is still given by a constant and we can write

$$\phi_0^{(\text{pbc})}(\tau, \vec{x}, z) = \chi_0 \frac{1}{\sqrt{L}}, \tag{4.34}$$

with $|\chi_0|^2$ having the dimension of a 2D number density. We can evaluate the effective action for this configuration to

$$\Gamma[\phi_0^{(\text{pbc})}] = \int_X \Big(m^2 |\chi_0|^2 + \frac{(\lambda_{3\text{D}}/L)}{2} |\chi_0|^4 \Big). \tag{4.35}$$

Notice that is has the structure of a two-dimensional Bose gas with a 2D coupling constant $\lambda_{2D} = \lambda_{3D}/L$. The same considerations can be done for a confinement in a box. However, the ground state is inhomogeneous and given by

$$\phi_0^{(\text{box})}(\tau, z, \vec{x}) = \chi_0 \sqrt{\frac{2}{L}} \sin\Big(\frac{\pi z}{L}\Big). \tag{4.36}$$

The effective action evaluates to

$$\Gamma[\phi_0^{(\text{box})}] = \int_X \left(\left(m^2 + \frac{\pi^2}{L^2} \right) |\chi_0|^2 + \frac{\lambda_{2\text{D}}}{2} |\chi_0|^4 \right) \tag{4.37}$$

with

$$\begin{aligned} \lambda_{2\text{D}} &= I_2 \frac{\lambda_{3\text{D}}}{L}, \\ I_2 &= \frac{4}{L} \int_0^L \mathrm{d}z \sin^4\left(\frac{\pi z}{L}\right) = \frac{3}{2}. \end{aligned} \tag{4.38}$$

Therefore, for a confinement in a box we find a nontrivial prefactor in the translation between the coupling constants on the mean-field level.

The FRG approach has been applied to study the effect of compactified dimensions on many-body system both in several relativistic and nonrelativistic setups. Finite volume effects, i.e., when *all* spatial directions are confined to a cube of size $[0, L]^d$, have been studied for quark-meson-models (Braun and Klein (2009); Braun et al. (2011b, 2012); Tripolt et al. (2014)) and the 3D BCS-BEC crossover (Braun et al. (2011a)). In particular, Ref. (Tripolt et al. (2014)) highlights the difference in periodic and antiperiodic boundary conditions. The latter result in a nonvanishing zero-point energy similar to the confinement in a box potential discussed above.

4.3 Flow equations

In the previous sections we set up our model by introducing the ansatz for the effective average action Γ_k, which has to coincide with the microscopic action S at the UV scale Λ. We ensure this by choosing the right initial conditions for our running couplings.

Remember from Ch. 3.2 that the Wetterich equation

$$\partial_t \Gamma_k = \frac{1}{2}\mathrm{Tr}\left[(\Gamma_k^{(2)} + R_k)^{-1}\partial_t R_k\right] \tag{4.39}$$

describes how the effective average action changes with the scale k. But we need to specify which regulator we want to choose within our calculations. Besides the general constraints a regulator has to fulfill in order to actually be a regulator, see Sec. 3.3, we require that it respects the underlying $U(1)$ symmetry, so that it does not spoil the previous symmetry considerations. Further, since we have to rely on truncations of the effective average action, the calculated effective actions might actually depend on the choice of regulator. Therefore, we choose a cutoff which is optimal in the sense discussed in Sec. 3.3. This regulator is given by a Litim-type cutoff (Litim (2001a); Wetterich (2008); Litim (2000))

$$\Delta S_k = \int_Q \bar{\phi}^* A_k(k^2 - \vec{q}^2 - k_n^2)\theta(k^2 - \vec{q}^2 - k_n^2)\bar{\phi}, \tag{4.40}$$

or, equivalently, in terms of the cutoff functions

$$R_k(Q, Q') = R_k(Q)\delta(Q + Q') \cdot \mathbb{1} \tag{4.41}$$

with $\mathbb{1}$ being the identiy matrix and

$$R_k(Q) = A_k(k^2 - \vec{q}^2 - k_n^2)\theta(k^2 - \vec{q}^2 - k_n^2). \tag{4.42}$$

Its derivative with respect to $t = \log(k/\Lambda)$ is given by

$$\dot{R}_k(Q) = A_k(2k^2 - \eta(k^2 - \vec{q}^2 - k_n^2))\theta(k^2 - \vec{q}^2 - k_n^2), \tag{4.43}$$

where we define the anomalous dimension by $\eta = -\dot{A}_k/A_k$. Note that this regulator does not serve as an UV cutoff for the Matsubara frequencies, however this also gives us the opportunity to carry out the Matsubara summation and the derivation of the flow equations analytically. This particular choice of Litim-cutoff essentially replaces $\vec{q}^2 + k_n^2$ with k^2 in the flow equations whenever $\vec{q}^2 + k_n^2 < k^2$ and thus provides us with an infrared cutoff by introducing an infrared mass term $A_k k^2$.

We present a detailed workout of the necessary calculations to deduce the flow equations in App. A. In brief, the crucial steps are as follows. On the right hand side of the Wetterich equation we see the inverse propagator or 2-point function $\Gamma_k^{(2)}$, which we need to evaluate for our choice of ansatz Γ_k. We work with a decomposition of the bosonic field ϕ into a real and imaginary part

$$\phi(X) = \frac{1}{\sqrt{2}}(\phi_1(X) + \mathrm{i}\phi_2(X)). \tag{4.44}$$

Whenever we evaluate equations for a physical ground state, we insert a constant real field $\phi(X) = \phi = \phi_1/\sqrt{2}$. The 2-point function is now a 2×2-matrix, where the components are given by

$$\left(\Gamma_k^{(2)}[\phi]\right)_{i,j}(X, Y) = \frac{\delta}{\delta\phi_i(X)}\frac{\delta}{\delta\phi_j(Y)}\Gamma_k[\phi] \tag{4.45}$$

The flow equation for the effective potential is given by

$$\dot{\bar{U}}_k(\bar{\rho}) = \frac{1}{2}\mathrm{tr}\int_Q \bar{G}_k(Q)\dot{R}_k(Q) \tag{4.46}$$

with the regularized propagator

$$\bar{G}_k(Q) = \frac{1}{\mathrm{det}_Q}\begin{pmatrix} p^q + \bar{U}' & \bar{Z}_k q_0 \\ -\bar{Z}_k q_0 & p^q + \bar{U}' + 2\bar{\rho}\bar{U}'' \end{pmatrix}, \tag{4.47}$$

where $Q = (q_0, \vec{q}, k_n)$, $\vec{q} = (q_1, \ldots, q_d)$ denotes the momentum vector in the noncompact dimensions of space, and k_n the component of the discrete momentum modes due to the transverse confinement. It can be derived from the Wetterich equation by evaluating it for a constant field. The regularized propagator $\bar{G}_k(Q)$ is obtained from the 2-point function by means of

$$\Gamma_k^{(2)}(Q, Q') + R_k(Q, Q') = \delta(Q + Q') \cdot \bar{G}_k^{-1}(Q), \tag{4.48}$$

where $\Gamma_k^{(2)}(Q, Q')$ is the Fourier transform of $\Gamma_k^{(2)}(X, Y)$, i.e.

$$\left(\Gamma_k^{(2)}[\phi]\right)_{i,j}(Q, Q') = \int_X \int_Y e^{iXQ} e^{iYQ'} \left(\Gamma_k^{(2)}[\phi]\right)_{i,j}(X, Y). \tag{4.49}$$

Further, we introduced

$$\begin{aligned} \mathrm{det}_Q &= (p^q + \bar{U}' + 2\bar{\rho}\bar{U}'')(p^q + \bar{U}') + (\bar{Z}_k q_0)^2, \\ p^q &= A_k(\vec{q}^2 + k_n^2) + R_k(Q), \end{aligned} \tag{4.50}$$

where a prime denotes a derivative with respect to $\bar{\rho}$. The integration in Eq. (4.46) consists of a q_0-integral, which is replaced by a sum over Matsubara frequencies $\omega_n = 2\pi n T$ for non-zero temperatures, and an integration over spatial dimensions. Therefore, we have

$$\int_Q = T\sum_{\omega_n} \frac{1}{L}\sum_{k_n} \int \frac{\mathrm{d}^d q}{(2\pi)^d}. \tag{4.51}$$

The flow equation for the effective potential can be written in the form

$$\begin{aligned} \dot{\bar{U}}_k &= \int_Q \frac{p^q + \bar{U}' + \bar{\rho}\bar{U}''}{\mathrm{det}_Q}\dot{R}_k \\ &= T\sum_{\omega_n} \frac{1}{L}\sum_{k_n} 4v_d \int_0^\infty \mathrm{d}q q^{d-1} \frac{p^q + \bar{U}' + \bar{\rho}\bar{U}''}{\mathrm{det}_Q} \\ &\times A_k\left(2k^2 - \eta(k^2 - q^2 - k_n^2)\right)\theta\left(k^2 - q^2 - k_n^2\right). \end{aligned} \tag{4.52}$$

The overall θ-function limits the integration to the region $q < \sqrt{k^2 - k_n^2}$ and we may replace $p^q \to A_k k^2$ in the integrand, so that the integration can be performed analytically.

We switch to renormalized quantities $Z_k = \bar{Z}_k/A_k$ and $\rho = A_k\bar{\rho}$ and find

$$\begin{aligned}
\dot{\tilde{U}}_k &= \frac{4v_d k^{3+d}}{dZ_k} G_1(T) F(\tilde{L}), \\
G_1(T) &= \left(\sqrt{\frac{1+w_1}{1+w_2}} + \sqrt{\frac{1+w_2}{1+w_1}}\right)\left(\frac{1}{2} + N_B\left(\frac{k^2\sqrt{(1+w_1)(1+w_2)}}{Z_k}\right)\right), \\
F(\tilde{L}) &= \frac{1}{Lk}\sum_{k_n}(1-(k_n/k)^2)^{d/2}\left(1-\eta\frac{1-(k_n/k)^2}{d+2}\right)\theta(k^2-k_n^2)
\end{aligned} \tag{4.53}$$

with $\tilde{L} = Lk$. Further, we introduced the dimensionless quantities $w_1 = U'/k^2$, $w_2 = (U' + 2\rho U'')/k^2$ and the Bose function $N_B(x) = (e^{x/T}-1)^{-1}$. $G_1(T)$ encodes the temperature-dependent part. Whenever we work in the zero temperature limit we can set the Bose function to zero. Specializing to two continuous dimensions and making a change of variable $\dot{U}_k = \dot{\tilde{U}}_k + \eta\rho U_k'$ the flow equation for the effective potential reads

$$\dot{U}_k = \eta\rho U_k' + \frac{k^5}{4\pi Z_k} G_1(T) F(\tilde{L}). \tag{4.54}$$

In this flow equation we see the emergence of the crossover function $F(\tilde{L})$, which evaluates for periodic boundary conditions to

$$\begin{aligned}
F_{\text{pbc}}(\tilde{L}) = \frac{2N+1}{\tilde{L}}\Bigg[1 - \frac{\eta}{4} - \frac{1}{\tilde{L}^2}\left(1-\frac{\eta}{2}\right)\frac{4\pi^2}{3}N(N+1) \\
- \frac{\eta}{\tilde{L}^4}\frac{4\pi^4}{15}N(N+1)(-1+3N+3N^2)\Bigg].
\end{aligned} \tag{4.55}$$

The crossover function is the crucial quantity for the dimensional crossover, because it encodes the influence of the trap. In the next section we discuss its shape and properties in detail.

Having the flow equation for the effective potential U_k, we can derive flow equations for the couplings that appear in our truncation of the effective potential (4.16) by means of a suitable projection. The flow is divided into two regimes. Whenever we are in the symmetric regime, we have $\rho_{0,k} = 0$, while in the spontaneously broken phase we have $m_k^2 = 0$. This means that we switch flow equations during the flow, depending on which phase we are in. The minimum of the effective potential is determined by the requirement

$$\left(\partial_\rho U\right)\left(\rho_{0,k}\right) \stackrel{!}{=} 0. \tag{4.56}$$

The flow of the minimum is therefore evaluated to

$$\begin{aligned}
0 &\stackrel{!}{=} \partial_t\left(U_k'\right)\Big|_{\rho=\rho_0} \\
&= \partial_\rho \dot{U}_k\Big|_{\rho=\rho_0} + U_k''\Big|_{\rho=\rho_0}\cdot\partial_t\rho_0 \\
\Rightarrow \quad \partial_t\rho_0 &= -\left(\frac{1}{U_k''}\partial_\rho\dot{U}_k\right)\Big|_{\rho=\rho_0} = -\frac{1}{\lambda_k}\partial_\rho\dot{U}_k\Big|_{\rho=\rho_0},
\end{aligned} \tag{4.57}$$

whereas in the symmetric regime we have

$$\partial_t m_k^2 = \partial_\rho \dot{U}_k \Big|_{\rho=0}. \tag{4.58}$$

For both regimes we have

$$\begin{aligned}\partial_t \lambda_k &= \partial_t \left(\partial_\rho^2 U_k\right)\Big|_{\rho=\rho_0} \\ &= \left(\partial_\rho^2 \dot{U}_k\right)\Big|_{\rho=\rho_0} + \left(\partial_\rho^3 U_k\right)\Big|_{\rho=\rho_0} \partial_t \rho_0 \\ &= \left(\partial_\rho^2 \dot{U}_k\right)\Big|_{\rho=\rho_0} + u_3 \cdot \partial_t \rho_0,\end{aligned} \tag{4.59}$$

however, we set $u_3 = 0$ in this thesis. In the same manner we arrive at flow equations for n_k and α_k, which read

$$\begin{aligned}\partial_t n_k &= -\left(\partial_{\mu'} \dot{U}_k\right)\Big|_{\rho=\rho_0} - \alpha_k \cdot \partial_t \rho_0, \\ \partial_t \alpha_k &= \left(\partial_\rho \partial_{\mu'} \dot{U}_k\right)\Big|_{\rho=\rho_0} + \left(\partial_\rho^2 \partial_{\mu'} U_k\right)\Big|_{\rho=\rho_0},\end{aligned} \tag{4.60}$$

where we neglect in the following the second term in the α_k flow equation. For better readability we have omitted $\mu' = \mu$, which has to be set after all derivatives have been performed.

Up to now the set of flow equations is not closed, since we are lacking flow equations for the wave function renormalizations A_k and $\bar{Z}_k$. We need to specify how to project the flow equation of the effective average action onto these couplings. We use the so-called derivative projection. Its motivation is found in the form of the inverse propagator

$$\bar{G}_k^{-1}(P) = \begin{pmatrix} A_k p^2 + \bar{U}' + 2\bar{\rho}\bar{U}'' & -\bar{Z}_k p_0 \\ \bar{Z}_k p_0 & A_k p^2 + \bar{U}' \end{pmatrix}. \tag{4.61}$$

We employ a projection of flow equations for $\bar{Z}_k$ and A_k according to

$$\begin{aligned}\partial_t \bar{Z}_k &= -\frac{\partial}{\partial p_0} \dot{\bar{G}}_{k,12}^{-1}(p_0, 0)\Big|_{p_0=0} \\ \partial_t A_k &= \frac{\partial}{\partial p^2} \dot{\bar{G}}_{k,22}^{-1}(0, p^2)\Big|_{p=0}.\end{aligned} \tag{4.62}$$

We get the flow equation of the inverse propagator by taking two functional derivatives of the flow equation of the effective action (4.39). It is given by (Wetterich (2008))

$$\begin{aligned}\dot{\bar{G}}_{k,ij}^{-1}(P) =& \mathrm{tr} \int_Q \bar{G}_k(Q) \gamma_i^{(3)} \bar{G}_k(Q - P) \gamma_j^{(3)} \bar{G}_k(Q) \dot{R}_k(Q) \\ & -\frac{1}{2} \mathrm{tr} \int_Q \bar{G}_k(Q) \gamma_{ij}^{(4)} \bar{G}_k(Q) \dot{R}_k(Q),\end{aligned} \tag{4.63}$$

where we introduced the 3- and 4-point vertices

$$\begin{aligned}\frac{\delta}{\delta\bar{\phi}_i(Q'')}\Gamma^{(2)}(Q,Q') &= \Gamma_i^{(3)}(Q,Q',Q'')\\ &= \gamma_i^{(3)}\delta(Q+Q'+Q''),\\ \frac{\delta}{\delta\bar{\phi}_i(Q'')}\frac{\delta}{\delta\bar{\phi}_j(Q''')}\Gamma^{(2)}(Q,Q') &= \Gamma_{ij}^{(4)}(Q,Q',Q'',Q''')\\ &= \gamma_{ij}^{(4)}\delta(Q+Q'+Q''+Q''').\end{aligned} \tag{4.64}$$

We want to work with the renormalized quantities $\eta = -\dot{A}_k/A_k$ and $Z_k = \bar{Z}_k/A_k$. The flow equation for the frequency coefficient evaluates to

$$\partial_t Z_k = \eta Z_k - \frac{\rho\lambda^2}{\pi k} G_2(T) F(\tilde{L}), \tag{4.65}$$

where we defined the temperature-dependent function

$$\begin{aligned}G_2(T) = &\frac{1}{(1+w_2)^{3/2}}\left(\frac{1}{2} + N_B(c) - cN_B'(c)\right)\\ &- \frac{3}{8}\frac{w_2(4+w_2)}{(1+w_2)^{5/2}}\left(\frac{1}{2} + N_B(c) - cN_B'(c) + \frac{c^2}{3}N_B''(c)\right).\end{aligned} \tag{4.66}$$

with $c = k^2\sqrt{1+w_2}/Z_k$. The anomalous dimension η evaluates to

$$\eta = \frac{\rho_0\lambda^2}{2\pi Z_k k} G_3(T) F_0(\tilde{L}), \tag{4.67}$$

with

$$G_3(T) = \frac{1}{(1+w_2)^{3/2}}\Big(\frac{1}{2} + N_B(c) - cN_B'(c)\Big). \tag{4.68}$$

$F_0(\tilde{L})$ is the crossover function with η set equal to zero, i.e.

$$F_0(\tilde{L}) = \frac{2N+1}{\tilde{L}}\left[1 - \frac{1}{\tilde{L}^2}\frac{4\pi^2}{3}N(N+1)\right]. \tag{4.69}$$

This completes the derivation of the flow equations. We arrived at a set of partial differential equations which is closed and can be computed with the help of the computational software program Mathematica.

4.4 Superfluid transition

In this section we study the superfluid phase transition of a Bose gas in the dimensional crossover. The system is influenced by a number of external parameters: the temperature T, the chemical potential μ, the scattering length a and the size L of the potential

well. Since we want to describe a gas with nonvanishing density which exhibits a second order phase transition at low temperatures, we choose a positive chemical potential and in addition, we set without loss of generality $\mu = 1$, since in the end we always express our results in dimensionless quantities. The flow of the effective average action Γ_k is initialized at some ultraviolet momentum scale $k = \Lambda$, where Γ_Λ coincides with the microscopic action of a three-dimensional Bose gas, see Sec. 4.1.2 for details. Besides the many-body scales the three-dimensional Bose gas now features another scale, which is defined by the size of the compactification length L in z-direction. For very large L the system behaves very similar to a three-dimensional system, however, if L^{-1} is much larger than the many-body scales, the system is effectively two-dimensional. We examine this scenario in Sec. 4.5. Nonetheless it is important that the ultraviolet scale Λ is always chosen in a way that $\Lambda \gg (L^{-1}, \mu^{1/2}, T^{1/2})$. Thus, we always start with a three-dimensional system with three-dimensional coupling constants. The initial value for the effective potential is given by

$$U_\Lambda(\rho) = \frac{\lambda_\Lambda}{2}(\rho - \rho_{0,\Lambda})^2 \tag{4.70}$$

with $\rho_{0,\Lambda} = \mu/\lambda_\Lambda$, so that it matches the microscopic potential. Even though we specified the "initial conditions" for the running couplings in Sec. 4.1.4, we have yet to define the actual scale Λ. From the considerations above we choose to initialize the flow at the ultraviolet scale $\Lambda/\sqrt{\mu} = 10^3$, and stop at the final scale $k_\mathrm{f} = \Lambda e^{-10}$, which is much smaller than the many body scales. Together with the initial conditions which we determined in Sec. 4.1.4 and the flow equations for the running couplings, see Sec. 4.3, we can deduce whether we are in the superfluid phase ($\rho_{0,0} > 0$) or in the disordered phase ($\rho_{0,0} = 0$). The flow equation of the effective average potential U_k is the central flow equation in our setting. It factorizes into a universal L-independent part $G_1(T)$ and a crossover function $F(\tilde{L})$ according to

$$k\frac{\partial}{\partial k}U_k(\rho) = \frac{k^5}{4\pi Z_k}G_1(T)F(\tilde{L}) + \eta\rho U_k'(\rho). \tag{4.71}$$

The crossover function $F(\tilde{L})$ encodes the influence of the trap and we plot it for periodic boundary conditions in Fig. 4.5. If we compare the flow equation for the effective average potential in this confined setting with the flow equation for the effective average potential in d continuous dimensions

$$k\frac{\partial}{\partial k}U_k(\rho) = 4v_d\frac{k^{d+2}}{Z_k d}\left(1 - \frac{\eta}{d+2}\right)G_1(T) + \eta\rho U_k'(\rho), \tag{4.72}$$

then we see that the function F interpolates between the two- and three-dimensional flow equations via the two limiting cases

$$F(\tilde{L}) = \begin{cases} \frac{2}{3\pi}\left(1 - \frac{\eta}{5}\right) & (\tilde{L} \gg 1) \\ \tilde{L}^{-1}\left(1 - \frac{\eta}{4}\right) & (\tilde{L} \ll 1) \end{cases}. \tag{4.73}$$

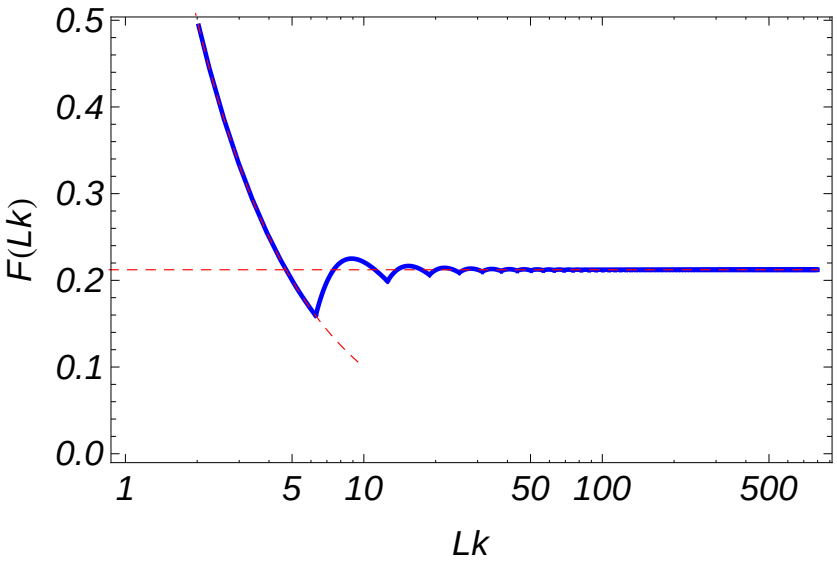

Figure 4.5: The key object in the dimensional crossover is the crossover function $F(\tilde{L})$, which appears in the flow equations of the three-dimensional system. We recover the three-dimensional flow equations for large $\tilde{L} = Lk$, while we obtain the two-dimensional flow equations for small $\tilde{L}$, where the crossover function diverges like $\tilde{L}^{-1}$. In this way we can interpolate between these to limites. Note that even when the system is confined by a very small trap size L, the description of the microscopic theory is still three-dimensional, because the ultraviolet scale $k_\Lambda = \Lambda$ ensures $L\Lambda \gg 1$. Figure taken from Lammers et al. (2016).

The flow equations coincide $\dot{U}_k = \dot{U}_{3\mathrm{D}}$ for $\tilde{L} \gg 1$, while we find $\dot{U}_k = \dot{U}_{2\mathrm{D}}/L$ for $\tilde{L} \ll 1$. Because we start with a three-dimensional system, the factor $1/L$ is there from dimensional reasons to arrive at a two-dimensional system. The crossover function changes its shape rather rapidly from the three-dimensional behavior for $k > \frac{2\pi}{L}$, where it is essentially constant, to the two-dimensional behavior for $k < \frac{2\pi}{L}$. The oscillatory behavior in the transition region is rapidly damped. In Fig. 4.5 we also show the limiting flow equations for two and three continuous dimensions with dashed red lines. Therefore, the dimensional reduction from three to two dimensions is very effectively realized by the flow and we could approximate this very well by simply switching from three to two dimensions as k decreases below $2\pi/L$. A similar sharp transition has been observed in the τ-direction for the transition between quantum and classical statistics (Tetradis and Wetterich (1993, 1994b)).

Our flow always starts in the symmetry broken regime, where the whole gas is condensed (on a microscopic level). Whenever the order parameter ρ_k vanishes during the flow, we need to activate the flow equation for m_k^2. If this happens we eventually arrive in the disordered regime for $k \to 0$. If the order parameter retains its nonzero

value, however, we are in the symmetry broken phase. In Figs. 4.6 – 4.8 we show the general behavior of ρ_k and m_k^2. Thus, we can determine the superfluid transition temperature T_c by monitoring the flow of $\rho_{0,k}$: It corresponds to the temperature for which $\rho_{0,k\to 0} = m_{k\to 0}^2 = 0$. We can repeat this calculation for every trap size L.

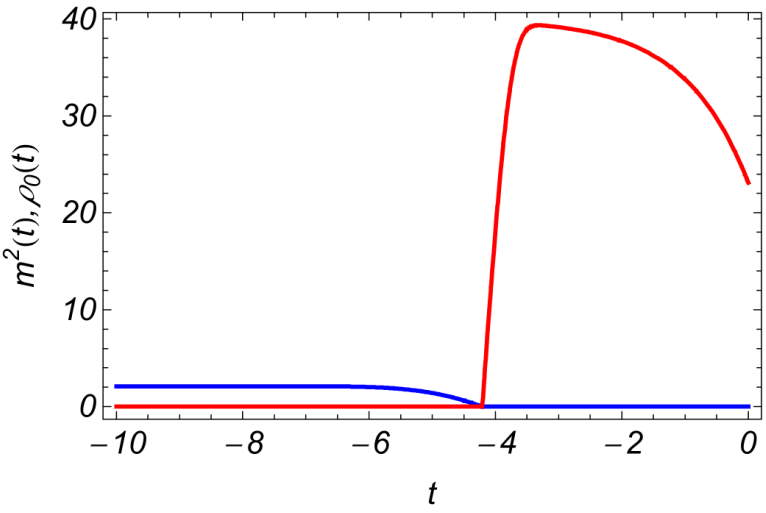

Figure 4.6: We determine in which phase we are by monitoring the flow of the order parameter $\rho_{0,k}$. To match the effective average action with the microscopic action in the ultraviolet, we start with a finite superlfuid density $\rho_{0,\Lambda}$. If the temperature is high enough, thermal fluctuations will destroy the long-range order and $\rho_{0,k}$ will eventually vanish during the flow. This activates the mass term m_k^2 and we arrive in the normal phase for $k \to 0$.

In this way we can plot the superfluid fraction ρ_0/n for different values of L in Fig. 4.9, covering the whole crossover from very small to very large L. Note that even for a two-dimensional system the ratio ρ_0/n of the 3D quantities ρ_0 and n gives the superfluid fraction, since $\rho_0^{2\mathrm{D}} = L\rho_0^{3\mathrm{D}}|_{L\to 0}$ and $n^{2\mathrm{D}} = Ln^{3\mathrm{D}}|_{L\to 0}$, so that L drops out. This is one of the reasons why we plot dimensionless quantities. For vanishing temperature we find $\rho_0/n = 1$, i.e. the whole gas becomes superfluid irrespective of L. But this does not mean that we have a Bose–Einstein condensate. Actually, to observe the condensate, we would need to keep track of the "unrenormalized" $\bar{\rho}$. In the three-dimensional limit the gas develops a small condensate depletion due to interactions (Floerchinger and Wetterich (2008)), which means that not the whole gas is condensed, i.e. $\bar{\rho}/n \lesssim 1$.

In Fig. 4.10 we show the superfluid transition temperature T_c for the whole 2D–3D dimensional crossover. Let us first discuss the three-dimensional limit that we approach for large L. The critical temperature for Bose–Einstein condensation (BEC) T_{BEC} of an

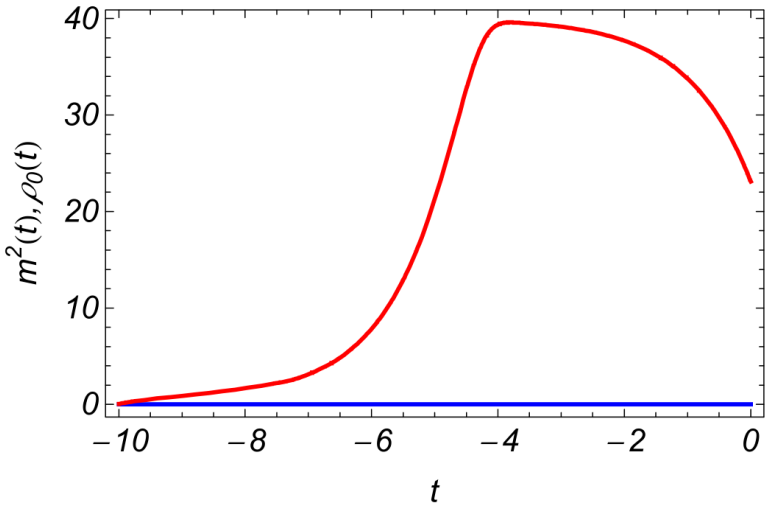

Figure 4.7: Flow at the critical temperature T_c. The temperature is tuned such that the flow of $\rho_{0,k}$ reaches zero asymptotically for $k \to 0$. Right above this temperature the superfluid density vanishes at a finite scale $k > 0$ and the mass term develops a nonzero value. Below the critical temperature the order parameter $\rho_{0,k\to 0}$ does not vanish and the system is in the superfluid phase.

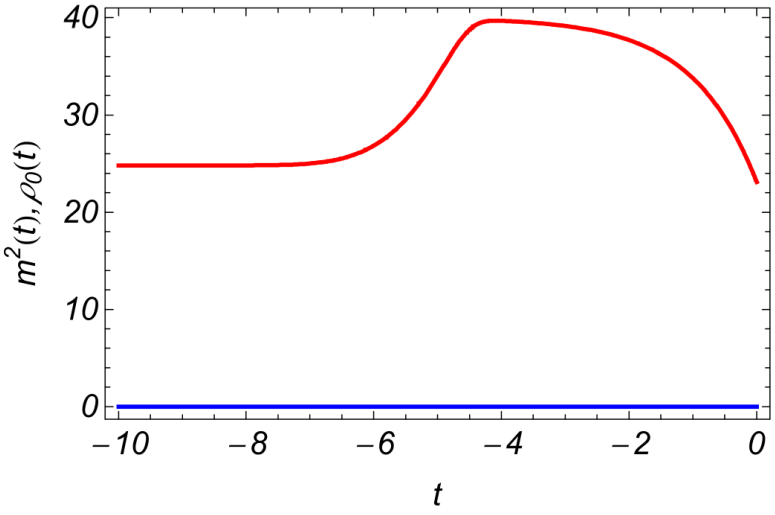

Figure 4.8: For low temperatures, the fluctuations are not strong enough to destroy the superfluid. Thus, we have $\rho_{0,k\to 0} > 0$ and $m^2_{k\to 0} = 0$. We then proceed to calculate the ratio $\rho_{0,k\to 0}/n_{k\to 0}$ to determine the superfluid fraction.

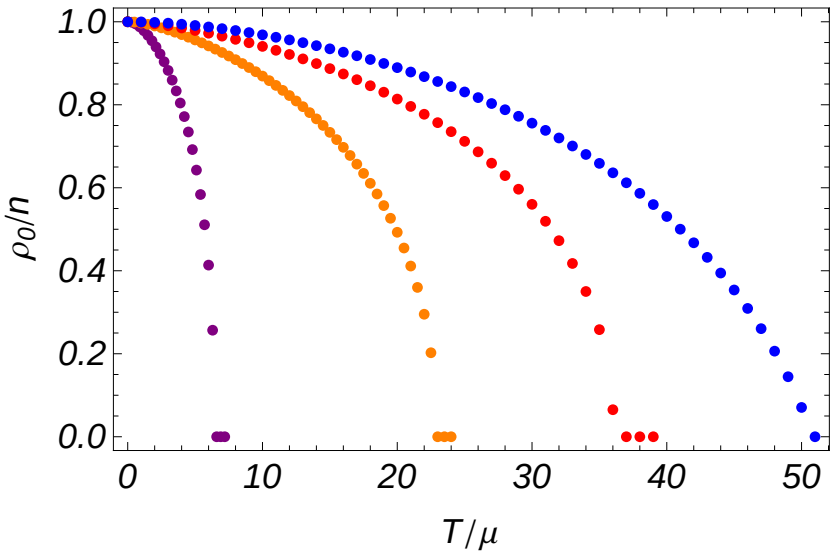

Figure 4.9: Superfluid fraction ρ_0/n at $k \to 0$ for different values of L. Larger values of L correspond to the curves further to the right. The critical temperature, here in units of the chemical potential μ, is higher in more 3D-like systems. For all compactification lengths L we recover the correct limit $\rho_0/n|_{T\to 0} = 1$, where the whole gas is superfluid due to Galilean invariance. The curves correspond to a coupling strength $g_{3D}\sqrt{\mu} = 0.025$. Figure taken from Lammers et al. (2016).

interacting gas is given by

$$\begin{aligned} T_{\mathrm{BEC}} &= T_{\mathrm{c,id}} + \Delta T_{\mathrm{c}}, \\ T_{\mathrm{c,id}} &= \frac{2\pi\hbar^2}{M k_{\mathrm{B}}} \Big(\frac{n}{\zeta(3/2)} \Big)^{2/3} = 6.625 n^{2/3}. \end{aligned} \tag{4.74}$$

We calculated the critical temperature of an ideal three-dimensional Bose gas in Ch. 2.2. Interactions change this transition temperature by a small amount, which we denote by ΔT_{c}. For a sufficiently small gas parameter $a_{3D} n^{1/3}$, this interaction induced shift of the critical temperature is given by (Grüter et al. (1997); Baym et al. (1999))

$$\frac{\Delta T_{\mathrm{c}}}{T_{\mathrm{c,id}}} = \kappa \, a_{3D} n^{1/3}, \tag{4.75}$$

where κ is a constant. Our calculation deduced $\kappa = 2.1$, which retrieves the value found in Ref. (Floerchinger and Wetterich (2008)). It also compares well with the Monte Carlo result (Holzmann and Krauth (1999); Arnold and Moore (2001); Kashurnikov et al. (2001)). Thus, our calculations in the dimensional crossover can reproduce the three-dimensional calculations for large L.

Often, the coupling constant $\lambda_{3D,k\to 0}$ is denoted as g_{3D}. We thus have

$$g_{3D} = 8\pi a_{3D} = \lambda_{3D,k\to 0}. \tag{4.76}$$

At the transition temperature we find $T_c/\mu = 51$ for $g_{3D}\sqrt{\mu} = 0.025$, which is equivalent to $\mu_c = 1.9 g_{3D} n$. We can compare this to Hartree–Fock theory, which predicts $\mu = 2 g_{3D} n$ above the transition temperature.

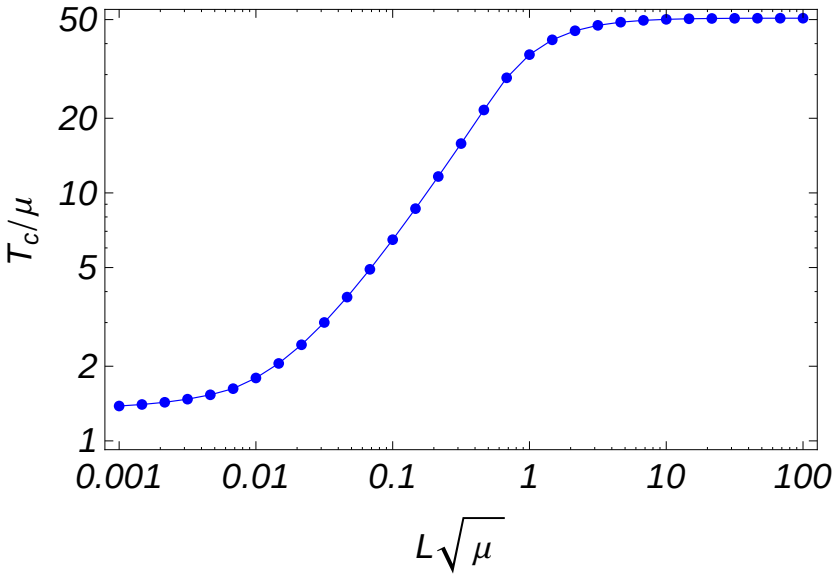

Figure 4.10: Dimensional crossover of the superfluid critical temperature T_c from two to three dimensions. For large L the superfluid transition goes along with Bose–Einstein condensation and the critical temperature coincides with the critical temperature of an interacting three-dimensional Bose gas. For smaller systems, that is for smaller compactification lengths L, the critical temperature is substantially lower. For any value of L we fix the three-dimensional coupling constant to the same value as in Fig. 4.9. This is typically the situation in cold atom experiments, where g_{3D} is controlled by a magnetic Feshbach resonance. Figure taken from Lammers et al. (2016).

What happens when we decrease the trap size L? We see in Fig. 4.10 that the critical temperature decreases and is reduced by a substantial factor as one goes through the crossover. We see that in the limit $L \to 0$ the critical temperature does not saturate to one value. To understand this, first note that we perform the dimensional crossover for a fixed value of a_{3D}, because this quantity is typically fixed by magnetic fields in cold atom experiments. As discussed before, this translates to a coupling λ_Λ^{3D} through the vacuum flow equation (see Eq. (4.28)), and leads to a characteristic behavior of T_c in the 2D limit of small L, which can be understood as follows: For $L \gtrsim \Lambda^{-1}$ the flow in Eq. (4.71) is solely determined by $F(\tilde{L}) \simeq \tilde{L}^{-1}(1 - \frac{\eta}{4})$, and thus resembles a truly two-dimensional renormalization group flow. In particular, this also applies to the initial value of the effectively two-dimensional coupling constant λ_{2D}, which in the

limit $L \to 0$ is given by

$$\lambda_{2\mathrm{D},\Lambda}\Big|_{L\Lambda\gtrsim 1} = \frac{1}{L}\lambda_{3\mathrm{D},\Lambda} \approx 8\pi\frac{a_{3\mathrm{D}}}{L}, \tag{4.77}$$

see Eq. (4.92). Hence, as we decrease L further an further in this regime, we simulate a whole class of strongly-interacting two-dimensional Bose gases, each corresponding to a certain coupling strength $\lambda_{2\mathrm{D}}(L)$ and critical temperature $T_\mathrm{c}(L)$. This is the reason why T_c does not fully saturate for small L, although the dependence becomes rather weak. We perform the dimensional crossover for fixed $a_{2\mathrm{D}}$ in Sec. 4.6.

4.5 2D limit

4.5.1 Effective 2D coupling constant

A particular strength of the functional renormalization group approach is that it can cope with a lot of different length scales. We saw that the flow of couplings can be described by a two-dimensional flow whenever the scale k is below an effective cutoff $\Lambda_\mathrm{eff} \ll L^{-1}$. In particular, if L^{-1} is much larger than the many-body scales $\sqrt{\mu}$ and $\sqrt{T}$, the many-body system can be described by an effective two-dimensional model with UV cutoff Λ_eff. We call this scenario the 2D limit. In this limit, even though we start with a three-dimensional microscopic action, the system experiences the "influence" of the trap quite early during the flow, so that it effectively switches to two-dimensional flow equations, long before many-body effects come into play. The aim of this section is to obtain a relation between $a_{2\mathrm{D}}$ and $a_{3\mathrm{D}}$. We achieve this by relating $\lambda_{2\mathrm{D}}(\Lambda_\mathrm{eff})$ of the effective two-dimensional action to the three-dimensional scattering length and further integrating the flow equations between Λ and Λ_eff in vacuum. We will see that the details of the relation between the two- and three-dimensional scattering lengths depends on the particular compactification or trap potential. Notice that once the renormalized coupling $\lambda_{2\mathrm{D}}(\Lambda_\mathrm{eff})$ is specified, it allows us to determine the many-body properties of the effective 2D system without any further knowledge of the 3D system.

We introduce the momentum scale Λ_eff via

$$\Lambda \gg L^{-1} \gg \Lambda_\mathrm{eff} \gg \sqrt{\mu}, \sqrt{T}. \tag{4.78}$$

Besides these constraints the new scale Λ_eff is arbitrary and will serve as an ultraviolet cutoff of the effective two-dimensional theory.

In the following we consider the regime $k \in [\Lambda_\mathrm{eff}, \Lambda]$ of the renormalization group flow. Since $\Lambda_\mathrm{eff} \gg \sqrt{\mu}, \sqrt{T}$, it is identical to the vacuum flow and characterized by $Z_k = 1$, $\eta = \rho_{0,k} = N_B = 0$, leading to a simple form of Eq. (4.71), which reads

$$\dot{U}(\rho) = \frac{k^5}{8\pi}F_0(\tilde{L})\left(\sqrt{\frac{1+w_1}{1+w_2}} + \sqrt{\frac{1+w_2}{1+w_1}}\right). \tag{4.79}$$

The crossover function $F|_{\eta=0} = F_0$ is evaluated for $\eta = 0$, see Eq. (4.69). In particular, for $\tilde{L} \ll 1$ we are left with

$$\dot{U}(\rho) = \frac{1}{L}\frac{k^4}{8\pi}\left(\sqrt{\frac{1+w_1}{1+w_2}} + \sqrt{\frac{1+w_2}{1+w_1}}\right) = \frac{1}{L}\dot{U}_{2\mathrm{D}}, \tag{4.80}$$

which is the flow equation of the two-dimensional potential defined via $U_{3\mathrm{D}} = \frac{1}{L} U_{2\mathrm{D}}$ and $\rho_{3\mathrm{D}} = \frac{1}{L}\rho_{2\mathrm{D}}$. With these definitions the quantities $w_1 = U'_{3\mathrm{D}}/k^2 = U'_{2\mathrm{D}}/k^2$ and $w_2 = (U'_{3\mathrm{D}} + 2\rho_{3\mathrm{D}} U''_{3\mathrm{D}})/k^2 = (U'_{2\mathrm{D}} + 2\rho_{2\mathrm{D}} U''_{2\mathrm{D}})/k^2$ are invariant. We define $\lambda^{2\mathrm{D}} = U''_{2\mathrm{D}}(0)$, such that the effective 2D coupling strength is given by

$$\lambda^{2\mathrm{D}}_{\Lambda_{\mathrm{eff}}} = \frac{1}{L}\lambda^{3\mathrm{D}}_{\Lambda_{\mathrm{eff}}}. \tag{4.81}$$

The aim is to connect $\lambda^{3\mathrm{D}}_{\Lambda_{\mathrm{eff}}}$ with $\lambda^{3\mathrm{D}}_{\Lambda}$ and further to connect both $\lambda^{3\mathrm{D}}_{\Lambda}$ and $\lambda^{2\mathrm{D}}_{\Lambda_{\mathrm{eff}}}$ with the scattering lengths $a_{3\mathrm{D}}$ and $a_{2\mathrm{D}}$, respectively.

We find that the running of the three-dimensional coupling constant λ_k in vacuum is given by

$$\dot{\lambda}_k = \frac{k^5}{4\pi} F_0(\tilde{L}) \frac{\lambda_k^2}{k^4}. \tag{4.82}$$

We can rewrite this differential equation according to

$$\partial_k \frac{1}{\lambda_k} = -\frac{1}{4\pi} F_0(\tilde{L}) \tag{4.83}$$

and arrive at

$$\frac{1}{\lambda^{3\mathrm{D}}_{\Lambda_{\mathrm{eff}}}} - \frac{1}{\lambda^{3\mathrm{D}}_{\Lambda}} = \frac{1}{4\pi L} \int_{L\Lambda_{\mathrm{eff}}}^{L\Lambda} \mathrm{d}\tilde{L}\; F_0(\tilde{L}). \tag{4.84}$$

Using Eq. (4.81) we can now relate the two-dimensional coupling constant at scale Λ_{eff} with the three-dimensional coupling constant λ_Λ coupling constant via

$$\frac{1}{\lambda^{2\mathrm{D}}_{\Lambda_{\mathrm{eff}}}} = \frac{L}{\lambda^{3\mathrm{D}}_{\Lambda}} + \frac{1}{4\pi} \int_{L\Lambda_{\mathrm{eff}}}^{L\Lambda} \mathrm{d}\tilde{L}\; F_0(\tilde{L}). \tag{4.85}$$

The coupling constants $\lambda^{3\mathrm{D}}_{\Lambda}$ and $\lambda^{2\mathrm{D}}_{\Lambda_{\mathrm{eff}}}$ can be related to the three- and two-dimensional scattering lengths $a_{3\mathrm{D}}$ and $a_{2\mathrm{D}}$ by means of the formulas

$$\begin{aligned} \frac{1}{\lambda^{3\mathrm{D}}_{\Lambda}} &= -\frac{\Lambda}{6\pi^2} + \frac{1}{8\pi a_{3\mathrm{D}}}, \\ \frac{1}{\lambda^{2\mathrm{D}}_{\Lambda_{\mathrm{eff}}}} &= -\frac{1}{8\pi} \log(\Lambda^2_{\mathrm{eff}} a^2_{2\mathrm{D}}) + \frac{1}{8\pi}. \end{aligned} \tag{4.86}$$

see Eqs. (4.127) and (4.128). We previously introduced the relation between $a_{3\mathrm{D}}$ and $\lambda^{3\mathrm{D}}_{\Lambda}$ in Eq. (4.28). If one wants to derive this relation for the two-dimensional case, it is quite difficult to obtain the additional term $+\frac{1}{8\pi}$. Thus, we employ T-matrix calculations below to find the relation in Eq. (4.86).

Finally, we insert the relations in Eq. (4.86) into Eq. (4.85) to obtain

$$a_{2\mathrm{D}} = L \exp\Big\{-\frac{1}{2}\frac{L}{a_{3\mathrm{D}}} + \Phi\Big\} \tag{4.87}$$

with

$$\Phi = \frac{2L\Lambda}{3\pi} - \log(L\Lambda_{\text{eff}}) + \frac{1}{2} - \int_{L\Lambda_{\text{eff}}}^{L\Lambda} \mathrm{d}\tilde{L}\, F_0(\tilde{L}). \tag{4.88}$$

This gives us the desired relation between a_{2D} and a_{3D}. Due to the particular limits of $F(\tilde{L})$ in Eq. (4.73), the artificial scales Λ_{eff} and Λ drop out and we can deduce a_{2D} purely from the values of a_{3D} and L. This is true for any crossover function $F(\tilde{L})$ that satisfies (4.73) and approaches these limits sufficiently fast in the variable $\tilde{L}$. In Sec. 4.8.1 we show how to deduce the crossover function for a box potential and we point out that we cannot take the $\Lambda \to \infty$ limit.

We evaluate the integral numerically to $\Phi = 0$ and are thus left with

$$a_{2D}^{(\text{pbc})} = L\, \exp\Big\{-\frac{1}{2}\frac{L}{a_{3D}}\Big\}. \tag{4.89}$$

Since Λ dropped out of the formula, a new effective cutoff of the two-dimensional theory emerges naturally by L^{-1}. The system lost all information about its third dimension, and its three-dimensional microscopic couplings just served as a way to define the two-dimensional theory with a new effective action. Relations like this have been obtained before, in particular, we can compare with the result obtained in a harmonic trap (Petrov and Shlyapnikov (2001); Bloch et al. (2008); Levinsen and Parish (2015)), which is given by

$$a_{2D} = \ell_z \sqrt{\frac{\pi}{A}} \exp\Big\{-\sqrt{\frac{\pi}{2}}\frac{\ell_z}{a_{3D}}\Big\} \tag{4.90}$$

with $A = 0.905$ and $\ell_z = \sqrt{\hbar/M\omega_0}$ the oscillator length. We can introduce the effective length scale $\ell_z^{\text{eff}} = L/\sqrt{2\pi}$ and an effective constant A_{eff} to completely match our results to Eq. (4.90) according to

$$a_{2D} = \ell_z^{\text{eff}} \sqrt{\frac{\pi}{A_{\text{eff}}}} \exp\Big\{-\sqrt{\frac{\pi}{2}}\frac{\ell_z^{\text{eff}}}{a_{3D}}\Big\}. \tag{4.91}$$

We have $A_{\text{eff}}^{(\text{pbc})} = \frac{1}{2}$ for a confinement along the z-direction with periodic boundary conditions.

Further, from Eqs. (4.81) and (4.86) we can deduce

$$\lambda_{2D,\Lambda_{\text{eff}}} = \frac{1}{L}\lambda_{3D,\Lambda_{\text{eff}}} = \frac{1}{\frac{L}{8\pi a_{3D}} - \frac{L\Lambda_{\text{eff}}}{6\pi^2}}. \tag{4.92}$$

If $a_{3D}/L \to 0$ is sufficiently small, we can ignore the term of order $\mathcal{O}(L\Lambda_{\text{eff}})$ in the denominator. Furthermore, neglecting the logarithmic running of the coupling, we can identify $g_{2D} \approx \lambda_{2D,\Lambda_{\text{eff}}}$ and thus arrive at

$$g_{2D} \approx 8\pi \frac{a_{3D}}{L}. \tag{4.93}$$

Written in terms of $\tilde{g} = g_{2\mathrm{D}}/2$ and ℓ_z^{eff} this assumes the familiar form

$$\tilde{g} \approx \sqrt{8\pi}\frac{a_{3\mathrm{D}}}{\ell_z^{\mathrm{eff}}} \tag{4.94}$$

known from the case of harmonic confinement (Bloch et al. (2008)).

We now employ T-matrix calculations for two reasons. First, we want to compare and benchmark our findings, in particular, we recover the relation between $a_{2\mathrm{D}}$ and $a_{3\mathrm{D}}$ from Eq. (4.89). In the T-matrix approach, the particle-particle loop is integrated directly without the use of a flow equation. It is interesting that we can solve the T-matrix in vacuum exactly, which is related to a decoupling property of the two-body sector in this particular system, see Ref. (Floerchinger (2014)). The route to determining the scattering properties of two particles in a box potential via the T-matrix has also been explored in Ref. (Yamashita et al. (2015)) and Eqs. (4.89) and (4.108) agree with the results therein for $L = 2\pi R$. The second reason why we employ T-matrix calculations is to obtain the additional term $+\frac{1}{8\pi}$ in Eq. (4.86), which is at this point difficult to obtain just with a functional renormalization group analysis.

In these calculations we use a sharp momentum cutoff, so that the momentum integration is equipped with an ultraviolet scale Λ. Since this is a different regularization procedure than the use of the regulator $R_k(Q)$ in Eq. (4.42), we denote the microscopic coupling constant with a superscript (sh), i.e. $\lambda_\Lambda^{(\mathrm{sh})}$.

The low-energy T-matrix $T(E)$ in d noncompact dimensions is defined as

$$\frac{1}{T(E)} = \frac{1}{\lambda_\Lambda^{(\mathrm{sh})}} - \int_{\vec{q}}^{\Lambda} \frac{1}{E + \mathrm{i}0 - 2q^2}, \tag{4.95}$$

where $2q^2 = q^2/2M_{\mathrm{r}}$ is the noninteracting part of the Hamiltonian with reduced mass $M_{\mathrm{r}} = M/2$, see, for instance, Ref. (Morgan et al. (2002); Levinsen and Parish (2015)) for a detailed discussion. We need to renormalize the interaction, since the integral diverges for $\Lambda \to \infty$ and we may use $\lambda_\Lambda^{(\mathrm{sh})}$ to relate to physical quantities $a_{2\mathrm{D}}$ or $a_{3\mathrm{D}}$. In fact, we define (compare to Eq. (2.41))

$$\frac{1}{8\pi a_{3\mathrm{D}}} = \lim_{E\to 0} \frac{1}{T(E)}. \tag{4.96}$$

By evaluating the integral we find

$$\frac{1}{8\pi a_{3\mathrm{D}}} = \frac{1}{\lambda_\Lambda^{(\mathrm{sh})}} + \frac{\Lambda}{4\pi^2}. \tag{4.97}$$

Therefore, the three-dimensional T-matrix evaluates to

$$\frac{1}{T^{3\mathrm{D}}(E)} = \frac{1}{8\pi}\Big(\frac{1}{a_{3\mathrm{D}}} - \sqrt{-(E+\mathrm{i}0)/2}\Big) \tag{4.98}$$

provided we choose

$$\frac{1}{\lambda_{3\mathrm{D},\Lambda}^{(\mathrm{sh})}} = -\frac{\Lambda}{4\pi^2} + \frac{1}{8\pi a_{3\mathrm{D}}}. \tag{4.99}$$

In the two-dimensional case we define the scattering length $a_{2\mathrm{D}}$ via

$$\frac{-\log\left(k^2 a_{2\mathrm{D}}^2\right)}{8\pi} = \frac{1}{T\left(E=2k^2\right)} = \frac{1}{\lambda^{(\mathrm{sh})}_{2\mathrm{D},\Lambda}} - \int_{\vec{q}}^{\Lambda} \frac{1}{2k^2 + \mathrm{i}0 - 2q^2}. \tag{4.100}$$

In contrast to the three-dimensional case, the limit $k \to 0$ does not serve for a definition of the scattering length, since the T-matrix vanishes in this limit. The integral evaluates to

$$\int_{\vec{q}}^{\Lambda} \frac{1}{2k^2 - 2q^2} = -\frac{1}{8\pi} \log\left(\frac{\Lambda^2}{k^2}\right), \tag{4.101}$$

so that the microscopic coupling $\lambda^{(\mathrm{sh})}_{2\mathrm{D},\Lambda}$ can be written in terms of $a_{2\mathrm{D}}$ as

$$\frac{1}{\lambda^{(\mathrm{sh})}_{2\mathrm{D},\Lambda}} = -\frac{1}{8\pi} \log(\Lambda^2 a_{2\mathrm{D}}^2). \tag{4.102}$$

Thus, the two-dimensional T-matrix is given by

$$\begin{aligned} \frac{1}{T^{2\mathrm{D}}(E)} &= -\frac{1}{8\pi} \log\Big(-\frac{(E+\mathrm{i}0)a_{2\mathrm{D}}^2}{2}\Big) \\ &= -\frac{1}{8\pi}\Big[\log\Big(\frac{E a_{2\mathrm{D}}^2}{2}\Big) - \mathrm{i}\pi\Big]. \end{aligned} \tag{4.103}$$

Having suitable definitions for the scattering lengths, we need to find a way to relate the two- and three-dimensional system. We generalize the T-matrix $T(E)$, where the z-direction is confined in a potential well of size L with periodic boundary conditions. We then have the quantization $q_z \to k_n = 2\pi n/L$, $n \in \mathbb{Z}$, for momenta in the z-direction, and need to replace the integration by a summation

$$\int_{-\infty}^{\infty} \frac{\mathrm{d}q_z}{2\pi} \to \sum_{n=-\infty}^{\infty} \frac{\Delta k_n}{2\pi} = \frac{1}{L} \sum_{n=-\infty}^{\infty}. \tag{4.104}$$

We introduce the abbreviation $A = -(E+\mathrm{i}0)/2$ and find

$$\begin{aligned} \frac{1}{T(E,L)} &= \frac{1}{\lambda^{(\mathrm{sh})}_{3\mathrm{D},\Lambda}} + \frac{1}{2L} \sum_n \int^{\Lambda'} \frac{\mathrm{d}^2 q}{(2\pi)^2} \frac{1}{k_n^2 + q^2 + A} \\ &= \frac{1}{\lambda^{(\mathrm{sh})}_{3\mathrm{D},\Lambda}} + \frac{1}{2} \int^{\Lambda'} \frac{\mathrm{d}^2 q}{(2\pi)^2} \frac{\frac{1}{2} + N_B(L\sqrt{q^2+A})}{\sqrt{q^2+A}} \\ &= \frac{1}{\lambda^{(\mathrm{sh})}_{3\mathrm{D},\Lambda}} + \frac{\Lambda' - \sqrt{A}}{8\pi} - \frac{1}{4\pi L} \log(1 - e^{-L\sqrt{A}}), \end{aligned} \tag{4.105}$$

where in the second line we evaluated the summation over the discrete modes, which results in the emergence of the Bose function N_B. To compare and match this result

with the previous found three-dimensional T-matrix, we consider the $L \to \infty$ limit. In this limit $T(E, L)$ reduces to the three-dimensional expression (4.98) provided we choose

$$\frac{1}{\lambda^{(\mathrm{sh})}_{\mathrm{3D},\Lambda}} = -\frac{\Lambda'}{8\pi} + \frac{1}{8\pi a_{\mathrm{3D}}},\ \Lambda' = \frac{2}{\pi}\Lambda. \tag{4.106}$$

Note that Λ and Λ' are not necessarily the same, because Λ' is a UV cutoff for the momenta in the two continuous dimensions. We define the three-dimensional scattering length more formally as

$$\frac{1}{8\pi a_{\mathrm{3D}}} := \lim_{E\to 0}\lim_{L\to\infty} \frac{1}{T(E,L)}. \tag{4.107}$$

We thus have

$$\frac{1}{T(E,L)} = \frac{1}{8\pi}\Big(\frac{1}{a_{\mathrm{3D}}} - \sqrt{A}\Big) - \frac{1}{4\pi L}\log(1 - e^{-L\sqrt{A}}). \tag{4.108}$$

We can now relate the generalized T-matrix with the effective 2D-T-matrix via

$$\frac{1}{T_{\mathrm{2D}}(E)} := \frac{L}{T(E,L)}, \tag{4.109}$$

which, for $E \to 0$ and therefore $A \to 0$ is given by

$$\begin{aligned}
\frac{1}{T_{\mathrm{2D}}(E)} &\overset{A\to 0}{\simeq} \frac{L}{8\pi a_{\mathrm{3D}}} - \frac{1}{4\pi}\log(L\sqrt{A}) \\
&= \frac{L}{8\pi a_{\mathrm{3D}}} - \frac{1}{4\pi}\log\Big(L\sqrt{-\frac{(E+\mathrm{i}0)}{2}}\Big) \\
&\overset{!}{=} -\frac{1}{4\pi}\log\Big(a_{\mathrm{2D}}\sqrt{-\frac{(E+\mathrm{i}0)}{2}}\Big) \\
&= -\frac{1}{8\pi}\log\Big(-\frac{(E+\mathrm{i}0)a_{\mathrm{2D}}^2}{2}\Big).
\end{aligned} \tag{4.110}$$

where in the third line we demand the T-matrix to coincide with the previously found low energy two-dimensional T-matrix (4.103).

Solving for a_{2D} yields the effective two-dimensional scattering length of the confined system

$$a^{(\mathrm{pbc})}_{\mathrm{2D}}(L) = L\exp\Big\{-\frac{1}{2}\frac{L}{a_{\mathrm{3D}}}\Big\}, \tag{4.111}$$

which agrees with the functional renormalization group result in Eq. (4.89).

The second application for the T-matrix calculations is to correctly define the initial conditions for λ_Λ of the renormalization group approach in Eq. (4.86). The T-matrix from Eq. (4.95) can be defined more generally as a function of $P = (p_0, \vec{p})$ by

$$\frac{1}{T(P)} = \frac{1}{\lambda^{(\mathrm{sh})}_{\Lambda}} + \int_Q^\Lambda \frac{1}{\mathcal{P}_\phi(Q+P)\mathcal{P}_\phi(-Q)}, \tag{4.112}$$

where we introduced the notation

$$\mathcal{P}_\phi(Q) = \mathcal{P}_\phi^Q = \mathrm{i}q_0 + q^2 - \mu. \tag{4.113}$$

Again, we can calculate the loop integral to obtain

$$\frac{1}{T(P)} = \begin{cases} \frac{1}{\lambda_{\mathrm{3D},\Lambda}^{(\mathrm{sh})}} + \frac{\Lambda}{4\pi^2} - \frac{1}{8\pi}\sqrt{A} & (d=3) \\ \frac{1}{\lambda_{\mathrm{2D},\Lambda}^{(\mathrm{sh})}} - \frac{1}{8\pi}\log(A/\Lambda^2) & (d=2) \end{cases}, \tag{4.114}$$

where we now have

$$A = \frac{\mathrm{i}p_0}{2} + \frac{p^2}{4} - \mu. \tag{4.115}$$

To recover the usual low energy T-matrix we can set $p^2 = \mu = 0$ and make an analytic continuation to energies E via $\mathrm{i}p_0 \to -(E + \mathrm{i}0)$. To make contact with the running coupling constant λ_k that we use in the functional renormalization group approach, we calculate its flow equation in vacuum (since we are interested in the scattering properties). We can project a flow equation for λ_k from the effective average potential U_k via

$$\dot{\lambda}_k = \dot{U}''(0), \tag{4.116}$$

where

$$\dot{U}(\rho) = \frac{1}{2}\int_Q \dot{R}_k(Q) \frac{L_\phi^Q + L_\phi^{-Q}}{L_\phi^Q L_\phi^{-Q} - (\rho U'')^2} \tag{4.117}$$

and $L_\phi^Q = \mathcal{P}_\phi(Q) + R_k(Q) + U' + \rho U''$. We obtain

$$\begin{aligned} \dot{\lambda}_k &= 2\lambda_k^2 \int_Q \frac{\dot{R}_k(Q)}{(\mathcal{P}_\phi^Q + R_k^Q)^2(\mathcal{P}_\phi^{-Q} + R_k^{-Q})} \\ &= -\lambda_k^2 \partial_t \int_Q \frac{1}{(\mathcal{P}_\phi^Q + R_k^Q)(\mathcal{P}_\phi^{-Q} + R_k^{-Q})}. \end{aligned} \tag{4.118}$$

We can rewrite this according to

$$\partial_t \frac{1}{\lambda_k} = \partial_t \int_Q \frac{1}{(\mathcal{P}_\phi^Q + R_k^Q)(\mathcal{P}_\phi^{-Q} + R_k^{-Q})}. \tag{4.119}$$

Thus, the running coupling λ_k is given by

$$\begin{aligned} \frac{1}{\lambda_k} &= \frac{1}{\lambda_\Lambda} + \int_Q \left(\frac{1}{(\mathcal{P}_\phi^Q + R_k^Q)(\mathcal{P}_\phi^{-Q} + R_k^{-Q})} - \frac{1}{(\mathcal{P}_\phi^Q + R_\Lambda^Q)(\mathcal{P}_\phi^{-Q} + R_\Lambda^{-Q})} \right) \\ &= \frac{1}{\lambda_\Lambda} + \frac{1}{2}\int_{\vec{q}} \Big(\frac{1}{q^2 + R_k(q)} - \frac{1}{q^2 + R_\Lambda(q)} \Big) \\ &\overset{(4.121)}{=} \frac{1}{\lambda_\Lambda} + \frac{1}{2}\int_{\vec{q}}^{\Lambda} \frac{1}{q^2 + R_k(q)} - \frac{1}{2}\int_{\vec{q}}^{\Lambda} \frac{1}{\Lambda^2}. \end{aligned} \tag{4.120}$$

In the last line we employed the particular form of the Litim-type regulator that we use in this thesis

$$R_k(q) = (k^2 - q^2)\theta(k^2 - q^2). \tag{4.121}$$

The last term in Eq. (4.120) evaluates to

$$\frac{1}{2}\int_{\vec{q}}^{\Lambda} \frac{1}{\Lambda^2} = \begin{cases} \frac{\Lambda}{12\pi^2} & (d=3), \\ \frac{1}{8\pi} & (d=2). \end{cases} \tag{4.122}$$

This term depends on the choice of regulator and is in general different for other regulators. Again, we can generalize this to a P-dependent scattering vertex by defining

$$\partial_t \frac{1}{\lambda_k(P)} := \partial_t \int_Q \frac{1}{(\mathcal{P}_\phi^{Q+P} + R_k^{Q+P})(\mathcal{P}_\phi^{-Q} + R_k^{-Q})}, \tag{4.123}$$

where we can take the limit $k \to 0$ for nonvanishing P to obtain

$$\frac{1}{\lambda_{k=0}(P)} = \frac{1}{\lambda_\Lambda} + \int_Q^{\Lambda} \frac{1}{\mathcal{P}_\phi^{Q+P}\mathcal{P}_\phi^{-Q}} - \frac{1}{2}\int_{\vec{q}}^{\Lambda} \frac{1}{\Lambda^2}, \tag{4.124}$$

where we used $R_{k=0} = 0$. Comparing this to Eq. (4.112) for the generalized T matrix $T(P)$ we conclude that we can identify

$$T(P) = \lambda_{k=0}(P). \tag{4.125}$$

Thus, we found the desired relation which "translates" the coupling constants according to

$$\frac{1}{\lambda_\Lambda^{(\mathrm{sh})}} = \frac{1}{\lambda_\Lambda} - \frac{1}{2}\int_{\vec{q}}^{\Lambda} \frac{1}{\Lambda^2}. \tag{4.126}$$

We find that the correct initial conditions for λ_Λ in two and three dimensions in terms of the scattering lengths is given by

$$\frac{1}{\lambda_\Lambda^{\mathrm{3D}}} = -\frac{\Lambda}{6\pi^2} + \frac{1}{8\pi a_{\mathrm{3D}}} \tag{4.127}$$

and

$$\frac{1}{\lambda_\Lambda^{\mathrm{2D}}} = -\frac{1}{8\pi}\log(\Lambda^2 a_{\mathrm{2D}}^2) + \frac{1}{8\pi}. \tag{4.128}$$

4.5.2 True 2D gas

In cold atom experiments, the two-dimensional coupling strength is commonly expressed by the coupling constant $\tilde{g} = (M/\hbar^2)g_{\mathrm{2D}} = g_{\mathrm{2D}}/2$. Due to the logarithmic energy dependence of the T-matrix in two dimensions the coupling g_{2D} needs to be defined with respect to a fixed energy or momentum scale. However, this scale dependence is only logarithmic and $\tilde{g}$ appears to be effectively constant in experiments. One

choice is to define the coupling strength at the momentum scale $k_n = \sqrt{n_{2D}}$, where $n_{2D} = Ln_{3D}$ is the two-dimensional density. For studying the phase transition, however, $T > \mu$ sets the appropriate scale. Thus we define the interaction strength via

$$g_{2D} = 2\tilde{g} = \lambda_{2D,k=\sqrt{T}} \tag{4.129}$$

in the functional renormalization group approach.

The critical phase space density for the BKT transition is $n\lambda_T^2 = \log(\xi/\tilde{g})$ for small couplings $\tilde{g}$. Monte Carlo calculations yield $\xi = 380$ (Prokof'ev et al. (2001); Prokof'ev and Svistunov (2002)). Solving for the superfluid transition temperature T_{BKT} yields

$$T_{\mathrm{BKT}} = \frac{4\pi n_{2D}}{\log(\xi/\tilde{g})}. \tag{4.130}$$

By employing $\mu_c/T = (\tilde{g}/\pi)\log(\xi_\mu/\tilde{g})$ for the critical chemical potential, we may also express the critical temperature for small $\tilde{g}$ by

$$\frac{T_{\mathrm{BKT}}}{\mu} = \frac{\pi}{\tilde{g}}\frac{A}{\log(\xi_\mu/\tilde{g})}. \tag{4.131}$$

Monte Carlo computations (Prokof'ev et al. (2001)) have evaluated the parameters to $A = 1$ and $\xi_\mu = 13.2$.

This limiting formula for the critical temperature of a two-dimensional superfluid Bose gas can be studied independently of the details of the dimensional crossover. For this calculation we set $\Lambda/\sqrt{\mu} = 10^3$ as before, and vary the values of $t_{\mathrm{f}} = \log(k_{\mathrm{f}}/\Lambda)$ and $\lambda_{2D,\Lambda}$.

In the dimensional crossover we have used $t_{\mathrm{f}} = -10$. For this choice we can reproduce the asymptotic form of Eq. (4.131) and find for the parameters $A = 0.99$ and $\xi_\mu = 6.0$. We visualize the coupling dependence of the critical temperature in Fig. 4.11. To check if this result depends on the infrared scale k_{f} we vary t_{f} in a reasonable range. Again we can reproduce the scaling behavior according to Eq. (4.131) with only mild variations of the parameters A and ξ_μ, as shown in Tab. 4.1. We obtained the values from a fit of T_{c}/μ to Eq. (4.131) in the interval $g_{2D} \in [10^{-4}, 0.01]$.

t_{f}	-8	-9	-10	-11	-12
A	0.94	0.98	0.99	0.99	0.99
ξ_μ	5.1	5.3	6.0	6.6	7.2

Table 4.1: Fitting parameters obtained from matching the critical temperature T_{c}/μ for different values of $t_{\mathrm{f}} = \log(k_{\mathrm{f}}/\Lambda)$ to Eq. (4.131) in the interval $g_{2D} \in [10^{-4}, 0.01]$.

The parametric form in Eq. (4.131) was also obtained with the functional renormalization group in Ref. (Rançon and Dupuis (2012)), where T_{BKT} was determined in a different manner than employed here, yielding $A = 0.982$ and $\xi_\mu = 9.48$.

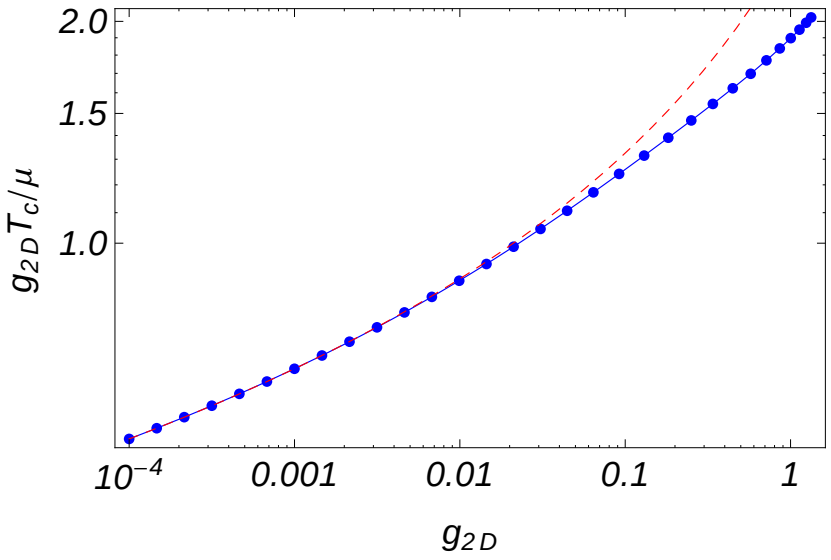

Figure 4.11: Critical temperature T_c/μ in two dimensions as a function of g_{2D} over four orders of magnitude. For better comparability with Eq. (4.131) we have multiplied the function by g_{2D}. The blue points and solid line constitute the result of functional renormalization group calculations for $t_f = -10$, whereas the red dashed line corresponds to the asymptotic form of Eq. (4.131) for small g_{2D}. For the dashed line we use the fit result from Tab. 4.1. Figure taken from Lammers et al. (2016).

4.6 Dimensional crossover for fixed a_{2D}

In the last sections we extracted physical properties of a Bose gas in a dimensional crossover where we fixed the three-dimensional scattering length a_{3D}. This follows a typical cold atom experiment protocol, where a_{3D} is fixed by means of an external magnetic field B, and decreasing the trap size L leads to a quasi-two-dimensional system. In this section we want to answer the question: If we attempt to quantum simulate two-dimensional systems, can we be sure to actually measure the two-dimensional critical temperature, given $L \neq 0$? Thus, we want to perform the dimensional crossover for fixed a_{2D}. In order to do this we need to choose the initial conditions for the flow equations rather carefully.

First of all, Eq. (4.86) implies that a_{3D} cannot be arbitrary large within our model with pointlike interactions. For a given fixed value of the ultraviolet scale Λ, the scattering length is bounded from above according to $a_{3D} < a_{\max} = (\frac{4\Lambda}{3\pi})^{-1} = 2.36\Lambda^{-1}$, see Ref. (Floerchinger and Wetterich (2008)). From this it can be deduced that for $\Lambda \to \infty$ we have $a_{3D} \to 0$, which means that the pointlike interaction approximation cannot describe the interacting system up to arbitrarily high energies.

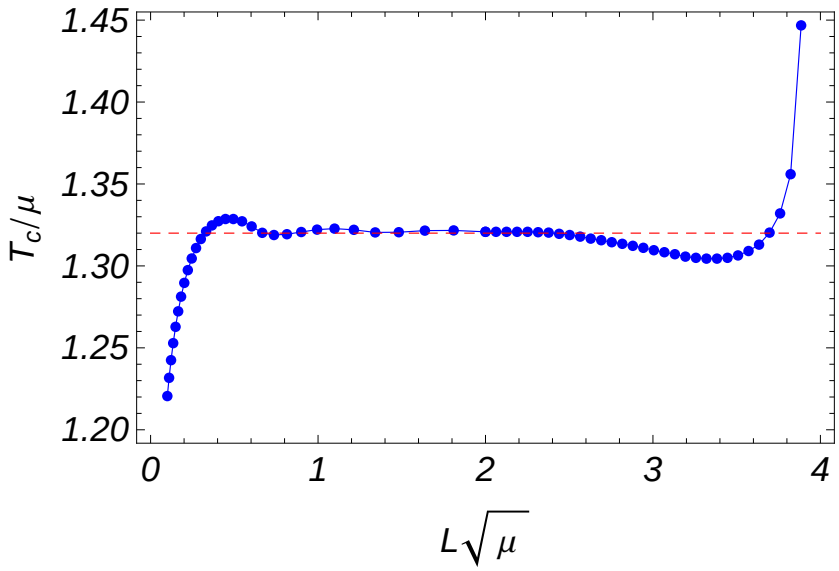

Figure 4.12: Dimensional crossover of the superfluid critical temperature T_c for a fixed value of a_{2D}. One observes three characteristic regimes for the behavior of the critical temperature: (i) For small $0.1 \leq L\sqrt{\mu} \leq 1$, the transition temperature increases. However, since we have chosen $\Lambda/\sqrt{\mu} = 10$ here, this region corresponds to $1 \leq L\Lambda \leq 10$ and thus violates the criterion $L \gg \Lambda^{-1}$. Thus it is not of relevance for this discussion. (ii) For intermediate $L\sqrt{\mu}$, the critical temperature settles at $T_c/\mu = 1.32$ (horizontal dashed line), which is the transition temperature for the corresponding 2D gas with the same value of a_{2D}. In this region, which corresponds to $L/a_{2D} = (1-3)\times 10^3$ in this particular case, the gas is truly two-dimensional. (iii) For larger L, we find an increase of the critical temperature. Note that the crossover scale $L\sqrt{\mu} \approx 3$ between the 2D and the quasi-2D regime is still much larger than $T^{-1/2}$ and $\mu^{-1/2}$. The slight dimple in T_c/μ before the rising seems to root in the same oscillatory crossover behavior as also found for small L, and we do not attribute any deep physical meaning to it at this point. Figure taken from Lammers et al. (2016).

For fixed L we can further deduce $a_{2D} < Le^{-\frac{1}{2}(L/a_{\max})}$ due to Eq. (4.89), which relates a_{2D} to a_{3D}. Thus, in typical experiments with fixed L, the range of accessible a_{2D} is also limited from above.

In this section we want to fix a_{2D} and Λ, where now the above considerations imply that not all values of the trap size L are allowed: We need to determine the possible values of L which realize this particular a_{2D}. Let us define the function $f(x) = 4\pi a_{2D}/\lambda_\Lambda^{3D} = \frac{\log(x)}{x} - \frac{2}{3\pi}(\Lambda a_{2D})$ with $x = L/a_{2D}$. To obtain a stable solution we require $f(x)$ to be positive. Thus, we obtain an interval of allowed x-values, which translates to a stability interval $[L_{\min}, L_{\max}]$ of possible L-values. From Eq. (4.86) we see

that, disregarding some modifications due to the regularization procedure, we have $\Lambda a_{2\mathrm{D}} < 1$. To make things more transparent, if we choose $\Lambda a_{2\mathrm{D}} = 0.1\ (0.01)$ we arrive at $x_{\mathrm{min}} \simeq 1.02\ (1.002)$ and $x_{\mathrm{max}} \simeq 260\ (3900)$. There is one last catch, however, since we still need to satisfy $L\Lambda \gg 1$. Thus the value of L_{min}, obtained from $f(x)$, will typically be too small, such that we set $L_{\mathrm{min}} = \Lambda^{-1}$.

For our discussion of the dimensional crossover at fixed $a_{2\mathrm{D}}$ we employ $\mu = 1$, $a_{2\mathrm{D}} = 10^{-3}$, $\Lambda = 10$ and $k_{\mathrm{f}} = 10^{-2}$. We choose $L_{\mathrm{min}} = \Lambda^{-1}$ from $L\Lambda > 1$ and $L_{\mathrm{max}} = 3885 a_{3\mathrm{D}}$ from the positivity of $f(x)$. The critical temperature of the pure two-dimensional gas for this set of parameters is given by $T_{\mathrm{c}}/\mu = 1.32$. The resulting crossover of the critical temperature is shown in Fig. 4.12, where the horizontal dashed line gives the critical temperature of the two-dimensional system.

We see that the critical temperature coincides with that of the pure two-dimensional system, if we choose $L/a_{2\mathrm{D}}$ sufficiently small. If we increase the trap size L we find that the critical temperature is enhanced. This makes sense, because systems with dimension $2 < d \leq 3$ can develop a condensate, which appears as an additional force to move the system to the superfluid state.

4.7 Anisotropic derivative expansion

We can improve and also check our truncation by including more running couplings and see if they might change the results qualitatively or quantitatively. The derivative expansion employed in Eq. (4.62) is spatially isotropic in the sense that excitations in the planar and transverse directions are treated equally. We might think that this is a bad ansatz due to the confinement in z-direction. Therefore, in the approach of this section, we more generally approximate the kinetic energy of spatial excitations by a dispersion relation

$$E_{\vec{q}} = \frac{1}{\bar{Z}(k)}\Big(A(k)(q_1^2 + \cdots + q_d^2) + A_{\mathrm{z}}(k) q_{d+1}^2\Big), \tag{4.132}$$

where we have in addition to $\bar{Z}(k)$ and $A(k)$ also the k-dependent running coupling $A_{\mathrm{z}}(k)$. This yields an anisotropic generalization of Eq. (4.12) given by

$$\bar{\Gamma}_k[\bar{\phi}^*, \bar{\phi}] = \int_X \Big(\bar{\phi}^*(\bar{Z}\partial_\tau - A\nabla^2 - A_{\mathrm{z}}\partial_z^2)\bar{\phi} + \bar{U}(\bar{\phi}^*\bar{\phi})\Big), \tag{4.133}$$

with $\nabla^2 = \partial_x^2 + \partial_y^2$ and the k-dependence of running couplings is understood implicitly. We write

$$\xi = \frac{A_{\mathrm{z}}}{A},\ \eta_{\mathrm{z}} = -\frac{\dot{A}_{\mathrm{z}}}{A}. \tag{4.134}$$

In this section we only present the main steps to arrive at the flow equations for A_{z} and the other couplings. A more detailed derivation is given in App. A.

First note that the isotropic case corresponds to $\xi = 1$ and $\eta = \eta_{\mathrm{z}}$. Due to $A_\Lambda = A_{z,\Lambda} = 1$ this implies $A = A_{\mathrm{z}}$ for all k. This behavior is recovered in the anisotropic

parametrization for large k. The infrared regulator function is chosen to be

$$R_k(Q) = A\Big(k^2 - q^2 - \xi q_z^2\Big)\theta\Big(k^2 - q^2 - \xi q_z^2\Big) \tag{4.135}$$

with $q^2 = \vec{q}^2 = q_x^2 + q_y^2$. The regulator is designed such that the usual replacement $p^q \to Ak^2$ in the integrand is applicable. Similar to the isotropic case, this allows us to perform the necessary integrations analytically. The β-functions for the effective potential $\bar{U}$ and frequency coefficient $\bar{Z}$ in Eqs. (4.54) and (4.65), respectively, need to be equipped with the modified crossover function

$$\begin{aligned} F_{\text{pbc}}(\tilde{L}) = \frac{2N+1}{\tilde{L}}\Bigg[1 - \frac{\eta}{4} - \frac{1}{\tilde{L}^2}\Big(\xi - \frac{\eta_z}{2}\Big)\frac{4\pi^2}{3}N(N+1) \\ - \frac{\xi(2\eta_z - \xi\eta)}{\tilde{L}^4}\frac{4\pi^4}{15}N(N+1)(-1+3N+3N^2)\Bigg] \end{aligned} \tag{4.136}$$

instead of Eq. (4.55). For the projection of the flow equations for A and A_z, respectively, we employ

$$\begin{aligned} \dot{A} &= \frac{\partial}{\partial p^2}\dot{\bar{G}}^{-1}_{k,22}(0, \vec{p}^2 = p^2, p_z = 0)\Big|_{P=0}, \\ \dot{A}_z &= \frac{\partial}{\partial p_z^2}\dot{\bar{G}}^{-1}_{k,22}(0, \vec{p}^2 = 0, p_z)\Big|_{P=0}. \end{aligned} \tag{4.137}$$

Although q_z is not a continuous variable for $L < \infty$, this is the natural generalization of the appropriate infinite volume projection, see also the definition of $\dot{\bar{Z}}$ from Eq. (4.62). For the anomalous dimensions η and η_z we obtain

$$\begin{aligned} \begin{Bmatrix} \eta \\ \eta_z \end{Bmatrix} = 8\rho_0\lambda^2 \int_Q \frac{1}{\det_Q^2}\Big[(2-\eta)k^2 + \eta q^2 + \eta_z q_z^2\Big] \\ \times \begin{Bmatrix} \frac{1}{d}q^2 \\ \xi^2 q_z^2 \end{Bmatrix}\delta(k^2 - q^2 - \xi q_z^2)\theta(k^2 - q^2 - \xi q_z^2). \end{aligned} \tag{4.138}$$

For $\tilde{L} = \infty$ we can employ $\int_Q q_z^2 = \frac{1}{d}\int_Q q^2$ such that $\eta = \eta_z$ and $\xi = 1$ is a consistent solution. For $\tilde{L} < \infty$, Eqs. (4.138) lead to a linear set of equations for η and η_z, which supplements the remaining flow equations. The flow of the running coupling ξ is given by

$$\dot{\xi} = \eta\xi - \eta_z. \tag{4.139}$$

From the solution of the renormalization group flow in the anisotropic derivative expansion we find the following features: The anomalous dimension η_z follows the behavior of η for $k > \frac{2\pi}{L}$ on average, though in a discontinuous manner. For $k \leq \frac{2\pi}{L}$, η_z vanishes, whereas η remains nonzero. This behavior is displayed in Fig. 4.13. Furthermore the value of $\xi = A_z/A$ at $k = k_f$ remains of order unity. It is close to $\xi = 1$ at zero temperature, whereas it is in the range $\xi \simeq 0.5$-1 at T_c, see Fig. 4.14. Accordingly,

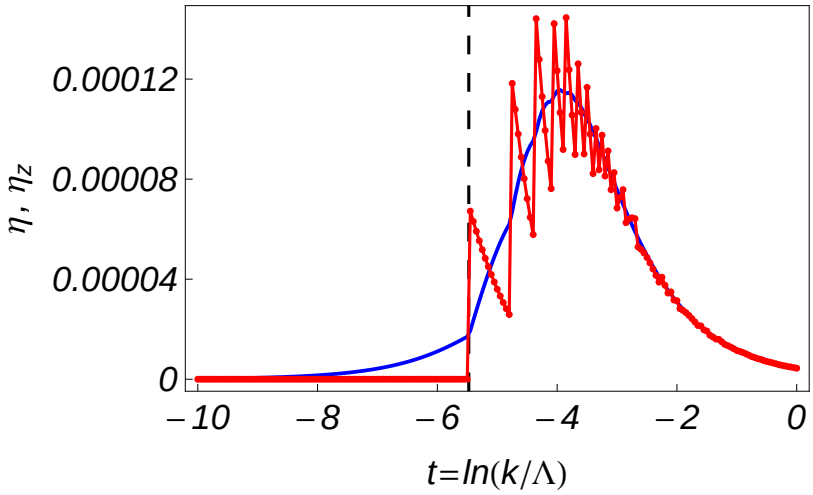

Figure 4.13: Characteristic flow of η and η_z within the anisotropic derivative expansion. We see that the planar anomalous dimension η (blue curve) remains continuous, while the transverse anomalous dimension η_z has discontinuous jumps due to the successive integration of modes and the step function in the regulator, Eq. (4.135). The function $\eta_z(k)$ follows the behavior of $\eta(k)$ on average for $k > \frac{2\pi}{L}$, and vanishes below $k = \frac{2\pi}{L}$ (shown as vertical dashed line). The plot is shown for $T = 0$, $L\sqrt{\mu} = 15$, $g_{3D}\sqrt{\mu} = 0.025$. The qualitative behavior of η and η_z is independent of this choice. Figure taken from Lammers et al. (2016).

excitations in the transverse direction with momentum $q_z \sim L^{-1}$ are still energetically costly for $L \to 0$ and thus decouple from the low-energy physics. We find that the extracted critical temperature T_c as a function of L and g_{3D} is identical to the one of the isotropic derivative expansion within the resolution of Fig. 4.10. This good agreement can be understood from the fact that η_z closely follows the behavior of η, but η itself is small. Hence the influence of η on T_c is already a subleading effect, such that the difference between η and η_z is only a second-order subleading effect.

The good agreement between results within the anisotropic and isotropic derivative expansions justify the use of the isotropic parametrization with $A_z = A$ for the computation of observables.

4.8 Non-homogeneous ground states

As a last chapter we deal with systems that deviate from a box with periodic boundary conditions. The reason why the system with periodic boundary conditions is easier than a system with a box potential with infinite walls is that the ground state is still homogeneous in space. Therefore, the ground state is minimizing not only the effective action, but also the effective potential. However, for nonhomogeneous settings we

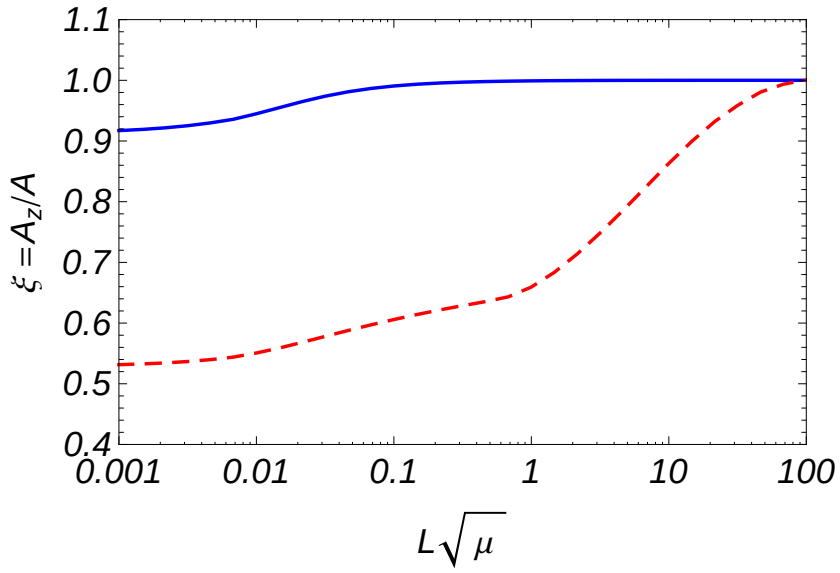

Figure 4.14: Ratio $\xi = A_z/A$ at the lowest momentum k_f with parameters as in Fig. 4.10 for zero temperature (upper curve, blue) and at T_c (lower curve, red). Since ξ is of order unity – and not exceptionally small – the isotropic derivative expansion is sufficient to compute observables like the critical temperature. Figure taken from Lammers et al. (2016).

still might be able to define a modified effective potential, so that within a reasonable approximation its minimum still captures the correct low-energy physics.

4.8.1 Crossover function in a box

Besides the problem of an inhomogeneous ground state in a box potential with infinite walls, the ground state energy E_0 is nonzero. Remember that in a box the boundary conditions lead to a quantization of energies in z-direction

$$E_z = \frac{\hbar^2 \kappa_n^2}{2M} \tag{4.140}$$

with

$$\kappa_n = \frac{\pi n}{L},\ n = 1, 2, \ldots \tag{4.141}$$

Therefore we have a nonvanishing zero-point energy $E_0 = \hbar^2 \pi^2/(2ML^2)$.

To properly address all fluctuations in the system we include an effective chemical potential, which is chosen in such a way that for $k \to 0$ we arrive at the right low energy modes. Motivated by the considerations in Fig. 4.4, we understand the existing modes as "stapled", that is for each κ_n in z-direction we find a whole plane of corresponding (q_x, q_y) modes.

So we can incorporate the effect of the chemical potential essentially via a shift in the momenta

$$\vec{q}_{d+1}^2 \to \vec{q}_{d+1}^2 - \mu \tag{4.142}$$

and the introduction of a modified regulator

$$\begin{aligned} R_k(Q) =& A_k(k^2 - \vec{q}_{d+1}^2)\theta(k^2 - \vec{q}_{d+1}^2) = A_k(k^2 - (q^2 + k_n^2))\theta(k^2 - (q^2 + k_n^2)) \\ \to& A_k(k^2 - (q^2 + k_n^2 - \mu))\theta(k^2 - (q^2 + k_n^2 - \mu)). \end{aligned} \tag{4.143}$$

If we now choose $\mu = \kappa_1^2 = \pi^2/L^2$, then as we lower the momentum scale k we flow smoothly "onto" the lowest lying momentum plane spanned by κ_1. If we performed the calculation similar to a box with periodic boundary conditions without introducing a chemical potential, the flow of the running couplings would stop as soon as k drops below the lowest momentum mode in z-direction. This is clearly the wrong physics, since there are actually fluctuations present with larger spatial extension than L.

Since the derivation of the flow equations is identical to the pbc-calculation, we just present the results here. To obtain the crossover function $F(\tilde{L})$ we just need to replace k_n^2 with $\kappa_n^2 - \mu$, which for $\eta = 0$ reads

$$F(\tilde{L}) = \frac{1}{Lk} \sum_{n=1}^{\infty} \left(1 - \frac{\kappa_n^2 - \mu}{k^2}\right) \theta\left(k^2 - (\kappa_n^2 - \mu)\right). \tag{4.144}$$

The summation is therefore limited to

$$\kappa_n = \frac{\pi}{L} n < \sqrt{k^2 + \mu} = \sqrt{k^2 + \kappa_1^2} \tag{4.145}$$

or

$$n < N = \left\lfloor \sqrt{\left(\tilde{L}/\pi\right)^2 + 1} \right\rfloor \tag{4.146}$$

again with $\tilde{L} = Lk$. With this we can evaluate the sum to arrive at the crossover function in a box

$$F(\tilde{L}) = \frac{N}{\tilde{L}} \left[1 - \frac{1}{\tilde{L}^2} \frac{\pi^2}{6} \left((N+1)(2N+1) - 6\right)\right]. \tag{4.147}$$

First notice that for $k \to 0$ we have $\tilde{L} \to 0$, but the floor function in the definition of N never evaluates to zero. Therefore we actually arrive at the correct low energy limit for $k \to 0$.

As a test we can check if the crossover function has the appropriate limits for $\tilde{L} \to \infty$ and $\tilde{L} \to 0$. This is important to recover the correct 3D and 2D limits of the theory. For large $\tilde{L}$ we may replace $N \to \tilde{L}/\pi$. We find

$$F(\tilde{L}) = \frac{1}{\pi} \left[1 - \frac{\pi^2}{6\pi^2} 2\right] = \frac{2}{3\pi}, \tag{4.148}$$

which is the same limit as it was found for periodic boundary conditions.

For small $\tilde{L}$ we may replace $N \to 1$. We find

$$F(\tilde{L}) = \frac{1}{\tilde{L}}\left[1 - \frac{\pi^2}{6}(2 \cdot 3 - 6)\right] = \frac{1}{\tilde{L}}, \tag{4.149}$$

which again is the correct limit to reproduce the 2D flow equations.

In Sec. 4.5.1 we showed how an effective 2D scattering length is inherited from a 3D scattering length. From Eqs. (4.150) and (4.151) we know that this relation only depends on the particular crossover function, which is characteristic for the respective system,

$$a_{2D} = L \exp\left\{-\frac{1}{2}\frac{L}{a_{3D}} + \Phi\right\} \tag{4.150}$$

with

$$\Phi = \frac{2L\Lambda}{3\pi} - \log(L\Lambda_{\text{eff}}) + \frac{1}{2} - \int_{L\Lambda_{\text{eff}}}^{L\Lambda} \mathrm{d}\tilde{L}\, F_0(\tilde{L}). \tag{4.151}$$

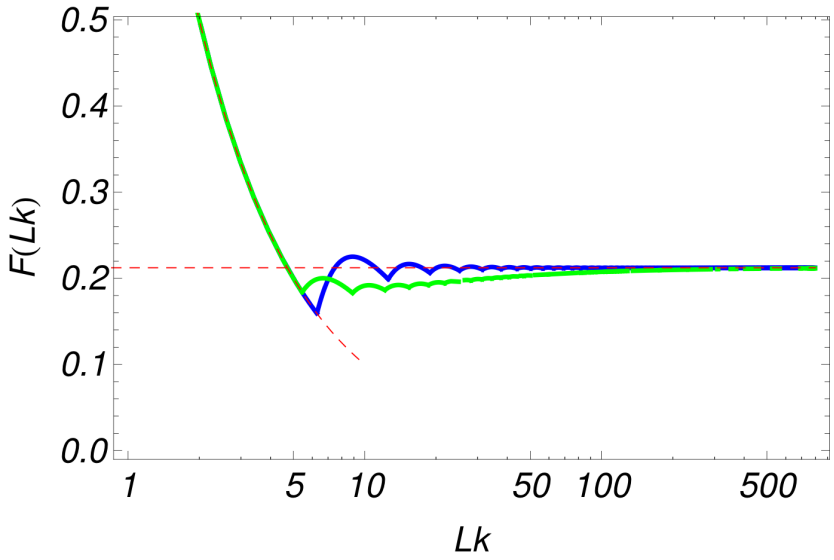

Figure 4.15: The crossover function $F_{\text{box}}(\tilde{L})$ (green) in comparison to the crossover function for periodic boundary conditions (blue). Both crossover functions approach the correct two- and three-dimensional limites. $F_{\text{box}}(\tilde{L})$, however, approaches the three-dimensional limit slower, so that we can not evaluate the integral to obtain a_{2D} for $\Lambda \to \infty$.

Even though the crossover function $F(\tilde{L})$ (4.147) has the correct large $\tilde{L}$ limit, it does not approach this fast enough. We can see this when we expand F for large values of

$\tilde{L}$. In this case we can replace

$$N = \left\lfloor \sqrt{(\tilde{L}/\pi)^2 + 1} \right\rfloor \to \tilde{L}/\pi - 1/2, \tag{4.152}$$

which leads to

$$F(\tilde{L}) = \frac{2}{3\pi} - \frac{1}{2\tilde{L}} \left(+ \frac{13}{12} \frac{\pi}{\tilde{L}^2} \right). \tag{4.153}$$

We see that this leads to a logarithmic divergence of the integral for large $\tilde{L}$

$$\begin{aligned} &\frac{2}{3\pi}\Lambda - \int_a^\Lambda \mathrm{d}\tilde{L} F(\tilde{L}) \\ =&\frac{2}{3\pi}\Lambda + \frac{2}{3\pi}a - \frac{1}{2}\log(a) - \frac{2}{3\pi}\Lambda + \frac{1}{2}\log(\Lambda) \\ =&f(a) + \frac{1}{2}\log(\Lambda). \end{aligned} \tag{4.154}$$

We show the shape of the crossover function F_{box} in Fig. 4.15 in comparison to the crossover function F_{pbc}. Future work needs to show how to understand and interprete the logarithmic divergence, which does not exist in the system with periodic boundary conditions.

4.8.2 Approximate flow equations in a harmonic trap

Up to now we have only considered systems where the eigenfunctions in z-direction could be sensibly written as a superposition of plane waves with momenta q_z. Depending on the boundary conditions the momenta were quantized either as

$$k_n = \frac{2\pi n}{L}, \quad n \in \mathbb{Z}, \tag{4.155}$$

or, in the case of infinitely high walls, as

$$\kappa_n = \frac{\pi n}{L}, \quad n = 1, 2, 3, \ldots. \tag{4.156}$$

In ultracold quantum experiments, however, the external magnetic trap is in good approximation given by a harmonic potential $V(\vec{x})$

$$V(\vec{x}) = \frac{1}{2} M \omega^2 z^2, \tag{4.157}$$

where ω is the trapping frequency. The potential can be rewritten as

$$V(\vec{x}) = V(z) = \frac{1}{2}\hbar\omega \left(\frac{z}{\alpha}\right)^2, \tag{4.158}$$

where

$$\alpha = \sqrt{\frac{\hbar}{M\omega}} \tag{4.159}$$

is the typical length scale in the potential and $\hbar\omega$ the typical energy.

To incorporate these trapping effects right from the beginning, we need to modify the microscopic action accordingly. We have

$$S[\varphi] = \int_X \varphi^* \Big(\partial_\tau - \nabla^2 - \mu + V(z)\Big)\varphi + \frac{\lambda}{2}(\varphi^*\varphi)^2 \tag{4.160}$$

where we also allow for an effective chemical potential, which we will use to arrive at the correct infrared limit for $k \to 0$, see the discussion in Sec. 4.8.1. For the effective average action we employ the ansatz

$$\Gamma_k[\phi] = \int_X \phi^* \Big(\partial_\tau - \nabla^2 - \mu + V(z)\Big)\phi + U(\rho). \tag{4.161}$$

In this approximation we set the anomalous dimension $\eta = 0$. We can again work in the real field basis

$$\phi(X) = \frac{1}{\sqrt{2}}(\phi_1(X) + \mathrm{i}\phi_2(X)) \tag{4.162}$$

and repeat the functional derivatives, see App. A, to arrive at the inverse propagator in position space

$$\bar{\Gamma}_k^{(2)}(X,Y) = \begin{pmatrix} -\nabla^2 + V(z) - \mu + U' + 2\rho U'' & \mathrm{i}\partial_\tau \\ -\mathrm{i}\partial_\tau & -\nabla^2 + V(z) - \mu + U' \end{pmatrix}_X \delta(X-Y). \tag{4.163}$$

where we have already inserted $\phi_1(X) = \sqrt{2\rho(\vec{x})}$ and $\phi_2(X) = 0$.

It is now natural to use the eigenstates of the harmonic oscillator for the function expansion in z-direction. The eigenstates are given by

$$\psi_n(z) = \frac{M\omega}{\hbar\pi}^{1/4} \frac{1}{(2^n n!)^{1/2}} e^{-\frac{M\omega}{\hbar}\frac{z^2}{2}} H_n\left(\left(\frac{M\omega}{\hbar}\right)^{1/2} z\right), \tag{4.164}$$

where

$$H_n(z) = (-1)^n e^{z^2} \frac{\mathrm{d}^n}{\mathrm{d}z^n}\left(e^{-z^2}\right), \quad H_0(z) = 1 \tag{4.165}$$

are the Hermite polynomials.

The transformation we are using therefore reads

$$\begin{aligned}\Gamma_k^{(2)}(Q,Q') = \int_{(x_0,y_0,\vec{x}_{2\mathrm{D}},\vec{y}_{2\mathrm{D}})} \int_{(z,z')} \Gamma_k^{(2)}(X,Y) e^{\mathrm{i}(x_0 q_0 + y_0 q_0' + \vec{x}_{2\mathrm{D}}\vec{q}_{2\mathrm{D}} + \vec{y}_{2\mathrm{D}}\vec{q}'_{2\mathrm{D}})} \\ \times \psi_n(z)\psi_{n'}(z')\delta(X-Y),\end{aligned} \tag{4.166}$$

with $Q = (q_0, \vec{q}_{2\mathrm{D}}, n)$. Essentially we now have to consider four different terms:

- ∂_τ
- $-\partial_x^2 - \partial_y^2$

- $-\partial_z^2 + V(z)$
- U' and $2\rho(\vec{x})U''$

The first two terms do not depend on z, therefore the calculation follows the one in App. A. The z and z' integrations in the calculation yield

$$\begin{aligned}&\int_z \int_{z'} \psi_n(z)\psi_{n'}(z')\delta_{zz'} \\ &= \int_z \psi_n(z)\psi_{n'}(z) \\ &= \delta_{nn'},\end{aligned} \tag{4.167}$$

where in the last equation we used the completeness relation for the eigenfunctions. Since the other transformations are independent of z, we are left with

$$\left(\frac{q_x^2}{2M} + \frac{q_y^2}{2M}\right) \delta_{q_0}\delta_{q_{2\mathrm{D}}}\delta_{nn'}, \tag{4.168}$$

where $\delta_{q_0} = \delta(q_0 - q_0')$ and the same for $\delta_{q_{2\mathrm{D}}}$.

To evaluate the third term we first reintroduce units to make the calculation and the result more transparent. The critical part of the transformation reads

$$I_3 = \int \cdots \int e^{\cdots} \left(-\frac{\hbar^2}{2M}\partial_z^2 + \frac{\hbar\omega}{2\alpha^2}z^2\right) \psi_n(z)\psi_{n'}(z')\delta(z - z'). \tag{4.169}$$

Again, since these terms do only depend on z, we obtain delta-functions for the q_0 and $\vec{q}_{2\mathrm{D}}$ integrals. The derivative ∂_z only acts on the first ψ. We evaluate the delta-function $\delta_{zz'}$ and write

$$I_3 = \delta_{q_0}\delta_{\vec{q}_{2\mathrm{D}}} \int_z \psi_{n'}(z) \left(-\frac{\hbar^2}{2M}\partial_z^2 + \frac{\hbar\omega}{2\alpha^2}z^2\right) \psi_n(z). \tag{4.170}$$

We may use the tricks from quantum mechanics to solve this integral. In particular, we introduce ladder operators

$$\begin{aligned}z^2 &= \frac{\alpha^2}{2}(a^\dagger + a)^2 \\ \partial_z^2 &= \frac{1}{2\alpha^2}(a^\dagger - a)^2\end{aligned} \tag{4.171}$$

to obtain

$$I_3 = \delta_{q_0}\delta_{\vec{q}_{2\mathrm{D}}} \int_z \psi_{n'}(z) \left(\frac{\hbar\omega}{4}\right) \left(-(a^\dagger - a)^2 + (a^\dagger + a)^2\right) \psi_n(z) \tag{4.172}$$

where we have inserted $\alpha^2 = \hbar/M\omega$. We write this in the intuitive bra-ket notation

$$I_3 = \delta_{q_0}\delta_{\vec{q}_{2\mathrm{D}}} \frac{\hbar\omega}{4} \left\langle n' \right| - (a^\dagger - a)^2 + (a^\dagger + a)^2 \left| n \right\rangle \tag{4.173}$$

and use

$$\begin{aligned} a^\dagger |n\rangle &= \sqrt{n+1}\,|n+1\rangle\,, \\ a\,|n\rangle &= \sqrt{n}\,|n-1\rangle\,, \\ N\,|n\rangle &= a^\dagger a\,|n\rangle = n\,|n\rangle \end{aligned} \tag{4.174}$$

to evaluate the integral to

$$\begin{aligned} I_3 &= \delta_{q_0}\delta_{\vec{q}_{2\mathrm{D}}}\frac{\hbar\omega}{4}\left\langle n'\right| 2(a^\dagger a + aa^\dagger)\,|n\rangle \\ &= \delta_{q_0}\delta_{\vec{q}_{2\mathrm{D}}}\frac{\hbar\omega}{4}\left\langle n'\right| 2(2a^\dagger a + \underbrace{[a,a^\dagger]}_{1})\,|n\rangle \\ &= \delta_{q_0}\delta_{\vec{q}_{2\mathrm{D}}}\hbar\omega\left\langle n'\right| N+\frac{1}{2}\,|n\rangle \\ &= \delta_{q_0}\delta_{\vec{q}_{2\mathrm{D}}}\hbar\omega\left(n+\frac{1}{2}\right)\delta_{nn'} \end{aligned} \tag{4.175}$$

and we recover the eigenenergies of the harmonic oscillator. To this point the inverse propagator reads

$$\begin{aligned} &\bar{\Gamma}_k^{(2)}(Q,Q') \\ &= \begin{pmatrix} q_x^2+q_y^2+\hbar\omega(n+\frac{1}{2})-\mu+\widetilde{U'}+2\widetilde{\rho U''} & -q_0 \\ q_0 & q_x^2+q_y^2+\hbar\omega(n+\frac{1}{2})-\mu+\widetilde{U'} \end{pmatrix}\delta_{q_0}\delta_{\vec{q}_{2\mathrm{D}}}\delta_{nn'}. \end{aligned} \tag{4.176}$$

Actually this is not quite correct, because we have just assumed that $\widetilde{U'}$ and $\widetilde{\rho U''}$ are proportional to $\delta_{nn'}$. This is, however, not correct, as we will see below.

In position space we again employ a Taylor expansion of the effective potential which is now, however, still z-dependent

$$U = m^2(\rho(\vec{x})-\rho_0(\vec{x})) + \frac{\lambda}{2}(\rho(\vec{x})-\rho_0(\vec{x}))^2. \tag{4.177}$$

Thus, the terms U' and $\rho U''$ are not that easy to transform anymore, since they now depend on z. We find

$$\begin{aligned} U' &= m^2 + \lambda(\rho(\vec{x})-\rho_0(\vec{x})), \\ U'' &= \lambda. \end{aligned} \tag{4.178}$$

Since we assume the couplings m^2 and λ to be independent of z, we find that essentially we have to transform $\rho(\vec{x})$. Besides the delta-functions for q_0 and $\vec{q}_{2\mathrm{D}}$ we have the integral

$$\int_z \rho(\vec{x})\psi_n(z)\psi_{n'}(z). \tag{4.179}$$

Next, we assume that the density is homogeneous in the two continuous dimensions, which is the same assumption that we used in the rest of this thesis, and furthermore

we expand the z-density in functions ψ_m^2 via

$$\rho(\vec{x}) = \rho_{2\mathrm{D}}\rho_z(z) = \rho_{2\mathrm{D}} \sum_m \alpha_m \psi_m^2(z). \tag{4.180}$$

This is a very natural way to expand the density: First of all, it is a sum of nonnegative terms and the unit of ψ_m^2 is the same as the unit of ρ_z, i.e. $1/L$. Thus, α_m are numbers. For low temperatures and strongly confined potentials, the ideal gas is dominated by the α_0-contribution. We make the assumption that this still holds for the interacting case and only consider the lowest lying mode , i.e. $m = 0$. The truncation can be improved by incorporating higher orders. The integral then reads

$$\begin{aligned} &\int_z \rho(\vec{x})\psi_n(z)\psi_{n'}(z) = \rho_{2\mathrm{D}} \int_z \rho_z(z)\psi_n(z)\psi_{n'}(z) \\ &= \rho_{2\mathrm{D}}\alpha_0 \int_z \psi_0^2(z)\psi_n(z)\psi_{n'}(z). \end{aligned} \tag{4.181}$$

The integral

$$I_{0nn'} = \int_z \psi_0^2 \psi_n \psi_{n'} \tag{4.182}$$

is further approximated by its diagonal contributions, that is we set $I_{0nn'} = 0$ for $n \neq n'$. This is, however, a crude approximation and further research might be able to improve this step in the future. However, this makes the inversion easier to obtain the regulated propagator. Further, the remaining integral has a simple closed form (Wang (2009))

$$I_{0nn} = \frac{1}{\sqrt{2\pi}} \frac{(2n)!}{(n!)^2 2^{2n}}, \tag{4.183}$$

which is very well approximated by

$$I_{0nn} = \frac{1}{\pi\sqrt{2n}} \tag{4.184}$$

for large n. Thus, the transformed $\tilde{\rho}$ is given by

$$\begin{aligned} \tilde{\rho} &= \int_z \rho(\vec{x})\psi_n(z)\psi_n(z) \\ &= \rho_{2\mathrm{D}}\alpha_0 \int_z \psi_0^2(z)\psi_n(z)\psi_n(z) \\ &= \tilde{\rho}_{2\mathrm{D}} I_{0nn} \end{aligned} \tag{4.185}$$

with $\tilde{\rho}_{2\mathrm{D}} = \rho_{2\mathrm{D}}\alpha_0$. Thus we can evaluate

$$\widetilde{U'} = m^2 + \lambda\widetilde{\Delta\rho} \tag{4.186}$$

with $\Delta\rho = \rho - \rho_0$ and the tilde denoting the transformation as in Eq. (4.185). Further, we have

$$\widetilde{\rho U''} = \tilde{\rho}\lambda. \tag{4.187}$$

Let us define the dimensionless quantities w_1 and w_2 in analogy to Eq. (4.53) and below as

$$\begin{aligned} w_1 &= \widetilde{U'} \\ w_2 &= \widetilde{U'} + 2\widetilde{\rho U''}. \end{aligned} \tag{4.188}$$

Notice that w_1 and w_2 now depend on n.

The inverse propagator now reads

$$\Gamma_k^{(2)}(Q,Q') = \begin{pmatrix} q^2 + \omega(n+\frac{1}{2}) - \mu + w_2 k^2 & -q_0 \\ q_0 & q^2 + \omega(n+\frac{1}{2}) - \mu + w_1 k^2 \end{pmatrix} \delta_{QQ'}, \tag{4.189}$$

where we used $\hbar = 2M = 1$. We set $\mu = \hbar\omega/2$ and choose the regulator

$$\begin{aligned} R &= \left(k^2 - (q^2+\omega n)\right)\theta\left(k^2-(q^2+\omega n)\right), \\ \dot{R} &= 2k^2\theta\left(k^2-(q^2+\omega n)\right). \end{aligned} \tag{4.190}$$

With

$$(\Gamma_k^{(2)} + R_k)^{-1}(Q,Q') = G(Q)\delta(Q+Q') \tag{4.191}$$

we obtain

$$G(Q) = \frac{1}{\mathrm{det}_Q}\begin{pmatrix} p^q + w_1 k^2 & q_0 \\ -q_0 & p^q + w_2 k^2 \end{pmatrix}, \tag{4.192}$$

where

$$\begin{aligned} \mathrm{det}_Q &= (p^q + w_1 k^2)(p^q + w_2 k^2) + q_0^2, \\ p^q &= q^2 + \omega n + \left(k^2 - (q^2+\omega n)\right)\theta\left(k^2-(q^2+\omega n)\right) \\ &= k^2 \text{ for } q^2 < (k^2 - \omega n). \end{aligned} \tag{4.193}$$

The flow equation for the effective potential therefore reads

$$\begin{aligned} \dot{\tilde{U}} &= \frac{1}{2}\mathrm{tr}\int_Q \frac{1}{\mathrm{det}_Q}\begin{pmatrix} p^q + w_1 k^2 & q_0 \\ -q_0 & p^q + w_2 k^2 \end{pmatrix} 2k^2\theta\left(k^2-(q^2+\omega n)\right) \\ &= \int_Q \frac{1}{\mathrm{det}_Q}\left(p^q + \frac{w_1+w_2}{2}k^2\right) 2k^2\theta\left(k^2-(q^2+\omega n)\right) \\ &= T\sum_{\omega_n}\sum_n 4v_2\int_0^\infty \mathrm{d}qq\frac{p^q + \frac{k^2}{2}(w_1+w_2)}{\mathrm{det}_Q} 2k^2\theta\left(k^2-(q^2+\omega n)\right) \\ &= 4v_2 T\sum_{\omega_n}\sum_n \int_0^{\sqrt{k^2-\omega n}} \mathrm{d}qq\frac{2+w_1+w_2}{(1+w_1)(1+w_2)+\left(\frac{q_0}{k^2}\right)^2}\theta(k^2-\omega n) \end{aligned} \tag{4.194}$$

Next, we insert $v_2 = 1/(8\pi)$ and evaluate the q-integration and the Matsubara summation to obtain

$$\begin{aligned}\dot{\tilde{U}} &= \frac{1}{2\pi} T \sum_{\omega_n} \sum_{n=0}^{\infty} \frac{2 + w_1 + w_2}{(1+w_1)(1+w_2) + \left(\frac{q_0}{k^2}\right)^2} \int_0^{\sqrt{k^2-\omega n}} \mathrm{d}q q \theta(k^2 - \omega n) \\ &= \frac{1}{4\pi} \sum_{n=0}^{\infty} \theta(k^2 - \omega n)(2 + w_1 + w_2)(k^2 - \omega n) T \sum_{\omega_n} \frac{1}{(1+w_1)(1+w_2) + \left(\frac{q_0}{k^2}\right)^2} \\ &= \frac{k^2}{4\pi} \sum_{n=0}^{\infty} \theta(k^2 - \omega n) \frac{2 + w_1 + w_2}{\sqrt{(1+w_1)(1+w_2)}} (k^2 - \omega n) \left(\frac{1}{2} + N_B \left(k^2 \sqrt{(1+w_1)(1+w_2)} \right) \right)\end{aligned} \tag{4.195}$$

with $N_B(x) = \frac{1}{e^{x/T}-1}$. The overall θ-function limits the summation to $N = \left\lfloor \frac{k^2}{\omega} \right\rfloor$. With this we find our final expression for the beta-function of the effective average potential

$$\dot{\tilde{U}} = \frac{k^4}{4\pi} \sum_{n=0}^{N} \left(\sqrt{\frac{1+w_1}{1+w_2}} + \sqrt{\frac{1+w_2}{1+w_1}} \right) \left(1 - \frac{\omega n}{k^2} \right) \left(\frac{1}{2} + N_B \left(k^2 \sqrt{(1+w_1)(1+w_2)} \right) \right). \tag{4.196}$$

To find suitable projections for the running couplings we might employ an expansion of the effective potential in lowest order as

$$\tilde{U}_0 = m^2 \left(\tilde{\rho}_{\mathrm{2D}} - \tilde{\rho}_{\mathrm{2D},0} \right) I_{000} + \frac{\lambda}{2} \left(\tilde{\rho}_{\mathrm{2D}} - \tilde{\rho}_{\mathrm{2D},0} \right)^2 I_{000}^2. \tag{4.197}$$

With this ansatz the flow equations for m_k^2, $\tilde{\rho}_{\mathrm{2D},0}$ and λ_k are given by

$$\begin{aligned}\dot{m}_k^2 &= \frac{1}{I_{000}} \partial_{\tilde{\rho}_{\mathrm{2D}}} \dot{\tilde{U}}_0 \Big|_{\tilde{\rho}_{\mathrm{2D}}=0}, \\ \dot{\tilde{\rho}}_{\mathrm{2D},0} &= -\frac{1}{\lambda_k I_{000}} \partial_{\tilde{\rho}_{\mathrm{2D}}} \dot{\tilde{U}}_0 \Big|_{\tilde{\rho}_{\mathrm{2D}}=\tilde{\rho}_{\mathrm{2D},0}}, \\ \dot{\lambda}_k &= \frac{1}{I_{000}^2} \partial_{\tilde{\rho}_{\mathrm{2D}}}^2 \dot{\tilde{U}}_0 \Big|_{\tilde{\rho}_{\mathrm{2D}}=\tilde{\rho}_{\mathrm{2D},0}}.\end{aligned} \tag{4.198}$$

Further research needs to be done to solve the set of flow equations. Since w_1 and w_2 are n-dependent, the sum in the flow equation for the effective average potential cannot be solved analytically any more. At this point, numerical calculations have been inconclusive.

CHAPTER 5

Discussion & Outlook

In this thesis we investigated the dimensional crossover of nonrelativistic bosons from three to two dimensions. We focused our work on a system, where the transverse dimension is confined in a trap of size L with periodic boundary conditions. This system is closest to its continuous two- and three-dimensional cousins: The ground state is still homogeneous and it can be obtained by minimizing the effective potential. However, we have argued why this system still captures the qualitative behavior of smooth trapping potentials which are found in experiments. Motivated by the recent progress in experiments with quasi-two-dimensional quantum gases we restricted the discussion to the crossover from two to three dimensions with its intriguing superfluid phase at low temperatures.

We obtained the superfluid transition temperature for all trap sizes L and recovered the three- and two-dimensional physics of a Bose gas for $L \to \infty$ and $L \to 0$, respectively. Further, we introduced the crossover function $F(\tilde{L})$ which encodes the trapping effects in the flow equations. In Sec. 4.4 we performed the dimensional crossover with fixed scattering length $a_{3\mathrm{D}}$. This follows a typical cold atom experimental protocol, where the external magnetic field B is tuned to obtain a particular value of $a_{3\mathrm{D}}$. In experiments trapping potentials strongly confine the system in one direction to study quasi-two-dimensional gases. The size of L is not that easily tunable, however, and rather fixed to one particular value. As we lower L in our calculations, the system can at some point be described by an effective two-dimensional system with an effective coupling constant $\lambda_{2\mathrm{D},\Lambda} \approx 8\pi \frac{a_{3\mathrm{D}}}{L}$, such that we simulate a whole class of strongly interacting Bose gases, each corresponding to a different $a_{2\mathrm{D}}(L)$. In order to plan and devise an experimental setup it is crucial to know the effective $a_{2\mathrm{D}}$ and $g_{2\mathrm{D}}$ which can be reached for a given L, and the formulas (4.90) and (4.94) are abundantly applied in the experimental cold atom literature.

In Sec. 4.6 we performed the dimensional crossover with fixed scattering length $a_{2\mathrm{D}}$ which tries to answer a different question. If we want to quantum simulate 2D systems, how can we be sure, given $L \neq 0$, that we actually measure the critical temperature of the two-dimensional system and not one of its quasi-two-dimensional relatives? We found that we recover the true critical temperature for a considerable range

of $(L/a_{2\mathrm{D}})$ values. For larger (but still small) values of L we found an enhanced critical temperature which we intuitively expected, because the possibility of a Bose–Einstein condensation in $d > 2$ should lead to the emergence of a superfluid state at higher temperatures.

Besides these many-body physics we also investigated the scattering properties of the Bose gas. In particular, we found a very intuitive route in the functional renormalization group approach to connect the two- and three-dimensional scattering lengths and explained how the lower-dimensional system inherits its properties from the higher-dimensional one. The relation that we found in Eq. (4.89) is in one-to-one correspondence to the results for harmonic confinement with ℓ_z once we identify $\ell_z^{\mathrm{eff}} = L/\sqrt{2\pi}$ as the effective oscillator length of the potential well.

We found the same relation by using T-matrix calculations and we were also able to correctly address the initial condition for the two-dimensional coupling strength $\lambda_{2\mathrm{D},\Lambda}$. We did this by introducing a generalized version of the T-matrix, which actually could resolve an obstacle of analyzing cold atom experiments. For large densities the typical momenta of the particles are not necessarily small. As a workaround, one could restrict the experiments to low densities, or one has to evaluate cross sections and effective coupling constants at finite momenta (Makhalov et al. (2014); Dyke et al. (2016); Fenech et al. (2016); Boettcher et al. (2016)). We may accomplish this effectively by using the energy- and momentum-resolved T-matrix of the confined system with its discrete mode spectrum such as in Eq. (4.108). To resolve this mode spectrum, one may restrict to phenomenological collective mode spectra such as in (Fuchs et al. (2003); Heiselberg (2004); Boettcher et al. (2011)).

In Sec. 4.7 we improved our truncation by an ansatz, where the excitations in the planar and transverse directions are not treated equally. With this anisotropic derivative expansion we wanted to credit the particular setup of the confined system. The results we obtained do not differ from the previously used isotropic derivative expansion, which just shows that the used truncation of the effective action already captures the relevant physics.

In the last section we depart from the trap with periodic boundary conditions and address important concepts which are not present in the system that we examined up to that point. In Sec. 4.8.1 we discuss the box potential with infinite walls, where the situation already becomes more complicated. In a Hamiltonian formulation the ground state of the interacting system is required to compute expectation values of observables, while in a functional integral formulation the interacting ground state enters by the need to evaluate the effective action at its minimum configuration. But the ground state is not homogeneous anymore! Thus, we can no longer find the ground state by minimizing the effective potential evaluated for constant field configurations. The second complication for trapping potentials different from a well with periodic boundary conditions is that the ground state energy is nonzero. We address this point in Sec. 4.8.1, where we introduce an effective chemical potential to accommodate the shift of energies due to the nonzero ground state energy. We showed how this leads to a different form of the crossover function. We can also understand the impact of a nonzero

ground state energy E_0 by comparing again to the T-matrix. In this approach, we found a logarithmic singularity of the effective two-dimensional T-matrix as $E \to 0$ for a well with periodic boundary conditions. To obtain the same behavior in a box we need to observe the limit $\Delta E \to 0$ to get the same logarithmic divergence, where now $E = E_0 + \Delta E$. This is true for harmonic confinement (Petrov and Shlyapnikov (2001); Levinsen and Parish (2015)). Consequently, as we have described in Fig. 4.4, the emergent two-dimensional physics appear in the effective two-dimensional continuum of states just above the zero-point energy.

In Sec. 4.8.2 we examine a system trapped in a harmonic confinement. We introduce the appropriate function space, which includes the eigenfunctions of the harmonic oscillator in z-direction, and derive the inverse propagator. For the following results we had to rely on a number of different approximations. We expanded the density in the non-interacting eigenstates and assumed that it is dominated by the lowest lying energy state. Even though the system exhibits a nonhomogeneous ground state, we define an effective potential which is essentially an expansion in the two-dimensional homogeneous density modified by a multiplication with a fixed z-density distribution. We obtain within these approximations a flow equation for the effective potential, from which flow equations for the running couplings can be obtained. Because of the complicated structure of the flow equation, we only obtained numerical results that are not yet conclusive.

Even though we derived the flow equations for the dimensional crossover from two to three dimensions, we may, however, extend our ansatz easily to other systems and dimensional crossovers from d to $d + 1$ dimensions. In future work, one might apply these flow equations to crossovers from 2D to 1D, or 3D to 1D, which are highly exciting from the point of view of quantum phase transitions. The finite temperature superfluid phase in the two-dimensional Bose gas that we considered in Sec. 2.4 and in the $L \to 0$ limit of the dimensional crossover is conceptually close to phases with quasi-long-range order in one dimension at zero temperature, see for example Refs. (Al Khawaja et al. (2003)) and (Al Khawaja et al. (2003)) for a mean-field study of the correlations in the dimensional crossover from 3D to 2D (1D) at $T > 0$ ($T = 0$). Since the confinement only affects spatial momenta, the characteristic frequency dependence which governs quantum critical phenomena will be resolved correctly with the functional renormalization group in the dimensional crossover if this is the case for the system without compact dimensions. Further, the nature of inhomogeneous phases of fermion pairs in dimensional crossovers have been discussed in Ref. (Sun and Bolech (2012); Dutta and Mueller (2016)).

We can also use the Bose gas as an effective description of bosonic degrees of freedom in other systems. In particular, the finite two-dimensional Bose gas and its BKT transition may be applied to the pseudogap phase of underdoped cuprates (Lee et al. (2006)). Further, the nonrelativistic nature of complex bosonic degrees of freedom is also found in open or non-equilibrium quantum systems such as exciton-polariton condensates in semiconductor microcavities (Carusotto and Ciuti (2013); Sieberer et al. (2016)).

In the future the question on how to properly incorporate inhomogeneous systems into the method of the functional renormalization group needs to be addressed. I think this is a very promising and interesting route to extend the applicability of functional renormalization to experimental setups beyond the order of a local density approximation.

Appendix

APPENDIX A

Flow equations

A.1 Isotropic derivative expansion

A.1.1 Flow of the effective potential

The first goal is to derive a flow equation for the effective average potential U_k. We can achieve this by evaluating the Wetterich equation

$$\partial_t \Gamma_k = \frac{1}{2}\mathrm{Tr}\left[\left(\Gamma_k^{(2)} + R_k\right)^{-1} \partial_t R_k\right] \tag{A.1}$$

for a homogeneous field, since the effective potential is the part of the action that contains no derivatives of the field. On the right hand side of the Wetterich equation we find the 2-point function or inverse propagator $\Gamma_k^{(2)}$. We need to evaluate this quantity for the ansatz of the effective average action Γ_k that we want to work with. The ansatz reads

$$\bar{\Gamma}_k\left[\bar{\phi}\right] = \int_Z \bar{\phi}_Z^*(\bar{Z}_k\partial_\tau - A_k\nabla^2)_Z\bar{\phi}_Z + \bar{U}_k(\bar{\rho}_Z). \tag{A.2}$$

It is not necessary to insert the Taylor expansion of the effective average potential - as we have described in the main text, it is sufficient to derive a flow equation for the general effective average potential and then project onto the corresponding couplings. Note also that we have indicated the derivative terms with a subscript Z to make clear on which variable it acts on. We do this to keep track in the following calculation.

We work with a decomposition of the complex field ϕ into a real and imaginary part

$$\phi(X) = \frac{1}{\sqrt{2}}\left(\phi_1(X) + \mathrm{i}\phi_2(X)\right). \tag{A.3}$$

Whenever we evaluate an equation for a physical ground state, which means that we consider homogeneous solutions, we choose the field to be real and assume it takes on a constant value, i.e.

$$\phi(X) = \phi = \frac{1}{\sqrt{2}}\phi_1. \tag{A.4}$$

The symmetry invariant $\rho = \phi^*(X)\phi(X)$ therefore relates to the field as

$$\rho_0 = \phi^*\phi = \phi^2 = \frac{1}{2}\phi_1^2 \tag{A.5}$$

or $\phi_1 = \sqrt{2\rho_0}$, because in the end we want to express the flow equations in terms of ρ_0. Note that ρ_0 might be zero, so we did not specify in which phase we are in.

In this decomposition the inverse propagator $\Gamma_k^{(2)}$ is given by a 2×2-matrix, i.e.

$$\left(\Gamma_k^{(2)}\left[\phi\right]\right)_{i,j}(X,Y) = \frac{\delta}{\delta\phi_i(X)}\frac{\delta}{\delta\phi_j(Y)}\Gamma_k\left[\phi\right]. \tag{A.6}$$

In the end we want to work in momentum space, which is the appropriate space to treat this system. We define the Fourier transformation for the fields via

$$\phi(Q) = \int_X e^{-iX\cdot Q}\phi(X), \tag{A.7}$$

whereas the Fourier transformation for the 2-point function is given by

$$\left(\Gamma_k^{(2)}\left[\phi\right]\right)_{i,j}(Q,Q') = \int_X\int_Y e^{iX\cdot Q}e^{iY\cdot Q'}\left(\Gamma_k^{(2)}\left[\phi\right]\right)_{i,j}(X,Y), \tag{A.8}$$

so that terms like $(\phi_1 \cdots \phi_N)\Gamma_k^{(N)}$, which do appear in a vertex expansion, are invariant. We will also use the shorthand notation

$$\begin{aligned}\phi_{i,X} &= \phi_i(X),\\ \delta\phi_{i,X} &= \frac{\delta}{\delta\phi_i(X)}.\end{aligned} \tag{A.9}$$

Inserting this decomposition into our ansatz for the effective average action yields

$$\bar{\Gamma}_k = \frac{1}{2}\int_Z(\bar{\phi}_{1,Z} - \mathrm{i}\bar{\phi}_{2,Z})(\bar{Z}_k\partial_\tau - A_k\nabla^2)_Z(\bar{\phi}_{1,Z} + \mathrm{i}\bar{\phi}_{2,Z}) + \int_Z \bar{U}_k(\bar{\rho}_Z). \tag{A.10}$$

The first functional derivative reads

$$\begin{aligned}(\delta\bar{\phi}_{1,X})\bar{\Gamma}_k\left[\bar{\phi}\right] = &\frac{1}{2}(\bar{Z}_k\partial_\tau - A_k\nabla^2)_X(\bar{\phi}_{1,X} + \mathrm{i}\bar{\phi}_{2,X})\\ &+ \frac{1}{2}(\bar{\phi}_{1,X} - \mathrm{i}\bar{\phi}_{2,X})(-\bar{Z}_k\partial_\tau - A_k\nabla^2)_X\\ &+ \bar{U}'(\bar{\rho}_X)\bar{\phi}_{1,X}.\end{aligned} \tag{A.11}$$

Here we have used the identity

$$\delta\bar{\phi}_{1,X}(\bar{\phi}_{1,Z}) = \delta(Z - X), \tag{A.12}$$

so that the integration becomes trivial. Further note the crucial minus sign in front of the second frequency coefficient $\bar{Z}_k$. This is due to the fact that we first need to do

a partial integration to be able to take the functional derivative of the fields behind the derivative operators. As a third point note that since the effective average potential $\bar{U}_k(\bar{\rho})$ is a function of the symmetry invariant $\bar{\rho}$ only, we denote a derivative with respect to $\bar{\rho}$ with a prime and make use of the chain rule

$$\delta\bar{\phi}_{1,X}\left(\bar{U}(\bar{\rho}_Z)\right) = \bar{U}'(\bar{\rho}_Z)\frac{\delta\bar{\rho}_Z}{\delta\bar{\phi}_{1,X}}, \tag{A.13}$$

which further evaluates to

$$\frac{\delta}{\delta\bar{\phi}_{1,X}}\bar{\rho}_Z = \frac{\delta}{\delta\bar{\phi}_{1,X}}\left(\frac{1}{2}(\bar{\phi}_{1,Z}^2+\bar{\phi}_{2,Z}^2)\right) = \bar{\phi}_{1,Z}\delta(Z-X). \tag{A.14}$$

To complete the calculation of the (1,1)-component of the 2-point function we need to take a second derivative with respect to $\bar{\phi}_1$

$$\begin{aligned}\delta\bar{\phi}_{1,Y}\left(\delta\bar{\phi}_{1,X}\bar{\Gamma}_k\left[\bar{\phi}\right]\right) =&\frac{1}{2}(\bar{Z}_k\partial_\tau - A_k\nabla^2)_X\delta(X-Y)\\ &+\frac{1}{2}(-\bar{Z}_k\partial_\tau - A_k\nabla^2)_X\delta(X-Y)\\ &+\bar{U}'(\bar{\rho}_X)\delta(X-Y)+\bar{U}''(\bar{\rho}_X)\bar{\phi}_{1,X}^2\delta(X-Y)\\ =&(-A_k\nabla^2+\bar{U}'+\bar{\phi}_1^2\bar{U}'')_X\delta(X-Y).\end{aligned} \tag{A.15}$$

In a similar way we calculate

$$\delta\bar{\phi}_{2,Y}\left(\delta\bar{\phi}_{2,X}\bar{\Gamma}_k\left[\bar{\phi}\right]\right) = (-A_k\nabla^2+\bar{U}'+\bar{\phi}_2^2\bar{U}'')_X\delta(X-Y). \tag{A.16}$$

The off-diagonal elements evaluate to

$$\begin{aligned}\delta\bar{\phi}_{2,Y}\left(\delta\bar{\phi}_{1,X}\bar{\Gamma}_k\left[\bar{\phi}\right]\right) =&\frac{1}{2}(\bar{Z}_k\partial_\tau - A_k\nabla^2)_X\mathrm{i}\delta(X-Y)\\ &+\frac{1}{2}(-\mathrm{i})(-\bar{Z}_k\partial_\tau - A_k\nabla^2)_X\delta(X-Y)\\ &+\bar{U}''(\bar{\rho}_X)\bar{\phi}_{1,X}\bar{\phi}_{2,X}\delta(X-Y)\\ =&(\mathrm{i}\bar{Z}_k\partial_\tau+\bar{\phi}_1\bar{\phi}_2\bar{U}'')_X\delta(X-Y).\end{aligned} \tag{A.17}$$

From symmetry arguments we can infer

$$\delta\bar{\phi}_{1,Y}\left(\delta\bar{\phi}_{2,X}\bar{\Gamma}_k\left[\bar{\phi}\right]\right) = (-\mathrm{i}\bar{Z}_k\partial_\tau+\bar{\phi}_1\bar{\phi}_2\bar{U}'')_X\delta(X-Y). \tag{A.18}$$

The inverse propagator therefore reads

$$\bar{\Gamma}_k^{(2)}(X,Y) = \begin{pmatrix} -A_k\nabla^2+\bar{U}'+\bar{\phi}_1^2\bar{U}'' & \mathrm{i}\bar{Z}_k\partial_\tau+\bar{\phi}_1\bar{\phi}_2\bar{U}'' \\ -\mathrm{i}\bar{Z}_k\partial_\tau+\bar{\phi}_1\bar{\phi}_2\bar{U}'' & -A_k\nabla^2+\bar{U}'+\bar{\phi}_2^2\bar{U}'' \end{pmatrix}_X\delta(X-Y). \tag{A.19}$$

Later we will also need the 3- and 4-point vertices to project flow equations for the wave function renormalizations. To label the different 3- and 4-point functions we use the notation

$$\begin{aligned}\bar{\Gamma}_i^{(3)}(X,Y,Z) &= \delta\bar{\phi}_{i,Z}\bar{\Gamma}^{(2)}(X,Y),\\ \bar{\Gamma}_{ij}^{(4)}(X,Y,Z,Z') &= \delta\bar{\phi}_{i,Z}\delta\bar{\phi}_{j,Z'}\bar{\Gamma}^{(2)}(X,Y).\end{aligned} \tag{A.20}$$

For better readability we omit the overbar in the following presentation of results. We find for the 3-point functions

$$\begin{aligned}\Gamma_1^{(3)}(X,Y,Z) &= \begin{pmatrix} 3\phi_1 U'' + \phi_1^3 U^{(3)} & \phi_2 U'' + \phi_2\phi_1^2 U^{(3)} \\ \phi_2 U'' + \phi_2\phi_1^2 U^{(3)} & \phi_1 U'' + \phi_1\phi_2^2 U^{(3)} \end{pmatrix}_X \delta(X-Y)\delta(X-Z), \\ \Gamma_2^{(3)}(X,Y,Z) &= \begin{pmatrix} \phi_2 U'' + \phi_2\phi_1^2 U^{(3)} & \phi_1 U'' + \phi_1\phi_2^2 U^{(3)} \\ \phi_1 U'' + \phi_1\phi_2^2 U^{(3)} & 3\phi_2 U'' + \phi_2^3 U^{(3)} \end{pmatrix}_X \delta(X-Y)\delta(X-Z),\end{aligned} \tag{A.21}$$

and the 4-point functions are given by

$$\begin{aligned}\Gamma_{11}^{(4)}(X,Y,Z,Z') &= \begin{pmatrix} 3U'' + 6\phi_1^2 U^{(3)} + \phi_1^4 U^{(4)} & 3\phi_1\phi_2 U^{(3)} + \phi_2\phi_1^3 U^{(4)} \\ 3\phi_1\phi_2 U^{(3)} + \phi_2\phi_1^3 U^{(4)} & U'' + (\phi_1^2+\phi_2^2)U^{(3)} + \phi_1^2\phi_2^2 U^{(4)} \end{pmatrix}_X \delta_{XY}\delta_{XZ}\delta_{XZ'}, \\ \Gamma_{22}^{(4)}(X,Y,Z,Z') &= \begin{pmatrix} U'' + (\phi_1^2+\phi_2^2)U^{(3)} + \phi_1^2\phi_2^2 U^{(4)} & 3\phi_1\phi_2 U^{(3)} + \phi_1\phi_2^3 U^{(4)} \\ 3\phi_1\phi_2 U^{(3)} + \phi_1\phi_2^3 U^{(4)} & 3U'' + 6\phi_2^2 U^{(3)} + \phi_2^4 U^{(4)} \end{pmatrix}_X \delta_{XY}\delta_{XZ}\delta_{XZ'}, \\ \Gamma_{12}^{(4)}(X,Y,Z,Z') &= \begin{pmatrix} 3\phi_1\phi_2 U^{(3)} + \phi_2\phi_1^3 U^{(4)} & U'' + (\phi_1^2+\phi_2^2)U^{(3)} + \phi_1^2\phi_2^2 U^{(4)} \\ U'' + (\phi_1^2+\phi_2^2)U^{(3)} + \phi_1^2\phi_2^2 U^{(4)} & 3\phi_1\phi_2 U^{(3)} + \phi_1\phi_2^3 U^{(4)} \end{pmatrix}_X \\ &\quad \times \delta_{XY}\delta_{XZ}\delta_{XZ'}, \\ \Gamma_{21}^{(4)}(X,Y,Z,Z') &= \Gamma_{12}^{(4)}(X,Y,Z,Z').\end{aligned} \tag{A.22}$$

Again we may simplify notation by using

$$\begin{aligned}\Gamma_i^{(3)}(X,Y,Z) &= \gamma_i^{(3)}\delta(X-Y)\delta(X-Z), \\ \Gamma_{ij}^{(4)}(X,Y,Z,Z') &= \gamma_{ij}^{(4)}\delta(X-Y)\delta(X-Z)\delta(X-Z').\end{aligned} \tag{A.23}$$

Since we do not need further functional derivatives (in our approximation of the effective average action), we may evaluate these expressions for a homogeneous field. We find

$$\begin{aligned}\gamma_1^{(3)} &= \sqrt{2\bar\rho}\bar U'' \begin{pmatrix} 3 + 2\bar\rho\frac{\bar U^{(3)}}{\bar U''} & 0 \\ 0 & 1 \end{pmatrix}, \\ \gamma_2^{(3)} &= \sqrt{2\bar\rho}\bar U'' \begin{pmatrix} 0 & 1 \\ 1 & 0 \end{pmatrix}, \\ \gamma_{11}^{(4)} &= \begin{pmatrix} 3\bar U'' + 12\bar\rho\bar U^{(3)} + 4\bar\rho^2\bar U^{(4)} & 0 \\ 0 & \bar U'' + 2\bar\rho\bar U^{(3)} \end{pmatrix}, \\ \gamma_{22}^{(4)} &= \begin{pmatrix} \bar U'' + 2\bar\rho\bar U^{(3)} & 0 \\ 0 & 3\bar U'' \end{pmatrix}, \\ \gamma_{12}^{(4)} &= \begin{pmatrix} 0 & \bar U'' + 2\bar\rho\bar U^{(3)} \\ \bar U'' + 2\bar\rho\bar U^{(3)} & 0 \end{pmatrix} = \gamma_{21}^{(4)}.\end{aligned} \tag{A.24}$$

Calculations have shown that bosonic multiple scattering, which is encoded in the higher order couplings of the effective average potential, does not enhance the quantitative precision. In our approximation we thus set $\bar U^{(3)} = \bar U^{(4)} = 0$. The 3- and 4-point

functions simplify to

$$\begin{aligned}
\gamma_1^{(3)} &= \sqrt{2\bar{\rho}}\bar{U}''\begin{pmatrix} 3 & 0 \\ 0 & 1 \end{pmatrix}, \\
\gamma_2^{(3)} &= \sqrt{2\bar{\rho}}\bar{U}''\begin{pmatrix} 0 & 1 \\ 1 & 0 \end{pmatrix}, \\
\gamma_{11}^{(4)} &= \bar{U}''\begin{pmatrix} 3 & 0 \\ 0 & 1 \end{pmatrix}, \\
\gamma_{22}^{(4)} &= \bar{U}''\begin{pmatrix} 1 & 0 \\ 0 & 3 \end{pmatrix}, \\
\gamma_{12}^{(4)} &= \bar{U}''\begin{pmatrix} 0 & 1 \\ 1 & 0 \end{pmatrix} = \gamma_{21}^{(4)}.
\end{aligned} \tag{A.25}$$

To obtain the flow equation for the effective average potential we evaluate $\bar{\Gamma}_k^{(2)}$ for a constant field

$$\bar{\phi}_1 = \sqrt{2\bar{\rho}}, \quad \bar{\phi}_2 = 0, \tag{A.26}$$

so that we are left with

$$\bar{\Gamma}_k^{(2)}(X,Y) = \begin{pmatrix} -A_k\nabla^2 + \bar{U}' + 2\bar{\rho}\bar{U}'' & \mathrm{i}\bar{Z}_k\partial_\tau \\ -\mathrm{i}\bar{Z}_k\partial_\tau & -A_k\nabla^2 + \bar{U}' \end{pmatrix}_X \delta(X-Y). \tag{A.27}$$

We arrive at the 2-point function in momentum space when we perform the Fourier transformation. The two nontrivial terms transform according to

$$\begin{aligned}
&\int_X\int_Y -A_k\nabla_X^2 e^{\mathrm{i}XQ}e^{\mathrm{i}YQ'}\delta(X-Y) \\
=&\int_X\int_Y -A_k\mathrm{i}^2|\vec{q}|^2 e^{\mathrm{i}XQ}e^{\mathrm{i}YQ'}\delta(X-Y) \\
=&A_k|\vec{q}|^2\int_X e^{\mathrm{i}X(Q+Q')} = A_k q^2\delta(Q+Q')
\end{aligned} \tag{A.28}$$

and

$$\begin{aligned}
&\int_X\int_Y \mathrm{i}\bar{Z}_k\partial_{\tau,X}e^{\mathrm{i}XQ}e^{\mathrm{i}YQ'}\delta(X-Y) \\
=&\int_X\int_Y \mathrm{i}^2\bar{Z}_k q_0 e^{\mathrm{i}XQ}e^{\mathrm{i}YQ'}\delta(X-Y) \\
=&-\bar{Z}_k q_0\delta(Q+Q')
\end{aligned} \tag{A.29}$$

We therefore find

$$\bar{\Gamma}_k^{(2)}(Q,Q') = \begin{pmatrix} A_k(\vec{q}^2+k_n^2) + \bar{U}' + 2\bar{\rho}\bar{U}'' & -\bar{Z}_k q_0 \\ \bar{Z}_k q_0 & A_k(\vec{q}^2+k_n^2) + \bar{U}' \end{pmatrix}\delta(Q+Q'), \tag{A.30}$$

where we have now specified to a confinement in z-direction with periodic boundary conditions, i.e. $Q = (q_0, \vec{q}, k_n)$, $\vec{q} = (q_1, \ldots, q_d)$ denotes the momentum vector in the

noncompact dimensions of space, and $k_n = 2\pi n/L, n \in \mathbb{Z}$ the component of the discrete momentum modes. Later we will specialize to the case that $d = 2$.

We use the Litim-type regulator

$$\begin{aligned} R_k(Q,Q') &= R_k(Q)\delta(Q+Q') \\ R_k(Q) &= A_k(k^2 - \vec{q}^2 - k_n^2)\theta(k^2 - \vec{q}^2 - k_n^2) \\ \dot{R}_k(Q) &= A_k(2k^2 - \eta(k^2 - \vec{q}^2 - k_n^2))\theta(k^2 - \vec{q}^2 - k_n^2), \end{aligned} \tag{A.31}$$

where we defined the anomalous dimension by $\eta = -\dot{A}_k/A_k$.

With the definition of the regularized inverse propagator

$$\bar{G}_k^{-1}\delta(Q+Q') = \bar{\Gamma}_k^{(2)}(Q,Q') + R_k(Q,Q') \tag{A.32}$$

we find

$$\bar{G}_k^{-1}(Q) = \begin{pmatrix} p^q + \bar{U}' + 2\bar{\rho}\bar{U}'' & -\bar{Z}_k q_0 \\ \bar{Z}_k q_0 & p^q + \bar{U}' \end{pmatrix} \tag{A.33}$$

with

$$p^q = A_k(\vec{q}^2 + k_n^2) + R_k(Q). \tag{A.34}$$

We can invert this and obtain

$$\bar{G}_k(Q) = \frac{1}{\det_Q}\begin{pmatrix} p^q + \bar{U}' & \bar{Z}_k q_0 \\ -\bar{Z}_k q_0 & p^q + \bar{U}' + 2\bar{\rho}\bar{U}'' \end{pmatrix}, \tag{A.35}$$

where

$$\det_Q = (p^q + \bar{U}' + 2\bar{\rho}\bar{U}'')(p^q + \bar{U}') + (\bar{Z}_k q_0)^2. \tag{A.36}$$

The flow equation for the effective average potential is obtained from the Wetterich equation by evaluating it for a constant field. This flow equation is given by

$$\dot{\bar{U}}_k(\bar{\rho}) = \frac{1}{2}\mathrm{tr}\int_Q \bar{G}_k(Q)\dot{R}_k(Q). \tag{A.37}$$

The integration consists of a q_0-integral, which is replaced by a sum over Matsubara frequencies $\omega_n = 2\pi n T$ for non-zero temperatures, and an integration over spatial dimensions. Therefore, we have

$$\int_Q = T\sum_{\omega_n}\frac{1}{L}\sum_{k_n}\int\frac{\mathrm{d}^d q}{(2\pi)^d}. \tag{A.38}$$

We can now insert the propagator and the expression for $\dot{R}_k$

$$\begin{aligned} \dot{\bar{U}}_k(\bar{\rho}) &= \frac{1}{2}\mathrm{tr}\int_Q \frac{1}{\det_Q}\begin{pmatrix} p^q + \bar{U}' & \bar{Z}_k q_0 \\ -\bar{Z}_k q_0 & p^q + \bar{U}' + 2\bar{\rho}\bar{U}'' \end{pmatrix} A_k(2k^2 - \eta(k^2 - q^2 - k_n^2))\theta(k^2 - q^2 - k_n^2) \\ &= \frac{1}{2}\int_Q \frac{1}{\det_Q}(2p^q + 2\bar{U}' + 2\bar{\rho}\bar{U}'')A_k(2k^2 - \eta(k^2 - q^2 - k_n^2))\theta(k^2 - q^2 - k_n^2) \\ &= \int_Q \frac{p^q + \bar{U}' + \bar{\rho}\bar{U}''}{\det_Q}A_k(2k^2 - \eta(k^2 - q^2 - k_n^2))\theta(k^2 - q^2 - k_n^2). \end{aligned} \tag{A.39}$$

Since the integral only depends on the absolute value of $\vec{q}$, we can directly perform the angular integration of the d-dimensional integral, which gives a factor of

$$4v_d = \left[2^{d-1}\pi^{d/2}\Gamma\left(\frac{d}{2}\right)\right]^{-1}, \tag{A.40}$$

where Γ is the gamma function. The flow equation can therefore be written in the form

$$\begin{aligned}\dot{\bar{U}}_k = T\sum_{\omega_n}\frac{1}{L}\sum_{k_n} 4v_d\int_0^\infty \mathrm{d}q q^{d-1}\frac{p^q + \bar{U}' + \bar{\rho}\bar{U}''}{\det_Q} \\ \times A_k\left(2k^2 - \eta(k^2 - q^2 - k_n^2)\right)\theta\left(k^2 - q^2 - k_n^2\right).\end{aligned} \tag{A.41}$$

The overall θ-function limits the integration to the region $q < \sqrt{k^2 - k_n^2}$. It is an advantage of this particular choice of Litim-cutoff that we can now replace $p^q \to A_k k^2$ in the integrand, which allows us to perform the integration analytically. Further the ω_n-summation factorizes. We now switch to renormalized quantities

$$\begin{aligned}Z_k &= \frac{\bar{Z}_k}{A_k}, \\ \rho &= A_k\bar{\rho},\end{aligned} \tag{A.42}$$

and find

$$\begin{aligned}\dot{\bar{U}}_k = 4v_d\left(T\sum_{\omega_n}\frac{k^2 + U' + \rho U''}{(k^2 + U')(k^2 + U' + 2\rho U'') + (Z_k\omega_n)^2}\right) \\ \times\frac{1}{L}\sum_{k_n}\int_0^{\sqrt{k^2-k_n^2}}\mathrm{d}q q^{d-1}\left(2k^2 - \eta(k^2 - q^2 - k_n^2)\right) \\ \times\theta(k^2 - q^2 - k_n^2).\end{aligned} \tag{A.43}$$

We can now perform the q-integration analytically. We obtain

$$\begin{aligned}\int_0^{\sqrt{k^2-k_n^2}}\mathrm{d}q q^{d-1}\left(2k^2 - \eta(k^2 - q^2 - k_n^2)\right)\theta(k^2 - q^2 - k_n^2) \\ = \frac{2}{d}k^{2+d}(1 - (k_n/k)^2)^{d/2}\left(1 - \eta\frac{1 - (k_n/k)^2}{d+2}\right)\theta(k^2 - k_n^2).\end{aligned} \tag{A.44}$$

The temperature-dependent part contains an evaluation of a Matsubara sum. We use

$$T\sum_{\omega_n}\frac{1}{a^2\omega_n^2 + b^2} = \frac{1}{ab}\left(\frac{1}{2} + N_B\left(\frac{b}{a}\right)\right), \tag{A.45}$$

where we introduced the Bose function

$$N_B(x) = \frac{1}{e^{x/T} - 1}. \tag{A.46}$$

The summation evaluates to

$$\begin{aligned} & T\sum_{\omega_n} \frac{k^2+U'+\rho U''}{(k^2+U')(k^2+U'+2\rho U'')+(Z_k\omega_n)^2} \\ &= \frac{1}{2Z_k}\left(\sqrt{\frac{1+w_1}{1+w_2}}+\sqrt{\frac{1+w_2}{1+w_1}}\right) \\ &\times\left(\frac{1}{2}+N_B\left(\frac{k^2\sqrt{(1+w_1)(1+w_2)}}{Z_k}\right)\right), \end{aligned} \tag{A.47}$$

where we also introduced the dimensionless quantities $w_1 = U'/k^2$ and $w_2 = (U' + 2\rho U'')/k^2$. We find

$$\begin{aligned} \dot{\bar{U}}_k =& 4v_d\frac{1}{2Z_k}\left(\sqrt{\frac{1+w_1}{1+w_2}}+\sqrt{\frac{1+w_2}{1+w_1}}\right)\left(\frac{1}{2}+N_B\left(\frac{k^2\sqrt{(1+w_1)(1+w_2)}}{Z_k}\right)\right) \\ &\times\frac{1}{L}\sum_{k_n}\frac{2}{d}k^{2+d}(1-(k_n/k)^2)^{d/2}\left(1-\eta\frac{1-(k_n/k)^2}{d+2}\right)\theta(k^2-k_n^2) \\ =&\frac{4v_dk^{3+d}}{dZ_k}\left(\sqrt{\frac{1+w_1}{1+w_2}}+\sqrt{\frac{1+w_2}{1+w_1}}\right)\left(\frac{1}{2}+N_B\left(\frac{k^2\sqrt{(1+w_1)(1+w_2)}}{Z_k}\right)\right) \\ =&\frac{1}{Lk}\sum_{k_n}(1-(k_n/k)^2)^{d/2}\left(1-\eta\frac{1-(k_n/k)^2}{d+2}\right)\theta(k^2-k_n^2). \end{aligned} \tag{A.48}$$

Here we see the emergence of the crossover function

$$F(\tilde{L}) = \frac{1}{Lk}\sum_{k_n}(1-(k_n/k)^2)^{d/2}\left(1-\eta\frac{1-(k_n/k)^2}{d+2}\right)\theta(k^2-k_n^2) \tag{A.49}$$

with $\tilde{L} = Lk$.

We now specialize to two continuous dimensions. Further, since we compactify on a torus, we label the crossover function with a subscript to show that it holds for periodic boundary conditions. The θ-function limits the range of summation to $|k_n| = \left|\frac{2\pi}{L}n\right| < k$, or, equivalently, $|n| < \frac{\tilde{L}}{2\pi}$. With $N = \left\lfloor\frac{\tilde{L}}{2\pi}\right\rfloor$ we can write

$$F_{\text{pbc}}(\tilde{L}) = \frac{1}{\tilde{L}}\left[\left(1-\frac{\eta}{4}\right)\sum_{n=-N}^{n=N}1-\left(1-\frac{\eta}{2}\right)\sum_{n=-N}^{n=N}\frac{k_n^2}{k^2}-\frac{\eta}{4}\sum_{n=-N}^{n=N}\frac{k_n^4}{k^4}\right]. \tag{A.50}$$

Together with

$$\begin{aligned} \sum_{n=-N}^{N}\frac{k_n^2}{k^2} &= 2\left(\frac{2\pi}{\tilde{L}}\right)^2\sum_{n=1}^{N}n^2, \\ \sum_{n=-N}^{N}\frac{k_n^4}{k^4} &= 2\left(\frac{2\pi}{\tilde{L}}\right)^4\sum_{n=1}^{N}n^2 \end{aligned} \tag{A.51}$$

and

$$\begin{aligned}\sum_{n=-N}^{n=N} 1 &= 1+2N,\\ \sum_{n=1}^{N} n^2 &= \frac{1}{6}N(1+N)(1+2N),\\ \sum_{n=1}^{N} n^4 &= \frac{1}{30}N(1+N)(1+2N)(-1+3N+3N^2)\end{aligned} \tag{A.52}$$

the crossover function evaluates to

$$\begin{aligned}F_{\text{pbc}}(\tilde{L}) = \frac{2N+1}{\tilde{L}}\Bigg[1-\frac{\eta}{4}-\frac{1}{\tilde{L}^2}\left(1-\frac{\eta}{2}\right)\frac{4\pi^2}{3}N(N+1)\\ -\frac{\eta}{\tilde{L}^4}\frac{4\pi^4}{15}N(N+1)(-1+3N+3N^2)\Bigg].\end{aligned} \tag{A.53}$$

We still need to make a change of variable from $\bar{\rho}$ to ρ. Thus, we get an additional term for the flow of the renormalized effective potential U_k

$$\dot{\bar{U}}_k = \dot{U}_k + \frac{\partial U}{\partial \rho}\frac{\partial \rho}{\partial t}\bigg|_{\bar{\rho}}. \tag{A.54}$$

With $\rho = A_k\bar{\rho}$ follows

$$\frac{\partial \rho}{\partial t}\bigg|_{\bar{\rho}} = (\partial_t A_k)\bar{\rho} = (\partial_t A_k)\frac{\rho}{A_k} \tag{A.55}$$

and therefore

$$\begin{aligned}\dot{U}_k &= \dot{\bar{U}}_k - U'\rho\frac{\partial_t A_k}{A_k}\\ &= \dot{\bar{U}}_k + \eta\rho U'.\end{aligned} \tag{A.56}$$

Together with $v_2 = \frac{1}{8\pi}$ the flow of the effective potential reads

$$\dot{U}_k = \eta\rho U_k' + \frac{k^5}{4\pi Z_k}G_1(T)F(\tilde{L}) \tag{A.57}$$

with

$$G_1(T) = \left(\sqrt{\frac{1+w_1}{1+w_2}}+\sqrt{\frac{1+w_2}{1+w_1}}\right)\left(\frac{1}{2}+N_B\left(\frac{k^2\sqrt{(1+w_1)(1+w_2)}}{Z_k}\right)\right). \tag{A.58}$$

A.1.2 Flow equations for kinetic coefficients

We use the derivative projection to obtain the flow equations for the kinetic coefficients $\bar{Z}_k$ and A_k. Recall the form of the inverse propagator

$$\bar{G}_k^{-1}(P) = \begin{pmatrix} A_k p^2 + \bar{U}' + 2\bar{\rho}\bar{U}'' & -\bar{Z}_k p_0 \\ \bar{Z}_k p_0 & A_k p^2 + \bar{U}' \end{pmatrix}. \tag{A.59}$$

We use the flow of $\bar{G}_k^{-1}$ to project flow equations for $\bar{Z}_k$ and A_k according to

$$\begin{aligned}\partial_t \bar{Z}_k &= -\frac{\partial}{\partial p_0}\dot{\bar{G}}^{-1}_{k,12}(p_0,0)\Big|_{p_0=0},\\ \partial_t A_k &= \frac{\partial}{\partial p^2}\dot{\bar{G}}^{-1}_{k,22}(0,p^2)\Big|_{p=0},\end{aligned} \tag{A.60}$$

where $G^{-1}_{k,ij}(p_0,p^2) = \delta^2\Gamma/(\delta\phi_i\delta\phi_j)|_{\rho_0}$ denotes the second functional derivative. The flow equation for the inverse propagator can be obtained by the second functional derivative of the Wetterich equation, see e.g. Ref. (Boettcher et al. (2014)) for details. It reads

$$\begin{aligned}\dot{\bar{G}}^{-1}_{k,ij}(P) =& \mathrm{tr}\int_Q \bar{G}_k(Q)\gamma^{(3)}_i\bar{G}_k(Q-P)\gamma^{(3)}_j\bar{G}_k(Q)\dot{R}_k(Q)\\ &-\frac{1}{2}\mathrm{tr}\int_Q \bar{G}_k(Q)\gamma^{(4)}_{ij}\bar{G}_k(Q)\dot{R}_k(Q)\end{aligned} \tag{A.61}$$

First we derive the flow equation of $\bar{Z}_k$. For this we need to evaluate the (1,2)-component of A.61. This yields

$$\begin{aligned}\partial_t\bar{Z}_k =& -\frac{\partial}{\partial p_0}\partial_t\bar{G}^{-1}_{12}(p_0,0)\Big|_{p_0=0}\\ =& -\frac{\partial}{\partial p_0}\Big[\mathrm{tr}\int_Q \bar{G}(Q)\gamma^{(3)}_1\bar{G}(Q-P)\gamma^{(3)}_2\bar{G}(Q)\dot{R}(Q)\\ &-\frac{1}{2}\mathrm{tr}\int_Q \bar{G}(Q)\gamma^{(4)}_{12}\bar{G}(Q)\dot{R}(Q)\Big]\Big|_{p_0=0=p}.\end{aligned} \tag{A.62}$$

Since the 4-point vertex $\gamma^{(4)}_{12}$ does not depend on the external momentum, it will vanish eventually when we perform the p_0-derivative. The flow equation simplifies to

$$\partial_t\bar{Z}_k = -\frac{\partial}{\partial p_0}\mathrm{tr}\int_Q \bar{G}(Q)\gamma^{(3)}_1\bar{G}(Q-P)\gamma^{(3)}_2\bar{G}(Q)\dot{R}(Q)\Big|_{p_0=0=p}. \tag{A.63}$$

Notice that due to the 3-point functions the flow equation for $\bar{Z}_k$ is proportional to an overall $\bar{\rho}$. Therefore $\bar{Z}_k$ experiences a renormalization only in the spontaneously broken phase where we have a nonvanishing $\bar{\rho}$. Since we do not need to take further derivatives with respect to the field $\bar{\phi}$ we can now directly insert $\bar{U}' = 0$. Again we can utilize $p^q \to A_k k^2$ for $q < \sqrt{k^2 - k_n^2}$ due to the overall θ-function. We can now perform the p_0-derivative of the now simplified expression

$$\bar{G}(Q-P)\Big|_{p=0} = \frac{1}{\det_{q_0-p_0}}\begin{pmatrix} A_k k^2 & \bar{Z}_k(q_0-p_0)\\ -\bar{Z}_k(q_0-p_0) & A_k k^2 + 2\bar{\rho}\bar{\lambda}\end{pmatrix} \tag{A.64}$$

with

$$\det_{q_0-p_0} = A_k k^2(A_k k^2 + 2\bar{\rho}\bar{\lambda}) + \bar{Z}_k^2(q_0-p_0)^2. \tag{A.65}$$

We obtain

$$\partial_{p_0}\bar{G}(Q-P)\Big|_{p=0} = \frac{1}{\det_{q_0-p_0}}\begin{pmatrix} 0 & -\bar{Z}_k \\ \bar{Z}_k & 0 \end{pmatrix} + \frac{2\bar{Z}_k^2(q_0-p_0)}{\det^2_{q_0-p_0}}\begin{pmatrix} A_k k^2 & \bar{Z}_k(q_0-p_0) \\ -\bar{Z}_k(q_0-p_0) & A_k k^2 + 2\bar{\rho}\bar{\lambda} \end{pmatrix} \tag{A.66}$$

and thus

$$\begin{aligned}\partial_{p_0}\bar{G}(Q-P)\Big|_{p_0=p=0} &= \frac{1}{\det_Q}\begin{pmatrix} 0 & -\bar{Z}_k \\ \bar{Z}_k & 0 \end{pmatrix} + \frac{2\bar{Z}_k^2 q_0}{\det_Q^2}\begin{pmatrix} A_k k^2 & \bar{Z}_k q_0 \\ -\bar{Z}_k q_0 & A_k k^2 + 2\bar{\rho}\bar{\lambda} \end{pmatrix} \\ &= \frac{1}{\det_Q}\begin{pmatrix} 0 & -\bar{Z}_k \\ \bar{Z}_k & 0 \end{pmatrix} + \frac{2\bar{Z}_k^2 q_0}{\det_Q}\bar{G}(Q).\end{aligned} \tag{A.67}$$

We insert this result into the flow equation and find

$$\begin{aligned}\partial_t \bar{Z}_k =& -2\bar{\rho}\bar{\lambda}^2 \mathrm{tr}\int_Q \dot{R}(Q)\frac{1}{\det_Q}\begin{pmatrix} A_k k^2 & \bar{Z}_k q_0 \\ -\bar{Z}_k q_0 & A_k k^2 + 2\bar{\rho}\bar{\lambda} \end{pmatrix}\begin{pmatrix} 3 & 0 \\ 0 & 1 \end{pmatrix} \\ &\times\frac{\bar{Z}_k}{\det_Q}\left[\begin{pmatrix} 0 & -1 \\ 1 & 0 \end{pmatrix} + \frac{2\bar{Z}_k q_0}{\det_Q}\begin{pmatrix} A_k k^2 & \bar{Z}_k q_0 \\ -\bar{Z}_k q_0 & A_k k^2 + 2\bar{\rho}\bar{\lambda} \end{pmatrix}\right] \\ &\times\frac{1}{\det_Q}\begin{pmatrix} 0 & 1 \\ 1 & 0 \end{pmatrix}\begin{pmatrix} A_k k^2 & \bar{Z}_k q_0 \\ -\bar{Z}_k q_0 & A_k k^2 + 2\bar{\rho}\bar{\lambda} \end{pmatrix}.\end{aligned} \tag{A.68}$$

This equation can be simplified to

$$\begin{aligned}\partial_t \bar{Z}_k =& -2\bar{\rho}\bar{\lambda}^2 \mathrm{tr}\int_Q \dot{R}(Q)\frac{\bar{Z}_k}{\det_Q^3}\begin{pmatrix} 3A_k k^2 & \bar{Z}_k q_0 \\ -3\bar{Z}_k q_0 & A_k k^2 + 2\bar{\rho}\bar{\lambda} \end{pmatrix} \\ &\times\left[\begin{pmatrix} -A_k k^2 & -\bar{Z}_k q_0 \\ -\bar{Z}_k q_0 & A_k k^2 + 2\bar{\rho}\bar{\lambda} \end{pmatrix} + \begin{pmatrix} 0 & 2\bar{Z}_k q_0 \\ 2\bar{Z}_k q_0 & 0 \end{pmatrix}\right] \\ =& 4\bar{\rho}\bar{\lambda}^2\int_Q \dot{R}(Q)\frac{\bar{Z}_k}{\det_Q^3}\left((A_k k^2)^2 - 2\bar{\rho}\bar{\lambda}(A_k k^2 + \bar{\rho}\bar{\lambda}) + (\bar{Z}_k q_0)^2\right).\end{aligned} \tag{A.69}$$

We can rewrite this in terms of renormalized couplings

$$\begin{aligned}\bar{Z}_k^{-1}\partial_t \bar{Z}_k = 4\rho U''^2 \int_Q & \frac{k^4 - 2\rho U''(k^2 + \rho U'') + (Z_k q_0)^2}{\left(k^2(k^2 + 2\rho U'') + (Z_k q_0)^2\right)^3} \\ &\times \left(2k^2 - \eta(k^2 - q^2 - k_n^2)\right)\theta(k^2 - q^2 - k_n^2).\end{aligned} \tag{A.70}$$

Again the integral factorizes according to

$$\begin{aligned}\bar{Z}_k^{-1}\partial_t \bar{Z}_k = 4\rho U''^2 &\left(T\sum_{\omega_n}\frac{k^4 - 2\rho U''(k^2 + \rho U'') + (Z_k q_0)^2}{\left(k^2(k^2 + 2\rho U'') + (Z_k q_0)^2\right)^3}\right) \\ &\times \frac{1}{L}\sum_{k_n}\int\frac{\mathrm{d}^d q}{(2\pi)^d}\left(2k^2 - \eta(k^2 - q^2 - k_n^2)\right)\theta(k^2 - q^2 - k_n^2).\end{aligned} \tag{A.71}$$

We know the result from the k_n summation and q-integration from the effective potential calculation. We have

$$\begin{aligned}&\frac{1}{L}\sum_{k_n}\int\frac{\mathrm{d}^d q}{(2\pi)^d}\left(2k^2-\eta(k^2-q^2-k_n^2)\right)\theta(k^2-q^2-k_n^2)\\&=4v_d\frac{2}{d}k^{3+d}F(\tilde{L}).\end{aligned}\tag{A.72}$$

With $\bar{Z}_k = Z_k A_k$ we obtain

$$\partial_t Z_k = \frac{\partial_t \bar{Z}_k}{A_k} + \eta Z_k. \tag{A.73}$$

Together with $U'' = \lambda$ we find

$$\begin{aligned}\partial_t Z_k = \eta Z_k - Z_k 4\rho\lambda^2\frac{8v_d k^{3+d}}{d}F(\tilde{L})\\ \times T\sum_{\omega_n}\frac{k^4-2\rho U''(k^2+\rho U'')+(Z_k\omega_n)^2}{\left(k^2(k^2+2\rho U'')+(Z_k\omega_n)^2\right)^3}.\end{aligned}\tag{A.74}$$

We are left with a summation over Matsubara frequencies. With a neat trick we can perform it analytically. For this we rewrite

$$\begin{aligned}T\sum_{\omega_n}\frac{k^4-2\rho\lambda(k^2+\rho\lambda)+(Z_k\omega_n)^2}{\left(k^2(k^2+2\rho\lambda)+(Z_k\omega_n)^2\right)^3} &= T\sum_{\omega_n}\frac{-\left(4\rho\lambda k^2+2(\rho\lambda)^2\right)}{\left(k^2(k^2+2\rho\lambda)+(S_k\omega_n)^2\right)^3}\\ &\quad + T\sum_{\omega_n}\frac{1}{\left(k^2(k^2+2\rho\lambda)+(S_k\omega_n)^2\right)^2}.\end{aligned}\tag{A.75}$$

From the known Matsubara summation

$$T\sum_{\omega_n}\frac{1}{\omega_n^2+c^2} = \frac{1}{c}\left(\frac{1}{2}+N(c)\right) \tag{A.76}$$

we can take derivatives with respect to c^2 to obtain a whole class of identities. We find

$$\begin{aligned}T\sum_{\omega_n}\frac{1}{(\omega_n^2+c^2)^2} &= -\frac{\partial}{\partial c^2}\left(T\sum_{\omega_n}\frac{1}{\omega_n^2+c^2}\right)\\ &= -\frac{\partial}{\partial c^2}\left[\frac{1}{c}\left(\frac{1}{2}+N(c)\right)\right]\\ &= -\frac{1}{2c}\frac{\partial}{\partial c}\left[\frac{1}{c}\left(\frac{1}{2}+N(c)\right)\right]\\ &= \frac{1}{2c^3}\left(\frac{1}{2}+N(c)\right)-\frac{1}{2c^2}N'(c)\\ &= \frac{1}{2c^3}\left(\frac{1}{2}+N(c)-cN'(c)\right).\end{aligned}\tag{A.77}$$

With one more derivative we obtain

$$\begin{aligned} T\sum_{\omega_n}\frac{1}{(\omega_n^2+c^2)^3} &= -\frac{1}{2}\frac{\partial}{\partial c^2}\left(T\sum_{\omega_n}\frac{1}{(\omega_n^2+c^2)^2}\right) \\ &= -\frac{1}{4c}\frac{\partial}{\partial c}\left[\frac{1}{2c^3}\left(\frac{1}{2}+N(c)-cN'(c)\right)\right] \\ &= -\frac{1}{4c}\left[\frac{1}{2c^3}\left(N'(c)-N'(c)-cN''(c)\right)\right. \\ &\quad \left.-\frac{3}{2c^4}\left(\frac{1}{2}+N(c)-cN'(c)\right)\right] \\ &= \frac{3}{8c^5}\left[\frac{1}{2}+N(c)-cN'(c)+\frac{c^2}{3}N''(c)\right]. \end{aligned} \tag{A.78}$$

We insert these expressions into the flow equation to arrive at the final form

$$\partial_t Z_k = \eta Z_k - Z_k 4\rho\lambda^2\frac{8v_d k^{3+d}}{d}\frac{1}{2Z_k k^6}G_2(T)F(\tilde{L}), \tag{A.79}$$

where we defined the temperature-dependent function

$$\begin{aligned} G_2(T) =& \frac{1}{(1+w_2)^{3/2}}\left(\frac{1}{2}+N_B(c)-cN_B'(c)\right) \\ &-\frac{3}{8}\frac{w_2(4+w_2)}{(1+w_2)^{5/2}}\left(\frac{1}{2}+N_B(c)-cN_B'(c)+\frac{c^2}{3}N_B''(c)\right), \end{aligned} \tag{A.80}$$

with $c = k^2\sqrt{1+w_2}/Z_k$ and $N_B(c) = (e^{c/T}-1)^{-1}$. Specifying to $d = 2$ noncompact dimensions we arrive at

$$\partial_t Z_k = \eta Z_k - \frac{\rho\lambda^2}{\pi k}G_2(T)F(\tilde{L}). \tag{A.81}$$

For the flow equation for A_k we need to take a derivative with respect to $|\vec{p}|^2$. We consider the external momentum as a two-dimensional vector $\vec{p} = (p_x, p_y)$. This time the crucial propagator is given by

$$\bar{G}_k(Q-P)\Big|_{p_0=0} = \frac{1}{\det_{\vec{q}_{d+1}-\vec{p}_{d+1}}}\begin{pmatrix} p^{\vec{q}_{d+1}-\vec{p}_{d+1}} & \bar{Z}_k q_0 \\ -\bar{Z}_k q_0 & p^{\vec{q}_{d+1}-\vec{p}_{d+1}}+2\bar{\rho}\bar{\lambda}\end{pmatrix}. \tag{A.82}$$

Again we set $\bar{U}' = 0$ from the beginning, because the flow is proportional to $\bar{\rho}$. We abbreviated

$$\begin{aligned} p^{\vec{q}_{d+1}-\vec{p}_{d+1}} &= A_k(\vec{q}_{d+1}-\vec{p}_{d+1})^2 + R\left((\vec{q}_{d+1}-\vec{p}_{d+1})^2\right) \\ &= A_k(q^2-2pqx+p^2+k_n^2) + A_k\left(k^2-k_n^2-(\vec{q}-\vec{p})^2\right)\theta(k^2-k_n^2-(\vec{q}-\vec{p})^2), \end{aligned} \tag{A.83}$$

where we have introduced $x = (\vec{q}\cdot\vec{p})/(qp)$. The easiest way to perform the p-derivatives is to Taylor expand this function in p. Higher order terms in p will vanish once we set p to zero. We expand

$$R\left((\vec{q}-\vec{p})^2\right) = A_k\left(k^2 - k_n^2 - (\vec{q}-\vec{p})^2\right)\theta(k^2 - k_n^2 - (\vec{q}-\vec{p})^2) \tag{A.84}$$

into

$$\begin{aligned} R\left((\vec{q}-\vec{p})^2\right) &= R(q^2) + R'(q^2)\left((\vec{q}-\vec{p})^2 - q^2\right) + \frac{1}{2}R''(q^2)\left((\vec{q}-\vec{p})^2 - q^2\right)^2 \\ &= R(q^2) + R'(q^2)\left(p^2 - 2pqx\right) + \frac{1}{2}R''(q^2)\left(2pqx\right)^2. \end{aligned} \tag{A.85}$$

We can calculate

$$\begin{aligned} R(q^2) &= A_k(k^2 - k_n^2 - q^2)\theta(k^2 - k_n^2 - q^2), \\ R'(q^2) &= -A_k\theta(k^2 - k_n^2 - q^2), \\ R''(q^2) &= A_k\delta(k^2 - k_n^2 - q^2). \end{aligned} \tag{A.86}$$

Inserting these expressions yields

$$\begin{aligned} p^{\vec{q}_{d+1}-\vec{p}_{d+1}} &= A_k(q^2 - 2pqx + p^2 + k_n^2) + A_k(k^2 - k_n^2 - q^2)\theta(k^2 - k_n^2 - q^2) \\ &\quad - A_k\theta(k^2 - k_n^2 - q^2)(p^2 - 2pqx) \\ &\quad + \frac{1}{2}A_k\delta(k^2 - k_n^2 - q^2)(2pqx)^2. \end{aligned} \tag{A.87}$$

Because of the overall θ-function in the flow equation we can evaluate the θ-functions in this expression to find

$$\begin{aligned} p^{\vec{q}_{d+1}-\vec{p}_{d+1}} &= A_k k^2 + \frac{1}{2}A_k\delta(k^2 - k_n^2 - q^2)(2pqx)^2 \\ &= A_k k^2 + 2A_k p^2 q^2 x^2 \delta(k^2 - k_n^2 - q^2). \end{aligned} \tag{A.88}$$

We obtain

$$\partial_{p^2} p^{\vec{q}_{d+1}-\vec{p}_{d+1}} = 2A_k q^2 x^2 \delta(k^2 - k_n^2 - q^2) \tag{A.89}$$

and further

$$\begin{aligned} \partial_{p^2}\bar{G}_k(Q-P)\Big|_{p_0=0} &= \partial_{p^2}\left[\frac{1}{\det_{\vec{q}-\vec{p}}}\begin{pmatrix} p^{\vec{q}-\vec{p}} & \bar{Z}_k q_0 \\ -\bar{Z}_k q_0 & p^{\vec{q}-\vec{p}} + 2\bar{\rho}\bar{\lambda} \end{pmatrix}\right] \\ &= -\frac{1}{\det^2_{\vec{q}-\vec{p}}}\left(2p^{\vec{q}-\vec{p}}(\partial_{p^2}p^{\vec{q}-\vec{p}}) + 2\bar{\rho}\bar{\lambda}(\partial_{p^2}p^{\vec{q}-\vec{p}})\right)\begin{pmatrix} p^{\vec{q}-\vec{p}} & \bar{Z}_k q_0 \\ -\bar{Z}_k q_0 & p^{\vec{q}-\vec{p}} + 2\bar{\rho}\bar{\lambda} \end{pmatrix} \\ &\quad + \frac{1}{\det_{\vec{q}-\vec{p}}}\begin{pmatrix} \partial_{p^2}p^{\vec{q}-\vec{p}} & 0 \\ 0 & \partial_{p^2}p^{\vec{q}-\vec{p}} \end{pmatrix}. \end{aligned} \tag{A.90}$$

We can evaluate the equation for $p = 0$ and plug it into the flow equation for the wave function renormalization. We also use $\bar{U}'' = \bar{\lambda}$ and find

$$\begin{aligned}
\partial_t A_k &= \frac{\partial}{\partial p^2} \dot{\bar{G}}^{(-1)}_{k,22}(0,p^2)\Big|_{p=0} \\
&= 2\bar{\rho}\bar{\lambda}^2 \mathrm{tr} \int_Q \frac{\dot{R}}{\mathrm{det}_Q^3} 2A_k q^2 x^2 \delta(k^2 - k_n^2 - q^2) \begin{pmatrix} p^q & \bar{Z}_k q_0 \\ -\bar{Z}_k q_0 & p^q + 2\bar{\rho}\bar{\lambda} \end{pmatrix} \begin{pmatrix} 0 & 1 \\ 1 & 0 \end{pmatrix} \\
&\times \left[\frac{-2(p^q + \bar{\rho}\bar{\lambda})}{\mathrm{det}_Q} \begin{pmatrix} p^q & \bar{Z}_k q_0 \\ -\bar{Z}_k q_0 & p^q + 2\bar{\rho}\bar{\lambda} \end{pmatrix} + \begin{pmatrix} 1 & 0 \\ 0 & 1 \end{pmatrix} \right] \\
&\times \begin{pmatrix} 0 & 1 \\ 1 & 0 \end{pmatrix} \begin{pmatrix} p^q & \bar{Z}_k q_0 \\ -\bar{Z}_k q_0 & p^q + 2\bar{\rho}\bar{\lambda} \end{pmatrix}.
\end{aligned} \tag{A.91}$$

This can be further simplified to

$$\begin{aligned}
\partial_t A_k &= A_k 4\bar{\rho}\bar{\lambda}^2 \int_Q \frac{\dot{R}}{\mathrm{det}_Q^3} q^2 x^2 \delta(k^2 - k_n^2 - q^2) \\
&\times \left[-2(p^q + \bar{\rho}\bar{\lambda})(p^q + p^q + 2\bar{\rho}\bar{\lambda}) + (p^q)^2 + (p^q + 2\bar{\rho}\bar{\lambda})^2 - 2(Z_k q_0)^2 \right] \\
&= -A_k 8\bar{\rho}\bar{\lambda}^2 \int_Q \frac{\dot{R}}{\mathrm{det}_Q^2} q^2 x^2 \delta(k^2 - k_n^2 - q^2).
\end{aligned} \tag{A.92}$$

Rewriting the equation in terms of renormalized couplings and using the definition of the anomalous dimension $\eta = -\frac{\partial_t A_k}{A_k}$ we then have

$$\begin{aligned}
\eta = 8\rho\lambda^2 &\left(T \sum_{\omega_n} \frac{1}{\mathrm{det}_Q^2} \right) \frac{1}{L} \sum_{k_n} \int \frac{\mathrm{d}^2 q}{(2\pi)^2} q^2 x^2 \delta(k^2 - q^2 - k_n^2) \\
&\times (2k^2 - \eta(k^2 - q^2 - k_n^2)) \theta(k^2 - q^2 - k_n^2).
\end{aligned} \tag{A.93}$$

Angle integration over x yields another factor of $1/2$. We have

$$\begin{aligned}
\eta = 8\rho\lambda^2 &\left(T \sum_{\omega_n} \frac{1}{\mathrm{det}_Q^2} \right) \frac{1}{L} \sum_{k_n} 4v_2 \frac{1}{2} \int \mathrm{d}q q q^2 \\
&\times (2k^2 - \eta(k^2 - q^2 - k_n^2)) \delta(k^2 - q^2 - k_n^2) \theta(k^2 - q^2 - k_n^2).
\end{aligned} \tag{A.94}$$

We further obtain

$$\begin{aligned}
\eta = \frac{32\rho\lambda^2 v_2}{2} &\left(T \sum_{\omega_n} \frac{1}{\mathrm{det}_Q^2} \right) \frac{1}{L} \sum_{k_n} \\
&\times \frac{1}{2} \int \mathrm{d}q q^3 (2k^2 - \eta(k^2 - q^2 - k_n^2)) \delta(k^2 - q^2 - k_n^2).
\end{aligned} \tag{A.95}$$

By reformulating the δ-function

$$\delta(k^2 - k_n^2 - q^2) = \frac{1}{2\sqrt{k^2 - k_n^2}} \left(\delta(\sqrt{k^2 - k_n^2} - q) + \delta(\sqrt{k^2 - k_n^2} + q) \right) \tag{A.96}$$

and using that the second δ-function gives no contribution to the integral, we get

$$\begin{aligned}\eta &= \frac{32\rho\lambda^2 v_2}{2}\left(T\sum_{\omega_n}\frac{1}{\det_Q^2}\right)\frac{1}{L}\sum_{k_n}\frac{1}{2}\frac{1}{2}(k^2-k_n^2)^{-1/2}(k^2-k_n^2)^{3/2}2k^2 \\ &= \frac{32\rho\lambda^2 v_2}{2}\left(T\sum_{\omega_n}\frac{1}{\det_Q^2}\right)\frac{1}{L}\sum_{k_n}\frac{1}{2}k^2(k^2-k_n^2).\end{aligned} \tag{A.97}$$

We find

$$\eta = \frac{32\rho\lambda^2}{32\pi}\left(T\sum_{\omega_n}\frac{1}{\det_Q^2}\right)\frac{k^4}{L}\sum_{k_n}\left(1-(k_n/k)^2\right). \tag{A.98}$$

And finally

$$\begin{aligned}\eta &= \frac{\rho\lambda^2}{\pi}k^5\left(T\sum_{\omega_n}\frac{1}{\det_Q^2}\right)\frac{1}{\tilde{L}}\sum_{k_n}\left(1-(k_n/k)^2\right) \\ &= \frac{\rho\lambda^2}{\pi}k^5\left(T\sum_{\omega_n}\frac{1}{\det_Q^2}\right)F_0(\tilde{L}),\end{aligned} \tag{A.99}$$

where $F_0(\tilde{L})$ is the crossover function with η set equal to zero, i.e.

$$F_0(\tilde{L}) = \frac{2N+1}{\tilde{L}}\left[1-\frac{1}{\tilde{L}^2}\frac{4\pi^2}{3}N(N+1)\right]. \tag{A.100}$$

The Matsubara summation yields

$$T\sum_{\omega_n}\frac{1}{\det_Q^2} = \frac{1}{2Z_k k^6}G_3(T) \tag{A.101}$$

with

$$G_3(T) = \frac{1}{(1+w_2)^{3/2}}\Big(\frac{1}{2}+N_B(c)-cN_B'(c)\Big), \tag{A.102}$$

$c = k^2(1+w_2)^{1/2}/Z_k$ and $N_B(c) = (e^{c/T}-1)^{-1}$ as before. The anomalous dimension then reads

$$\eta = \frac{\rho_0\lambda^2}{2\pi Z_k k}G_3(T)F_0(\tilde{L}). \tag{A.103}$$

A.2 Anisotropic derivative expansion

In the following we consider the anisotropic extension of Eq. (A.2) given by

$$\Gamma_k[\bar{\phi}^*,\bar{\phi}] = \int_X\Big(\bar{\phi}^*(\bar{Z}\partial_\tau - A\nabla^2 - A_z\partial_z^2)\bar{\phi}+\bar{U}(\bar{\phi}^*\bar{\phi})\Big), \tag{A.104}$$

with $\nabla^2 = \partial_x^2 + \partial_y^2$. The k-dependence of the running couplings is understood implicitly. The regularized propagator is given by

$$\bar{G}_k(Q) = \frac{1}{\det_Q} \begin{pmatrix} p^q + \bar{U}' & \bar{Z}_k q_0 \\ -\bar{Z}_k q_0 & p^q + \bar{U}' + 2\bar{\rho}\bar{U}'' \end{pmatrix}, \tag{A.105}$$

where we now have

$$p^q = A\vec{q}^2 + A_z q_z^2 + R_k(Q), \tag{A.106}$$

again with $q^2 = q_x^2 + q_y^2$. We write

$$\xi = \frac{A_z}{A},\ \eta_z = -\frac{\dot{A}_z}{A}. \tag{A.107}$$

The isotropic case corresponds to $\xi = 1$ and $\eta = \eta_z$. Due to $A_\Lambda = A_{z,\Lambda} = 1$ this implies $A = A_z$ for all k. This behavior is recovered in the anisotropic parametrization for large k. The infrared regulator function is chosen to be

$$R_k(Q) = A\Big(k^2 - q^2 - \xi q_z^2\Big)\theta\Big(k^2 - q^2 - \xi q_z^2\Big) \tag{A.108}$$

The regulator is designed such that the usual replacement $p^q \to Ak^2$ in the integrand is applicable. Further we have

$$\dot{R}_k = A\left(2k^2 - \dot{\xi}_k q_z^2 - \eta(k^2 - q^2 - \xi q_z^2)\right)\theta(k^2 - q^2 - \xi q_z^2). \tag{A.109}$$

The flow of the running coupling ξ is given by

$$\dot{\xi} = \frac{\dot{A}_z}{A} - \frac{A_z}{A}\frac{\dot{A}}{A} = -\eta_z + \xi\eta. \tag{A.110}$$

The flow of the effective potential reads

$$\begin{aligned}\dot{\bar{U}}_k = 4v_d &\left(T\sum_{\omega_n} \frac{k^2 + U' + \rho U''}{(k^2 + U')(k^2 + U' + 2\rho U'') + (Z_k\omega_n)^2}\right) \\ &\times \frac{1}{L}\sum_{k_n}\int_0^{\sqrt{k^2 - \xi k_n^2}} \mathrm{d}q q^{d-1}\left(2k^2 - \dot{\xi}k_n^2 - \eta(k^2 - q^2 - \xi k_n^2)\right)\theta(k^2 - q^2 - \xi k_n^2).\end{aligned} \tag{A.111}$$

The integrand of the q-integration can be rewritten as

$$\begin{aligned}&2k^2 - \dot{\xi}k_n^2 - \eta(k^2 - q^2 - \xi k_n^2) \\ =&2k^2 + \eta_z k_n^2 - \eta(k^2 - q^2) \\ =&(2 - \eta)k^2 + \eta_z k_n^2 + \eta q^2.\end{aligned} \tag{A.112}$$

For the q-integration we obtain analytically

$$\begin{aligned}
&\int_0^{\sqrt{k^2-\xi k_n^2}} \mathrm{d}q q^{d-1} \left((2-\eta)k^2 + \eta_\mathrm{z} k_n^2 + \eta q^2\right) \theta(k^2 - q^2 - \xi k_n^2) \\
=&\frac{1}{d} q^d \left(2k^2 - \eta k^2 + \eta_\mathrm{z} k_n^2\right) + \frac{\eta}{d+2} q^{d+2} \Big|_0^{\sqrt{k^2-\xi k_n^2}} \theta(k^2 - \xi k_n^2) \\
=&\frac{2}{d} k^{2+d} \left(1 - \xi (k_n/k)^2\right)^{d/2} \cdot \left\{1 - \frac{\eta}{d+2}\left(1 - (k_n/k)^2 \left[\frac{d}{2}(\eta_\mathrm{z}/\eta - \xi) + \eta_\mathrm{z}/\eta\right]\right)\right\} \theta(k^2 - \xi k_n^2)
\end{aligned} \tag{A.113}$$

The flow of the effective potential therefore reads

$$\begin{aligned}
\dot{\tilde{U}}_k &= \frac{4 v_d k^{3+d}}{dZ_k} G_1(T) F(\tilde{L}), \\
G_1(T) &= \left(\sqrt{\frac{1+w_1}{1+w_2}} + \sqrt{\frac{1+w_2}{1+w_1}}\right)\left(\frac{1}{2} + N_B\right), \\
F(\tilde{L}) &= \frac{1}{Lk} \sum_{k_n} (1 - \xi (k_n/k)^2)^{d/2} \\
&\quad \times \left\{1 - \frac{\eta}{d+2}\left(1 - (k_n/k)^2 \left[\frac{d}{2}(\eta_\mathrm{z}/\eta - \xi) + \eta_\mathrm{z}/\eta\right]\right)\right\} \theta(k^2 - \xi k_n^2)
\end{aligned} \tag{A.114}$$

The range of summation is limited to $|k_n| = \left|\frac{2\pi}{L} n\right| < \frac{k}{\sqrt{\xi}}$ or $|n| < \frac{\tilde{L}}{2\pi\xi^{1/2}}$. We define $N = \left\lfloor \frac{\tilde{L}}{2\pi\xi^{1/2}} \right\rfloor$ and specify to two continuous dimensions to get the modified crossover function

$$\begin{aligned}
F_{\mathrm{pbc}}(\tilde{L}) = \frac{2N+1}{\tilde{L}} \Bigg[&1 - \frac{\eta}{4} - \frac{1}{\tilde{L}^2}\Big(\xi - \frac{\eta_\mathrm{z}}{2}\Big)\frac{4\pi^2}{3} N(N+1) \\
&- \frac{\xi(2\eta_\mathrm{z} - \xi\eta)}{\tilde{L}^4} \frac{4\pi^4}{15} N(N+1)(-1 + 3N + 3N^2) \Bigg].
\end{aligned} \tag{A.115}$$

For $\xi = 1$, $\eta = \eta_\mathrm{z}$ we recover the isotropic crossover function.

The flow equation for the frequency coefficient Z deviates from the isotropic equation only in the different crossover function.

For the projection of the flow equations for A and A_z, respectively, we employ

$$\begin{aligned}
\dot{A} &= \frac{\partial}{\partial p^2} \dot{\bar{G}}^{-1}_{k,22}(0, \vec{p}^2 = p^2, p_z = 0)\Big|_{P=0}, \\
\dot{A}_\mathrm{z} &= \frac{\partial}{\partial p_z^2} \dot{\bar{G}}^{-1}_{k,22}(0, \vec{p}^2 = 0, p_z)\Big|_{P=0}.
\end{aligned} \tag{A.116}$$

Although q_z is not a continuous variable for $L < \infty$, this is the natural generalization of the appropriate infinite volume projection. We follow closely the isotropic calculation for the flow equation for η and note that we now have

$$p^{q-p} = Aq^2 - 2Apqx + Ap^2 + A_\mathrm{z} q_z^2 + R_k(Q - P). \tag{A.117}$$

Again we can expand the regulator as

$$R_k(Q-P) = R_k(q^2) + R'(q^2)\cdot((\vec{q}-\vec{p})^2 - q^2) + \frac{1}{2}R''(q^2)\cdot((\vec{q}-\vec{p})^2 - q^2) \tag{A.118}$$

with

$$\begin{aligned} R_k(q^2) &= A(k^2 - q^2 - \xi q_z^2)\theta(k^2 - q^2 - \xi q_z^2), \\ R_k'(q^2) &= -A\theta(k^2 - q^2 - \xi q_z^2), \\ R_k''(q^2) &= A\delta(k^2 - q^2 - \xi q_z^2). \end{aligned} \tag{A.119}$$

We find

$$\begin{aligned} p^{q-p} &= Ak^2 + 2Ap^2q^2x^2\delta(k^2 - q^2 - \xi q_z^2) \\ \partial_{p^2}p^{q-p} &= 2Aq^2x^2\delta(k^2 - q^2 - \xi q_z^2). \end{aligned} \tag{A.120}$$

The rest of the calculation follows the isotropic calculation. We find

$$\begin{aligned} \eta &= 8\rho\lambda^2\left(T\sum_{\omega_n}\frac{1}{\det_Q^2}\right)\frac{1}{L}\sum_{k_n}\int\frac{\mathrm{d}^2q}{(2\pi)^2}q^2x^2 \\ &\times(2k^2 - \eta k^2 + \eta q^2 + \eta_{\mathrm{z}}q_z^2)\theta(k^2 - q^2 - \xi q_z^2)\delta(k^2 - q^2 - \xi q_z^2) \\ &= \frac{\rho\lambda^2}{2\pi}\left(T\sum_{\omega_n}\frac{1}{\det_Q^2}\right)\frac{1}{L}\sum_{k_n}(k^2 - \xi q_z^2)(2k^2 - (\eta\xi - \eta_{\mathrm{z}})q_z^2). \end{aligned} \tag{A.121}$$

The calculation for η_{z} is pretty similar and we present the differences below. We have

$$p^{q-p} = Aq^2 + A_{\mathrm{z}}(q_z^2 - 2q_zp_z + p_z^2) + R_k(Q-P) \tag{A.122}$$

and the regulator expansion gives

$$\begin{aligned} R_k(q_z^2) &= A(k^2 - q^2 - \xi q_z^2)\theta(k^2 - q^2 - \xi q_z^2), \\ R_k'(q_z^2) &= -\xi A\theta(k^2 - q^2 - \xi q_z^2), \\ R_k''(q_z^2) &= \xi^2 A\delta(k^2 - q^2 - \xi q_z^2). \end{aligned} \tag{A.123}$$

We find

$$\begin{aligned} p^{q-p} &= Ak^2 + 2\xi^2Ap_z^2q_z^2\delta(k^2 - q^2 - \xi q_z^2), \\ \partial_{p_z^2}p^{q-p} &= 2\xi^2Aq_z^2\delta(k^2 - q^2 - \xi q_z^2), \end{aligned} \tag{A.124}$$

and

$$\eta_{\mathrm{z}} = \frac{\rho\lambda^2}{\pi}\left(T\sum_{\omega_n}\frac{1}{\det_Q^2}\right)\frac{1}{L}\sum_{k_n}(\xi q_z)^2(2k^2 - (\eta\xi - \eta_{\mathrm{z}})q_z^2). \tag{A.125}$$

Together with

$$\begin{aligned} A &= \frac{\rho\lambda^2}{2\pi}\frac{G_3}{kZ_k}\frac{1}{\tilde{L}}, \\ s_0 &= \sum_{n=-N}^{N} 1 = 2N+1, \\ s_2 &= \sum_{n=-N}^{N}\left(\frac{k_n}{k}\right)^2 = \left(\frac{2\pi}{\tilde{L}}\right)^2 2\sum_{n=1}^{N} n^2, \\ s_4 &= \sum_{n=-N}^{N}\left(\frac{k_n}{k}\right)^4 = \left(\frac{2\pi}{\tilde{L}}\right)^4 2\sum_{n=1}^{N} n^4, \end{aligned} \tag{A.126}$$

we are led to a linear set of equations for η and η_z, which supplements the remaining flow equations

$$\begin{aligned} \eta &= \frac{A}{2}\left(2s_0 - 2\xi s_2 + \eta(\xi^2 s_4 - \xi s_2) + \eta_z(s_2 - \xi s_4)\right), \\ \eta_z &= A\left(2\xi^2 s_2 - \eta\xi^3 s_4 + \eta_z\xi^2 s_4\right). \end{aligned} \tag{A.127}$$

List of Figures

2.1 Velocity distribution for Bose–Einstein condensation 18
2.2 Condensate fraction N_0/N as a function of temperature T. 19
2.3 Phase of the Bose field in presence of a vortex configuration 24

3.1 Effective average action in theory space 34

4.1 The effective potential U as a function of the complex field ϕ 40
4.2 Effective potential in presence of a second order phase transition 41
4.3 Vacuum- and many-body-flow of the effective average action 46
4.4 Schematics of the energy spectrum in the dimensional crossover 48
4.5 Crossover function $F_{\text{pbc}}(\tilde{L})$ 57
4.6 Flow in the normal phase 58
4.7 Flow at the critical temperature 59
4.8 Flow in the superfluid phase 59
4.9 Superfluid fraction ρ_0/n at $k \to 0$ for different values of L 60
4.10 Dimensional crossover of the superfluid critical temperature T_{c} 61
4.11 Critical temperature T_{c}/μ in two dimensions as a function of g_{2D} 71
4.12 Dimensional crossover of T_{c} for a fixed value of a_{2D} 72
4.13 Characteristic flow of η and η_{z} 75
4.14 Ratio $\xi = A_{\text{z}}/A$ at the lowest momentum k_{f} 76
4.15 The crossover function $F_{\text{box}}(\tilde{L})$ 78

Bibliography

Al Khawaja, U., Proukakis, N. P., Andersen, J. O., Romans, M. W. J., and Stoof, H. T. C. (2003). Dimensional and temperature crossover in trapped bose gases. *Phys. Rev. A*, 68:043603.

Altland, A. and Simons, B. D. (2010). *Condensed Matter Field Theory*. Cambridge University Press, 2 edition.

Anderson, M. H., Ensher, J. R., Matthews, M. R., Wieman, C. E., and Cornell, E. A. (1995). Observation of Bose–Einstein condensation in a dilute atomic vapor. *Science*, 269(5221):198–201.

Arnold, P. and Moore, G. (2001). Bec transition temperature of a dilute homogeneous imperfect bose gas. *Phys. Rev. Lett.*, 87:120401.

Baym, G., Blaizot, J.-P., Holzmann, M., Laloë, F., and Vautherin, D. (1999). The transition temperature of the dilute interacting bose gas. *Phys. Rev. Lett.*, 83:1703–1706.

Berezinskii, V. L. (1971). Destruction of long-range order in one-dimensional and two-dimensional systems having a continuous symmetry group I. classical systems. *Sov. Phys. JETP*, 32(3):493.

Berezinskii, V. L. (1972). Destruction of long-range order in one-dimensional and two-dimensional systems possessing a continuous symmetry group. II. quantum systems. *Sov. Phys. JETP*, 34(3):610–616.

Berges, J., Tetradis, N., and Wetterich, C. (2002). Nonperturbative renormalization flow in quantum field theory and statistical physics. *Phys.Rept.*, 363:223–386.

Bloch, I., Dalibard, J., and Zwerger, W. (2008). Many-body physics with ultracold gases. *Rev. Mod. Phys.*, 80:885–964.

Boettcher, I., Bayha, L., Kedar, D., Murthy, P. A., Neidig, M., Ries, M. G., Wenz, A. N., Zürn, G., Jochim, S., and Enss, T. (2016). Equation of state of ultracold fermions in the 2d bec-bcs crossover region. *Phys. Rev. Lett.*, 116:045303.

Boettcher, I., Floerchinger, S., and Wetterich, C. (2011). Hydrodynamic collective modes for cold trapped gases. *J. Phys.*, B44:235301.

Boettcher, I., Pawlowski, J. M., and Diehl, S. (2012). Ultracold atoms and the Functional Renormalization Group. *Nucl.Phys.Proc.Suppl.*, 228:63–135.

Boettcher, I., Pawlowski, J. M., and Wetterich, C. (2014). Critical temperature and superfluid gap of the unitary fermi gas from functional renormalization. *Phys. Rev. A*, 89:053630.

Bose, S. N. (1924). Plancks Gesetz und Lichtquantenhypothese. *Z. Phys.*, 26:178.

Bradley, C. C., Sackett, C. A., Tollett, J. J., and Hulet, R. G. (1995). Evidence of Bose–Einstein condensation in an atomic gas with attractive interactions. *Phys. Rev. Lett.*, 75:1687–1690.

Braun, J., Diehl, S., and Scherer, M. M. (2011a). Finite-size and particle-number effects in an ultracold Fermi gas at unitarity. *Phys. Rev. A*, 84(6):063616.

Braun, J. and Klein, B. (2009). Finite-size scaling behavior in the O(4) model. *European Physical Journal C*, 63:443–460.

Braun, J., Klein, B., and Piasecki, P. (2011b). On the scaling behavior of the chiral phase transition in QCD in finite and infinite volume. *European Physical Journal C*, 71:1576.

Braun, J., Klein, B., and Schaefer, B.-J. (2012). On the phase structure of QCD in a finite volume. *Physics Letters B*, 713:216–223.

Carusotto, I. and Ciuti, C. (2013). Quantum fluids of light. *Rev. Mod. Phys.*, 85:299–366.

Cladé, P., Ryu, C., Ramanathan, A., Helmerson, K., and Phillips, W. D. (2009). Observation of a 2D Bose Gas: From Thermal to Quasicondensate to Superfluid. *Phys. Rev. Lett.*, 102:170401.

Davis, K. B., Mewes, M. O., Andrews, M. R., van Druten, N. J., Durfee, D. S., Kurn, D. M., and Ketterle, W. (1995). Bose–Einstein condensation in a gas of sodium atoms. *Phys. Rev. Lett.*, 75:3969–3973.

Desbuquois, R., Chomaz, L., Yefsah, T., Léonard, J., Beugnon, J., Weitenberg, C., and Dalibard, J. (2012). Superfluid behaviour of a two-dimensional Bose gas. *Nat. Phys.*, 8(9):645–648.

Dupuis, N. (2009). Unified picture of superfluidity: From bogoliubov's approximation to popov's hydrodynamic theory. *Phys. Rev. Lett.*, 102:190401.

Dutta, S. and Mueller, E. J. (2016). Dimensional crossover in a spin-imbalanced fermi gas. *Phys. Rev. A*, 94:063627.

Dyke, P., Fenech, K., Peppler, T., Lingham, M. G., Hoinka, S., Zhang, W., Peng, S.-G., Mulkerin, B., Hu, H., Liu, X.-J., and Vale, C. J. (2016). Criteria for two-dimensional kinematics in an interacting fermi gas. *Phys. Rev. A*, 93:011603.

Einstein, A. (1924). Quantentheorie des einatomigen idealen Gases. *Sitzungsberichte, Preussische Akademie der Wissenschaften*, 1924:261–267.

Einstein, A. (1925). Quantentheorie des einatomigen idealen Gases, 2. Abhandlung. *Sitzungsberichte, Preussische Akademie der Wissenschaften*, 1925:3–10.

Fenech, K., Dyke, P., Peppler, T., Lingham, M. G., Hoinka, S., Hu, H., and Vale, C. J. (2016). Thermodynamics of an attractive 2d fermi gas. *Phys. Rev. Lett.*, 116:045302.

Feynman, R. P. (1982). Simulating Physics with Computers. *International Journal of Theoretical Physics*, 21:467–488.

Fisher, D. S. and Hohenberg, P. C. (1988). Dilute bose gas in two dimensions. *Phys. Rev. B*, 37:4936–4943.

Fletcher, R. J., Robert-de Saint-Vincent, M., Man, J., Navon, N., Smith, R. P., Viebahn, K. G. H., and Hadzibabic, Z. (2015). Connecting berezinskii-kosterlitz-thouless and bec phase transitions by tuning interactions in a trapped gas. *Phys. Rev. Lett.*, 114:255302.

Floerchinger, S. (2014). Few-body hierarchy in non-relativistic functional renormalization group equations and a decoupling theorem. *Nuclear Physics A*, 927:119–133.

Floerchinger, S. and Wetterich, C. (2008). Functional renormalization for bose-einstein condensation. *Phys. Rev. A*, 77:053603.

Floerchinger, S. and Wetterich, C. (2009a). Nonperturbative thermodynamics of an interacting bose gas. *Phys. Rev. A*, 79:063602.

Floerchinger, S. and Wetterich, C. (2009b). Superfluid bose gas in two dimensions. *Phys. Rev. A*, 79:013601.

Fuchs, J. N., Leyronas, X., and Combescot, R. (2003). Hydrodynamic modes of a one-dimensional trapped bose gas. *Phys. Rev. A*, 68:043610.

Gersdorff, G. v. and Wetterich, C. (2001). Nonperturbative renormalization flow and essential scaling for the kosterlitz-thouless transition. *Phys. Rev. B*, 64:054513.

Gies, H. (2012). Introduction to the functional RG and applications to gauge theories. *Lect.Notes Phys.*, 852:287–348.

Goldstone, J. (1961). Field theories with superconductor solutions. *Il Nuovo Cimento (1955-1965)*, 19(1):154–164.

Grüter, P., Ceperley, D., and Laloë, F. (1997). Critical temperature of bose-einstein condensation of hard-sphere gases. *Phys. Rev. Lett.*, 79:3549–3552.

Hadzibabic, Z. and Dalibard, J. (2011). Two-dimensional Bose fluids: An atomic physics perspective. *Riv. del Nuovo Cim.*, 34(389).

Hadzibabic, Z., Krüger, P., Cheneau, M., Battelier, B., and Dalibard, J. (2006). Berezinskii-Kosterlitz-Thouless crossover in a trapped atomic gas. *Nature*, 441(7097):1118–1121.

Heiselberg, H. (2004). Collective modes of trapped gases at the bec-bcs crossover. *Phys. Rev. Lett.*, 93:040402.

Hohenberg, P. C. (1967). Existence of long-range order in one and two dimensions. *Phys. Rev.*, 158(2):383–386.

Holzmann, M., Baym, G., Blaizot, J.-P., and Laloë, F. (2007). Superfluid transition of homogeneous and trapped two-dimensional Bose gases. *Proc. Natl. Acad. Sci. U.S.A.*, 104(5):1476–1481.

Holzmann, M. and Krauth, W. (1999). Transition temperature of the homogeneous, weakly interacting bose gas. *Phys. Rev. Lett.*, 83:2687–2690.

Holzmann, M. and Krauth, W. (2008). Kosterlitz-Thouless Transition of the Quasi-Two-Dimensional Trapped Bose Gas. *Phys. Rev. Lett.*, 100:190402.

Hung, C.-L., Zhang, X., Gemelke, N., and Chin, C. (2011). Observation of scale invariance and universality in two-dimensional Bose gases. *Nature*, 470(7333):236–239.

Jakubczyk, P., Dupuis, N., and Delamotte, B. (2014). Reexamination of the nonperturbative renormalization-group approach to the kosterlitz-thouless transition. *Phys. Rev. E*, 90:062105.

Kadanoff, L. P. (1966). Scaling laws for Ising models near T(c). *Physics*, 2:263–272.

Kagan, Y., Svistunov, B. V., and Shlyapnikov, G. V. (1987). Influence on inelastic processes of the phase transition in a weakly collisional two-dimensional bose gas. *Sov. Phys. JETP*, 66:314.

Kaluza, T. (1921). Zum Unitätsproblem der Physik. *Sitzungsberichte der Königlich Preußischen Akademie der Wissenschaften (Berlin), Seite p. 966-972*, pages 966–972.

Kashurnikov, V. A., Prokof'ev, N. V., and Svistunov, B. V. (2001). Critical temperature shift in weakly interacting bose gas. *Phys. Rev. Lett.*, 87:120402.

Klein, O. (1926). Quantentheorie und fünfdimensionale Relativitätstheorie. *Zeitschrift fur Physik*, 37:895–906.

Kosterlitz, J. M. (1974). The critical properties of the two-dimensional *xy* model. *J. Phys. C: Solid State Phys.*, 7:1046.

Kosterlitz, J. M. and Thouless, D. J. (1973). Ordering, metastability and phase transitions in two-dimensional systems. *J. Phys. C: Solid State Phys.*, 6(7):1181–1203.

Lammers, S., Boettcher, I., and Wetterich, C. (2016). Dimensional crossover of nonrelativistic bosons. *Phys. Rev. A*, 93:063631.

Lee, P. A., Nagaosa, N., and Wen, X.-G. (2006). Doping a mott insulator: Physics of high-temperature superconductivity. *Rev. Mod. Phys.*, 78:17–85.

Levinsen, J. and Parish, M. M. (2015). Strongly interacting two-dimensional Fermi gases. *Annual Review of Cold Atoms and Molecules*, 3(1):1–71.

Lewenstein, M., Sanpera, A., Ahufinger, V., Damski, B., De, A. S., and Sen, U. (2006). Ultracold atomic gases in optical lattices: mimicking condensed matter physics and beyond. *Advances in Physics*, 56:135.

Litim, D. F. (2000). Optimization of the exact renormalization group. *Phys.Lett.*, B486:92–99.

Litim, D. F. (2001a). Mind the gap. *Int.J.Mod.Phys.*, A16:2081–2088.

Litim, D. F. (2001b). Optimized renormalization group flows. *Phys.Rev.*, D64:105007.

Makhalov, V., Martiyanov, K., and Turlapov, A. (2014). Ground-state pressure of quasi-2d fermi and bose gases. *Phys. Rev. Lett.*, 112:045301.

Mermin, N. D. and Wagner, H. (1966). Absence of Ferromagnetism or Antiferromagnetism in One- or Two-Dimensional Isotropic Heisenberg Models. *Phys. Rev. Lett.*, 17:1133–1136.

Morgan, S. A., Lee, M. D., and Burnett, K. (2002). Off-shell t matrices in one, two, and three dimensions. *Phys. Rev. A*, 65:022706.

Morris, T. R. (1994a). Derivative Expansion of the Exact Renormalization Group. *Phys. Lett. B*, 329:241–248.

Morris, T. R. (1994b). On Truncations of the Exact Renormalization Group. *Phys. Lett. B*, 334:355–362.

Murthy, P. A., Boettcher, I., Bayha, L., Holzmann, M., Kedar, D., Neidig, M., Ries, M. G., Wenz, A. N., Zürn, G., and Jochim, S. (2015). Observation of the berezinskii-kosterlitz-thouless phase transition in an ultracold fermi gas. *Phys. Rev. Lett.*, 115:010401.

Pawlowski, J. M. (2007). Aspects of the functional renormalisation group. *Annals of Physics*, 322(12):2831 – 2915.

Pethick, C. and Smith, H. (2002). *Bose–Einstein condensation in dilute gases*. Cambridge University Press.

Petrov, D. S. and Shlyapnikov, G. V. (2001). Interatomic collisions in a tightly confined bose gas. *Phys. Rev. A*, 64:012706.

Pitaevskii, L. and Stringari, S. (2003). *Bose–Einstein condensation*. Oxford University Press.

Plisson, T., Allard, B., Holzmann, M., Salomon, G., Aspect, A., Bouyer, P., and Bourdel, T. (2011). Coherence properties of a two-dimensional trapped Bose gas around the superfluid transition. *Phys. Rev. A*, 84:061606.

Popov, V. N. (1983). *Functional Integrals in Quantum Field Theory and Statistical Physics*. Reidel, Dordrecht.

Popov, V. N. (1988). *Functional Integrals and Collective Excitations*. Cambridge Monographs on Mathematical Physics. Cambridge University Press.

Prokof'ev, N., Ruebenacker, O., and Svistunov, B. (2001). Critical point of a weakly interacting two-dimensional bose gas. *Phys. Rev. Lett.*, 87:270402.

Prokof'ev, N. and Svistunov, B. (2002). Two-dimensional weakly interacting bose gas in the fluctuation region. *Phys. Rev. A*, 66:043608.

Rançon, A. and Dupuis, N. (2012). Universal thermodynamics of a two-dimensional bose gas. *Phys. Rev. A*, 85:063607.

Ries, M. G., Wenz, A. N., Zürn, G., Bayha, L., Boettcher, I., Kedar, D., Murthy, P. A., Neidig, M., Lompe, T., and Jochim, S. (2015). Observation of pair condensation in the quasi-2d bec-bcs crossover. *Phys. Rev. Lett.*, 114:230401.

Schnoerr, D., Boettcher, I., Pawlowski, J. M., and Wetterich, C. (2013). Error estimates and specification parameters for functional renormalization. *Annals Phys.*, 334:83–99.

Sieberer, L. M., Buchhold, M., and Diehl, S. (2016). Keldysh field theory for driven open quantum systems. *Rep. Prog. Phys.*, 79:096001.

Sun, K. and Bolech, C. J. (2012). Oscillatory pairing amplitude and magnetic compressible-incompressible transitions in imbalanced fermionic superfluids in optical lattices of elongated tubes. *Phys. Rev. A*, 85:051607.

Tetradis, N. and Wetterich, C. (1993). The high temperature phase transition for phi4 theories. *Nucl. Phys.*, B398:659–696.

Tetradis, N. and Wetterich, C. (1994a). Critical exponents from the effective average action. *Nuclear Physics B*, 422(3):541 – 592.

Tetradis, N. and Wetterich, C. (1994b). High temperature phase transitions without infrared divergences. *Int. J. Mod. Phys.*, A9:4029–4062.

Tong, D. (2012). Lectures on statistical physics.

Tripolt, R.-A., Braun, J., Klein, B., and Schaefer, B.-J. (2014). Effect of fluctuations on the QCD critical point in a finite volume. *Phys. Rev. D*, 90(5):054012.

Tung, S., Lamporesi, G., Lobser, D., Xia, L., and Cornell, E. A. (2010). Observation of the Presuperfluid Regime in a Two-Dimensional Bose Gas. *Phys. Rev. Lett.*, 105:230408.

Wang, W.-M. (2009). Integrals of products of hermite functions.

Wetterich, C. (1993). Exact evolution equation for the effective potential. *Physics Letters B*, 301(1):90–94.

Wetterich, C. (2008). Functional renormalization for quantum phase transitions with nonrelativistic bosons. *Phys. Rev. B*, 77:064504.

Wilson, K. G. (1971). The Renormalization group and critical phenomena 1. *Phys. Rev. B.*, 4:3174–3183.

Yamashita, M. T., Bellotti, F. F., Frederico, T., Fedorov, D. V., Jensen, A. S., and Zinner, N. T. (2015). Weakly bound states of two- and three-boson systems in the crossover from two to three dimensions. *Journal of Physics B Atomic Molecular Physics*, 48(2):025302.

Yefsah, T., Desbuquois, R., Chomaz, L., Günter, K. J., and Dalibard, J. (2011). Exploring the thermodynamics of a two-dimensional bose gas. *Phys. Rev. Lett.*, 107:130401.

Zee, A. (2010). *Quantum field theory in a nutshell*. Princeton University Press.

Zhang, X., Hung, C.-L., Tung, S.-K., and Chin, C. (2012). Observation of quantum criticality with ultracold atoms in optical lattices. *Science*, 335(6072):1070–1072.

Danksagung

Mein größter Dank gilt meinem Betreuer Prof. Christof Wetterich für die Möglichkeit, auf diesem faszinierenden Gebiet zu forschen. Die vielen Gespräche und Diskussionen waren immer sehr lehrreich und zugleich motivierend.

Weiterhin bedanke ich mich sehr herzlich bei Prof. Thomas Gasenzer für die Übernahme der Zweitbegutachtung.

Igor Böttcher danke ich für eine tolle Zusammenarbeit, die vielen Diskussionen und seine unzähligen hilfreichen Erklärungen.

Für das tolle Arbeitsklima bedanke ich mich beim gesamten Team vom 16er, insbesondere bei allen aus dem Dachzimmer.

Der Heidelberg Graduate School for Fundamental Physics danke ich für die finanzielle Unterstützung.

Sehr viel zu verdanken habe ich Kristin, meinen Eltern und meinen Geschwistern, die mich in allen Belangen während der Promotion unterstützt haben.

Erklärung:

Ich versichere, dass ich diese Arbeit selbstständig verfasst habe und keine anderen als die angegebenen Quellen und Hilfsmittel benutzt habe.

Heidelberg, den 02.08.2017 .....